New Rock-Eval method for Pyritic and Organic Sulphur quantification : Application to study Organic Matter preservation in Jurassic sediments

Anabel Aboussou

Sorbonne Université

ED 398 : Géosciences, ressources naturelles et environnement

IFP Energies nouvelles (IFPEN) / Géofluides et roches

New Rock-Eval method for Pyritic and Organic Sulphur quantification: Application to study Organic Matter preservation in Jurassic sediments.

By Anabel ABOUSSOU

Doctoral thesis in Geosciences

Supervised by Thomas WAGNER and Bruno GARCIA

Presented and publicly defended on 17/12/2018

To a jury composed of:

Armelle RIBOULLEAU, Senior Lecturer at the University of Lille	Reviewer
Mohammed BOUSSAFIR, Senior Lecturer at the University of Orleans	Reviewer
François BAUDIN, Professor at Sorbonne University	Examiner
François GELIN, Research Engineer / Project Manager at Total	Examiner
Thomas WAGNER, Professor at Heriot-Watt University - Lyell Centre	Co-Director
Bruno GARCIA, Research Engineer / Project Manager at IFPEN	Co-Director
Christian MÄRZ, Associate Professor at the University of Leeds	Guest scientist
Violaine LAMOUREUX-VAR, Research Engineer / Project Manager at IFPEN	Guest scientist

A mes très chers parents,

Aucune dédicace, aucun mot ne pourrait exprimer à leur juste valeur l'amour que je vous porte. Loin de vous, votre soutien, votre amour et vos encouragements m'ont toujours donné la force de persévérer et d'avancer dans la vie.

Merci d'être mes parents

Acknowledgements

I would like to express my gratitude to all my supervisors: Professor Thomas Wagner (Heriot Watt University-Lyell centre), Dr Bruno Garcia (IFPEN), Dr Christian März (University of Leeds), Dr Violaine Lamoureux-Var (IFPEN), Dr Isabelle Kowalewski (IFPEN) and Dr Brigitte Doligez (IFPEN). I am very thankful for the opportunity they give me to work on this project and for their guidance during the entire PhD. This paper would not be possible without their invaluable contributions, for which I am deeply indebted.

Special mention to Professor Thomas Wagner and Christian März for welcoming me during my 5 months visit at the Lyell centre of Heriot Watt University and University of Leeds, as well as for their helpful advices during the entire PhD.

It would be remiss of me not to acknowledge the outstanding technical and scientific assistance provided by several people at IFP Energies nouvelles (France), Institute of Petroleum Engineering of Heriot-Watt University (United Kingdom) and Institut des sciences de la Terre de Paris (ISTeP) - Sorbonne Université (France) namely Daniel Pillot, Herman Ravelojaona, Dr Jim Buckman, Dr Johann Schnyder, Geremie Letort, Said Youssouf, Patience Ekambas, Dr Eric Kohler, Isabelle Clemençon, Dr Benjamin Bruneau and Matthieu Mascle.

I would like to greet members of the IFPEN Geoscience department and those of the Lyell centre of Heriot Watt University as well as my fellow PhD students from these two sites, for the enthusiastic collaboration and the enjoyable work atmosphere.

I am very grateful to my two reviewers, Dr Armelle Riboulleau and Dr Mohammed Boussafir, and members of my jury, Professor François Baudin and Dr François Gelin, who kindly agreed to judge this work. Anyone working in the field of Organic Geochemistry owes a great debt to these leading researchers, whose presence in my jury is the best honours I can have.

Finally, many thanks to my family and all my friends who have been very supportive during the entire PhD. Without you all, it would not have been possible to juggle the extensive work which this PhD entailed.

I especially thank my parents, my brother and my partner for their unfailing support throughout the duration of this PhD.

Abstract

This study was focused on development of the new Rock-Eval 7S which presents the same functionalities as the current version (Rock-Eval 6), complemented by a system of sulphur detection during the two phases of the analysis: pyrolysis phase and oxidation phase. The main goal of this PhD was to provide and highlight different carbon and sulphur Rock-Eval 7S parameters which can be used to describe OM preservation in marine sediments. The longer-term perspective of this project being to lay the scientific foundation to apply Rock-Eval 7S carbon and sulphur parameters as routine descriptors in basin models.

To reach the main goal of this PhD, developing and validating new analytical method for sulphur speciation and quantification was required. Rock-Eval 7S calibration for total sulphur (S^{Total}) quantification was done first, followed by characterization of Rock-Eval 7S signals of different sulphur species found in marine sediments (pyritic sulphur: S^{Pyrite}; organic sulphur: $S^{Organic}$; sulphates: $S^{Sulphate}$ and elemental sulphur: $S^{Elemental}$). These phases decompose at different specific ranges of temperatures, except S^{Pyrite} and $S^{Organic}$. Indeed, during the pyrolysis phase, $_{Pyrolysis}S^{Pyrite}$ and $_{Pyrolysis}S^{Organic}$ can be distinguished from each other and quantified separately because they are represented by two distinct sulphur peaks. However, during the oxidation phase, $_{Oxidation}S^{Pyrite}$ and $_{Oxidation}S^{Organic}$ are covered by one single peak. This limits the Rock-Eval 7S direct quantification of S^{Pyrite} and $S^{Organic}$, two essential parameters to study OM preservation and paleoenvironmental conditions in marine sediments. Indeed, S^{Pyrite} *vs* TOC relationships can be used as indicators of bottom water oxygenation, which is an important environmental controlling factor of OM preservation. And, the $S^{Organic}$ parameter informs about OM sulfurization degree, an important OM preservation mechanism.

Therefore, an analytical method for S^{Pyrite} and $S^{Organic}$ quantification using Rock-Eval 7S was developed. Knowing that with Rock-Eval 7S we can quantify $_{Pyrolysis}S^{Pyrite}$, the strategy was to study of pyrite thermal transformation during Rock-Eval 7S pyrolysis and its interaction with OM and minerals commonly found in organic rich marine sediments. The aim being to estimate the total S^{Pyrite} from the $_{Pyrolysis}S^{Pyrite}$, and then deduce the total $S^{Organic}$.

This new Rock-Eval 7S method was validated using a set of organic rich marine sediment samples from the Grey Shale Member (North-Yorkshire, UK), Kimmeridge Clay Fm. (Dorset, UK) and a set of sedimentary mixtures with known S^{Pyrite} and $S^{Organic}$ contents (sedimentary rocks containing only $S^{Organic}$ + pyrite). The results obtained show that the new Rock-Eval 7S method provides an satisfying quantification of both S^{Pyrite} and $S^{Organic}$.

The new Rock-Eval 7S method for S^{Pyrite} and $S^{Organic}$ quantification, developed and validated in this study, was then applied to study of OM preservation in Jurassic sediments. Three Jurassic sedimentary sections were studied, Dorset section (KCF), North-Yorkshire section (Grey Shale Member) and Somerset section (Blue Lias Fm.). Indeed, only with a rapid Rock-Eval 7S analysis, we obtained relevant carbon and sulphur parameters, including TOC, S^{Total}; S^{Pyrite} and $S^{Organic}$, that were used as indicators of paleoenvironmental conditions which impacted the OM preservation, such as bottom water oxygenation and OM sulfurization degree.

This advanced Rock-Eval 7S methodology, the first quick, efficient and reliable quantitative method that allows direct quantification of S^{Pyrite} and $S^{Organic}$ in a single analysis, provides important analytical advantages including: (i) rapid analysis time (2 hours per sample); (ii) no chemical preparation steps, which are laborious and hazardous due to the use of strong acids; (iii) automatic analysis; and (iv) simultaneous quantification of organic/inorganic carbon and organic/inorganic sulphur in a single run.

In addition to its application to better understand and parameterise OM preservation, the new Rock-Eval 7S method for S^{Pyrite} and $S^{Organic}$ quantification has numerous potential applications and opportunities. Indeed, this method can provide useful data for a wide range of applications including petroleum exploration and production, paleoenvironmental/paleoclimate reconstruction, coal exploration and production, and soil pollution.

Résumé

Cette étude a consisté au développement du nouveau Rock-Eval 7S possédant les mêmes fonctionnalités que la version actuelle (Rock-Eval 6) couplée à un système de détection du soufre pendant les deux phases de l'analyse (pyrolyse et oxydation). Le but principal de cette étude a été de définir et de mettre en évidence différents paramètres Rock-Eval 7S, carbone et soufre, nécessaires à l'étude de la préservation de la matière organique dans les sédiments marins. La perspective à long terme de ce projet étant d'établir les bases scientifiques en vue de l'utilisation des paramètres Rock-Eval 7S comme descripteurs de préservation de la matière organique dans les logiciels de modélisation de bassin.

Le développement et la validation d'une nouvelle méthode de spéciation et de quantification du soufre a été nécessaire pour répondre au but principal de cette étude. Cela a consisté en plusieurs étapes. Dans un premier temps, la calibration du Rock-Eval 7S pour la quantification du soufre total (S^{Total}) a été effectuée. Deux coefficients de calibration, KSO_2-pyrolyse et KSO_2-oxydation, pour chacune des phases de l'analyse Rock-Eval 7S, ont été déterminés. Les résultats obtenus avec ces nouveaux coefficients de calibration montrent que le Rock-Eval 7S fournit une quantification précise du S^{Total}.

Par la suite, le signal des différentes d'espèces de soufre rencontrées dans les sédiments marins (soufre pyritique : S^{Pyrite}, soufre organique : $S^{Organic}$, sulfates : $S^{Sulphates}$ et soufre natif : $S^{Elemental}$) a été caractérisé avec le Rock-Eval 7S. Chaque espèce de soufre se décompose à des gammes de températures spécifiques, à l'exception du S^{Pyrite} et du $S^{Organic}$. En effet, pendant la phase de pyrolyse, le S^{Pyrite} et le $S^{Organic}$ de pyrolyse peuvent être distingués et quantifiés séparément car ils sont représentés par deux pics distincts. Cependant, pendant la phase d'oxydation, le S^{Pyrite} et le $S^{Organic}$ se décomposent aux mêmes gammes de températures. Cela limite donc la quantification directe du S^{Pyrite} et du $S^{Organic}$ avec le Rock-Eval 7S, qui sont deux importants paramètres pour l'étude de la préservation de la matière organique. En effet, les relations entre S^{Pyrite} et Carbone Organique Total (COT) peuvent être utilisées comme indicateurs de l'oxygénation de la colonne d'eau, un facteur environnemental important pour la préservation de la matière organique. De plus, le paramètre $S^{Organic}$ renseigne sur le degré de sulfuration de la matière organique, un important mécanisme de préservation de la matière organique.

Par conséquent, une méthode pour la quantification du S^{Pyrite} et du $S^{Organic}$ avec le Rock-Eval 7S a été développée. Sachant qu'avec le Rock-Eval 7S on peut quantifier le S^{Pyrite} de pyrolyse ($_{Pyrolysis}S^{Pyrite}$), la stratégie a donc été d'étudier la transformation thermique de la pyrite pendant la phase

pyrolyse du Rock-Eval 7S et son interaction avec la matière organique et les minéraux communément présents dans les sédiments marins riches en organique. Le but étant d'estimer la quantité totale de S^{Pyrite} à partir du S^{Pyrite} de pyrolyse, et ensuite déduire la quantité totale de $S^{Organic}$. Les formules suivantes ont été définies pour la quantification de S^{Pyrite} et de $S^{Organic}$ dans les sédiments marins riches en matière organique :

$$S^{Pyrite} = \frac{(1+\beta+\gamma)}{\alpha} \cdot {}_{Pyrolysis}S^{Pyrite}$$

$$S^{Organic} = S_{total} - S^{Pyrite}$$

Dans ces formules, le facteur α représente le pourcentage de S^{Pyrite} libéré pendant la phase de pyrolyse. Les facteurs β et γ sont des facteurs de correction qui visent à prendre en compte la quantité de S^{Pyrite} de pyrolyse piégée dans la matière organique et dans la matrice minérale pendant la phase de pyrolyse.

Cette nouvelle méthode Rock-Eval 7S a été validée sur une série de sédiments provenant du Grey Shale Member (Toarcien, North-Yorkshire, Royaume-Uni) et de la Kimmeridge Clay Fm. (Tithonien-Kimmeridgien, Dorset, Royaume-Uni) ainsi que sur une série de mélanges sédimentaires synthétiques avec des teneurs fixées et connues en S^{Pyrite} et $S^{Organic}$ (mélanges de roches sédimentaires ne contenant que du $S^{Organic}$ + pyrite). Les résultats obtenus montrent que la nouvelle méthode Rock-Eval 7S permet une quantification précise du S^{Pyrite} et du $S^{Organic}$.

La nouvelle méthode Rock-Eval 7S pour la quantification du S^{Pyrite} et du $S^{Organic}$, développée et validée dans cette étude, a ensuite été utilisée pour aider à la description de la préservation de la matière organique dans des sédiments marins. Trois sections sédimentaires ont été étudiées : la section du Dorset (Tithonien-Kimmeridgien, Kimmeridge Clay Fm), la section du North-Yorkshire (Toarcien, Grey Shale Member) et la section du Somerset (Hettangien-Sinemurien, Blue Lias Fm.). En effet, l'analyse Rock-Eval 7S d'échantillons de ces formations sédimentaires nous a permis d'obtenir de pertinents paramètres carbone et soufre, principalement le COT, le S^{Total}, le S^{Pyrite} et le $S^{Organic}$, qui ont été utilisés comme indicateurs de conditions paléo-environnementales impactant la préservation de la matière organique tels que l'oxygénation de la colonne d'eau et le degré de sulfuration de la matière organique.

Cette méthode Rock-Eval 7S, la première méthode rapide, efficace et fiable permettant la quantification directe du S^{Pyrite} et du $S^{Organic}$ en une seule analyse, offre des avantages analytiques importants : i) le cout temps d'analyse (2 heures par échantillon) ; ii) l'absence d'étapes de préparation chimique laborieuses et dangereuses en raison de l'utilisation d'acides forts ; iii) les analyses

automatisées; et iv) la quantification simultanée du carbone organique/inorganique et du soufre organique/inorganique en une seule analyse.

En plus de son application dans l'étude de la préservation de la matière organique, cette nouvelle méthode Rock-Eval 7S pour la quantification du S^{Pyrite} et du $S^{Organic}$ a de nombreuses autres applications potentielles. En effet, cette méthode peut fournir des données utiles pour un large éventail d'applications, telles que : (i) l'exploration et la production pétrolières, (ii) la reconstruction paléoenvironnementale et paléoclimatique, (iii) l'exploration et la production du charbon et (vi) la pollution des sols.

List of publications

Aboussou, A., Lamoureux-Var, V., Pillot, D., Kowalewski, I., Garcia, B., Wagner, T., März C. (writing in progress). Pyritic and organic sulphur quantification in organic rich marine sediments using Rock-Eval 7S.

Aboussou, A., Lamoureux-Var, V., Wagner, T., Pillot, D., Kowalewski, I., März C., Garcia, B., Doligez, B. (2018). Pyritic sulphur and organic sulphur quantification in organic rich sediment using Rock-Eval. 1st EAGE/IFPEN Conference on Sulphur Risk Management in E&P, Rueil-Malmaison, 2018.

Aboussou, A., Lamoureux-Var, V., Wagner, T., Pillot, D., Kowalewski, I., März C., Garcia, B., Doligez, B. (2018). Application of an advanced method for pyritic and organic sulphur quantification to organic rich marine sediments. 80th European Association of Geoscientists and Engineers Conference and Exhibition: EAGE, Copenhagen, 2018.

Aboussou, A., Lamoureux-Var, V., Pillot, D., Kowalewski, I., Garcia, B., Wagner, T., März C. (2018). Procédé pour la quantification du soufre pyritique et du soufre organique d'un échantillon de roche (Perfectionnement). **Pending patent FR 18/56.042**.

Aboussou, A., Lamoureux-Var, V., Wagner, T., Pillot, D., Buckman, J., März C., Kowalewski, I., Doligez, B., Garcia, B. (2017). Advanced sulphur speciation and quantification in marine shales: emerging perspectives from Jurassic North Yorkshire black shale. 28th International Meeting on Organic Geochemistry: IMOG, Florence, 2017.

Aboussou, A., Lamoureux-Var, V., Pillot, D., Kowalewski, I., Doligez, B., Garcia, B., Wagner, T., Buckman, J., März C. (2017). Procédé pour la quantification du soufre pyritique et du soufre organique d'un échantillon de roche. **Pending patent FR 17/58.413**.

Aboussou, A., Lamoureux-Var, V., Pillot, D., Letort, G., Garcia, B., D., Kowalewski, I., Doligez, B. (2016). Développement d'une méthode de spéciation et de quantification des différents composés soufrés contenus dans les roches mères marines avec un Rock-Eval 6 couplé à un système d'analyse du soufre. 3rd French Researcher in Organic Geochemistry Conference and Exhibition: FROG, Poitiers, 2016.

Table of contents

Acknowledgements II
Abstract III
Résumé V
List of publications VIII
Table of contents IX
List of figures XIII
List of tables XV
List of abbreviations XVI

Chapter 1: INTRODUCTION 1

1.1- POTENTIAL APPLICATIONS OF A NEW METHOD FOR PYRITIC SULPHUR AND ORGANIC SULPHUR QUANTIFICATION USING ROCK-EVAL 7S 3
1.1.1- Petroleum exploration and production 3
1.1.2- Paleoenvironmental/Paleoclimate reconstruction 3
1.1.3- Coal exploration and production 4
1.1.4- Soil pollution 4
1.2- OM PRESERVATION IN MARINE SEDIMENTS: THE LINK TO GEOCHEMICAL PROPERTIES OF CARBON AND SULPHUR 5
1.2.1- Environmental factors controlling OM preservation in marine sediments 5
1.2.2- Overview of the different mechanisms of OM preservation in marine environments 7
1.2.3- Formation of sulphur species in marine sediments 10
1.2.4- Geochemical properties of carbon and sulphur as descriptors of OM preservation in marine environments 13
1.3- ROCK-EVAL 7S 15
1.3.1- Rock-Eval 7S principle 15
1.3.2- Rock-Eval 7S sulphur speciation: state of the art 19
1.4- PHD OBJECTIVES 20
1.4.1- First objective: Developing and validating new analytical methodology on Rock-Eval 7S for sulphur quantification and speciation 20
1.4.2- Second objective: Using Rock-Eval 7S carbon and sulphur parameters as descriptors of OM preservation 20

Chapter 2: ROCK-EVAL 7S CALIBRATION STUDIES 22

2.1- INTRODUCTION 22
2.2- ROCK-EVAL 7S S^{Total} CALIBRATION 23
2.2.1- Samples 23
2.2.2- Methodology 24
2.2.3- S^{Total} calibration results 26
2.3- ROCK-EVAL 7S CHARACTERISATION OF THE MAIN TYPES OF SULPHUR SPECIES FOUND IN MARINE SEDIMENTS 28
2.3.1- Samples and methodology 28
2.3.2- Rock-Eval 7S characterisation of the main sulphur species found in marine sediments 32
2.4- CONCLUSIONS 35

Chapter 3: PYRITIC AND ORGANIC SULPHUR QUANTIFICATION IN ORGANIC RICH MARINE SEDIMENTS USING ROCK-EVAL 7S 36

3.1- CHAPTER INTRODUCTION 36
3.2- DEVELOPMENT OF A NEW METHOD FOR PYRITIC SULPHUR AND ORGANIC SULPHUR QUANTIFICATION USING ROCK-EVAL 7S 39
3.2.1- Introduction 39
3.2.2- Samples and methods 39
3.2.3- Results 43
3.2.4- Discussions 54
3.2.5- Conclusions 61
3.3- VALIDATION OF THE NEW ROCK-EVAL 7S METHODOLOGY FOR PYRITIC SULPHUR AND ORGANIC SULPHUR QUANTIFICATION ON ORGANIC RICH SEDIMENTS 63
3.3.1- Introduction 63
3.3.2- Samples and methods 63
3.3.3- Results and discussions 68
3.3.4- Conclusions 74
3.4- CHAPTER CONCLUSIONS 75

Chapter 4: APPLICATION OF ROCK-EVAL 7S TO THE DESCRIPTION OF OM PRESERVATION OF JURASSIC BLACK SHALES FROM NORTH YORKSHIRE, DORSET AND SOMERSET 76

4.1-INTRODUCTION 76
4.2- METHODOLOGY 78
4.2.1- Dorset section: Kimmeridge Clay Formation 78

4.2.2- North Yorkshire section: Grey Shale Member 79
4.2.3- Somerset section: Blue Lias 79
4.3- ROCK EVAL 7S RESULTS 80
4.3.1- Dorset section: Kimmeridge Clay Formation (Appendix J and N) 82
4.3.2- North Yorkshire section: Grey Shale Member (Appendix J and N) 84
4.3.3- Somerset section: Blue Lias (Appendix J and N) 86
4.4- CONTRIBUTION OF NEW ROCK-EVAL 7S DATA IN THE DESCRIPTION OF OM PRESERVATION 89
4.4.1- Dorset section: Kimmeridge Clay Formation 89
4.2.2- North Yorkshire section: Grey Shale Member 90
4.2.3- Somerset section: Blue Lias 91
4.5- CONCLUSIONS 92

Chapter 5: SUMMARY AND OUTLOOK 93

5.1-SUMMARY 93
5.2-OUTLOOK 95
5.2.1- Development of Rock-Eval 7S for S^{Pyrite} and $S^{Organic}$ quantification 95
5.2.2- Using the Rock-Eval 7S carbon and sulphur properties as descriptors of OM preservation in DIONISOS sedimentary basin model 95
APPENDIX 98

Appendix A: Rock-Eval 7S sulphur calibration (SO_2 signals of Elemental sulphur and B2323 coal samples) 98
Appendix B: Rock-Eval 7S sulphur calibration: Determination of the KSO_2 coefficients 100
Appendix C: Rock-Eval 7S sulphur calibration: Assessment of the calibration coefficients 101
Appendix D: SO_2 pyrolysis sulphur signals (Altered pyrite *vs* Normal pyrite) 102
Appendix E: Rock-Eval 7S signals Type II and Type III Kerogens, Pyrite and mixtures “Pyrite + Kerogens” 103
Appendix F: Rock-Eval 7S results of mixture “Pure igneous pyrite + Kerogen”: Raw data 104
Appendix G: Rock-Eval 7S results of mixture “Pure igneous pyrite + Kerogen”: Processed data 106
Appendix H: Rock-Eval 7S results of mixture “Pure igneous pyrite + Mineral” 108
Appendix I: Rock-Eval 7S CO_2 signal of mixtures “Pyrite + carbonates” 110
Appendix J: S^{Pyrite} and $S^{Organic}$ quantification using Rock-Eval 7S 111
Appendix K: S^{Pyrite} and $S^{Organic}$ quantification using elemental analysis method 116
Appendix L: S^{Pyrite} and $S^{Organic}$ quantification in validation mixtures 118

Appendix M: XRD Characterisation 120
Appendix N: Basic Rock-Eval 7S parameters 122
Appendix O: Rock-Eval 7S standard deviation estimation for less than 10 analysis 124
REFERENCES 125

List of figures

Figure 1. 1 : Conceptual biochemical and geochemical changes undergone by living OM (top) as it is preserved and condensed as kerogen (bottom). Diagram is modified from Curiale and Curtis (2016) 9

Figure 1. 2 : A diagrammatic representation of the principal processes allowing pyrite (green pathway) and organo-sulphur (red pathway) formation 12

Figure 1. 3 : Rock-Eval 7S principle using the total sulphur temperature program 18

Figure 1. 4 : Example of sulphur detection with Rock-Eval 7S 19

Figure 2. 1: Cross plot of sulphur masses and the corresponding peak areas obtained during pyrolysis and oxidation phases of Rock-Eval 7S 27

Figure 2. 2: Comparison of the determination of S^{Total} contents: Rock-Eval 7S vs Infrared (Orbagnoux samples) and RE 7S vs LECO (North Yorkshire samples) 28

Figure 2. 3: Composite graph presenting a synthesis of Rock-Eval 7S signals of the different types of sulphur species found in marine sediments 34

Figure 3. 1: Flow chart presenting the different sections of chapter 3 and the strategy applied in each section. (Pyrite = Pure igneous pyrite)....38

Figure 3. 2: Rock-Eval 7S SO_2 signals of different masses of pure igneous pyrite 43

Figure 3. 3: Rock-Eval 7S response linearity between the areas of the SO_2 peak and the sample mass of pyrite 44

Figure 3. 4: *In-situ* XRD analyses of a pure igneous pyrite sample simulating the conditions created during Rock-Eval 7S analysis....45

Figure 3. 5: 5a) Rock-Eval 7S sulphur signals of mixtures (pure igneous pyrite + type II kerogen), of the pure igneous pyrite and of type II kerogen sample. 5b) Rock-Eval 7S sulphur signal of mixtures (pure igneous pyrite + type III kerogen), of the pure igneous pyrite and of type III kerogen sample. S. P.: sulphur peaks 48

Figure 3. 6: Evolution of the OM_{effect} in function of the Hydrogen Index (HI) and in function of the Oxygen Index (OI)....49

Figure 3. 7: Rock-Eval 7S sulphur signal of pyrite sample and sulphur signal of mixtures pure igneous pyrite + silicate minerals. S. P. (sulphur peaks)....51

Figure 3. 8: Rock-Eval 7S sulphur signal of pyrite sample and sulphur signal of mixtures pure igneous “pyrite + carbonate minerals”. S. P. (sulphur peaks)....52

Figure 3. 9: Min_{effect} on the amount of ${}_{Pyrolysis}S^{Pyrite}$ released during Rock-Eval 7S pyrolysis phase for each mineral....53

Figure 3. 10: The OM_{effect} obtained by the analysis of mixtures "pyrite + kerogen" vs $OM_{effect\ predicted}$ from HI and OI 58

Figure 3. 11: Min_{effect} *vs* MinC calibration curves corresponding to minimal, mean and maximal Min_{effect} calibration mixtures 60

Figure 3. 12: Comparison of Rock-Eval 7S and elemental analysis in the quantification of the S^{Total} content of the organic rich marine sediment samples 69

Figure 3. 13: Comparison of Rock-Eval 7S method and elemental analysis method in the quantification of the S^{Pyrite} content of the organic rich marine sediment samples 70

Figure 3. 14: Comparison of Rock-Eval 7S method and elemental analysis method in the quantification of the $S^{Organic}$ content of the organic rich marine sediment samples 70

Figure 3. 15: Comparison of Rock-Eval 7S method and elemental analysis method in the quantification of the $S^{Organic}$ content of the organic rich marine sediment samples without samples presenting misscorrélation between both method for S^{Total} and S^{Pyrite} sulphur quantification 71

Figure 3. 16: Rock-Eval 7S sulphur signals of the selected sedimentary rocks from Orbagnoux Fm. (O), Phosphoria Fm. (P) and Limagne Fm. (L). S.P.: Sulphur peak 72

Figure 3. 17: Comparison between S^{Total} content of the mixtures "sedimentary rocks + pyrite" obtained with Rock-Eval 7S and the expected S^{Total} content. 73

Figure 3. 18: Comparison between S^{Pyrite} content of the mixtures "sedimentary rocks + pyrite" obtained with the Rock-Eval 7S method and the expected S^{Pyrite} content. 73

Figure 3. 19: Comparison between $S^{Organic}$ content of the mixtures "sedimentary rocks + pyrite" obtained with the Rock-Eval 7S method and the expected $S^{Organic}$ content. 74

Figure 4. 1: HI vs IO diagram (Espitalie *et al.*, 1986)allowing characterisation of OM type in the different studied sections 81

Figure 4. 2: Rock-Eval 7S sulphur parameters *vs* TOC for the Dorset section. Dashed line: Normal marine C/S relationship (Berner, 1982) 83

Figure 4. 3: Rock-Eval 7S sulphur parameters vs TOC for the North-Yorkshire section. Dashed line: Normal marine C/S relationship (Berner, 1982) 85

Figure 4. 3: Rock-Eval 7S sulphur parameters vs TOC for the Somerset section. Dashed line: Normal marine C/S relationship (Berner, 1982) 88

Figure 5. 1 : Quantified factor in Dionisos^{TM} simulations 96

List of tables

Table 2. 1 : Masses of sulphur in reference samples 25

Table 2. 2: XRD and elemental analysis samples characterisation 31

Table 3. 1: Kerogen samples used in mixtures of “pure igneous pyrite+ kerogen” 41

Table 3. 2: Mineral samples used in mixtures of “pure igneous pyrite+ minerals” 41

Table 3. 3: Rock-Eval 7S results of sulphur content of the pure igneous pyrite sample 45

Table 3. 4: Rock-Eval 7S results of sulphur content of the altered pyrite samples *vs* the unaltered pyrite sample 46

Table 3. 5: Basic Rock-Eval parameters of the selected samples.....65

Table 3. 6: Sedimentary rock samples used in mixtures “sedimentary rocks + pyrite”, their weights and total sulphur contents. Pyrite weights used in the mixtures “sedimentary rocks + pyrite” and its total sulphur content.....66

List of abbreviations

- OM: Organic Matter
- BSR: Bacterial Sulphate Reduction
- S^{Total}: Total sulphur
- S^{Pyrite}: Pyritic sulphur
- $S^{Organic}$: Organic sulphur
- ${}_{Pyrolysis}S^{Pyrite}$: Pyrolysis pyritic sulphur
- ${}_{Oxidation}S^{Pyrite}$: Oxidation pyritic sulphur
- ${}_{Pyrolysis}S^{Organic}$: Pyrolysis organic sulphur
- ${}_{Oxidation}S^{Organic}$: Oxidation organic sulphur
- OM_{effect}: Organic matter effect
- Min_{effect}: Mineral effect

Chapter 1: INTRODUCTION

A petroleum system corresponds to a sedimentary basin, or part of a sedimentary basin that typically includes different core elements: source rock; carrier system; reservoir rock; seal or cap rock; and structural or stratigraphic trap. In addition to these elements, a petroleum system is defined by the occurrence and timing of processes leading to accumulation and preservation of oil and gas in reservoir units. A better knowledge of petroleum systems is of great importance for the exploration and production of new resources, as has been shown in the discovery of many new hydrocarbon occurrences and in improved production from existing ones (Huc, 2013). Studying the origin and development of any active petroleum system, specifically the processes leading to source rock formation and evolution, is essential and fundamental for oil and gas exploration strategies.

This PhD project entitled ***"New Rock-Eval method for Pyritic and Organic Sulphur quantification: Application to study Organic Matter preservation in Jurassic sediments"***, aims to contribute to a better understanding of source rock formation, by the use of carbon and sulphur paleo-environmental descriptors, based on the novel technology of Rock-Eval 7S, to improve the characterisation of organic matter (OM) source and preservation in Jurassic sediments. The longer-term perspective of this project is to lay the scientific foundation to apply Rock-Eval 7S carbon and sulphur parameters as routine descriptors in sedimentary basin models.

To provide the different carbon and sulphur parameters that can be used for this purpose, developing and validating a new analytical method for sulphur speciation and quantification using Rock-Eval 7S is primary required. The development of this Rock-Eval 7S method faces different challenges: (i) mineral sulphur and organic sulphur peak convolution and (ii) chemical reactions involving and modifying the original sulphur compounds. These different challenges will be addressed in this PhD project in order to establish an analytical method for mineral and organic sulphur quantification using Rock-Eval 7S.

Therefore, this PhD project has two the main targets (i) developing and validating a new analytical method on the using Rock-Eval 7S for quantifying mineral and organic sulphur in organic rich sediments and, (ii) identifying Rock-Eval 7S derived-descriptors to support the description and parameterisation of OM preservation in marine sediments.

Sulphur characterization has become essential given that the new Petroleum Exploration and Production targets which are often rich in sulphur and because of the sulphur environmental standard of

refining products which have become increasing drastic. Moreover, there is currently no existing laboratory instrument on the market that allows the fast quantification of both organic and mineral sulphur in a single analysis. Therefore, this PhD project provides a good framework to improve greatly the interest of the Rock-Eval 7S technology. With this perspective, the Rock-Eval 7S technology could provide fast, cost-effective and detailed characterization of organic carbon and sulphur in natural samples (shale, soils, etc.) and anthropogenic products (e.g. waste), urgently needed in the strategic investigation of fossil fuel resources (e.g. unconventionals), soil carbon stocks, and environmental pollution sites.

1.1- POTENTIAL APPLICATIONS OF A NEW METHOD FOR PYRITIC SULPHUR AND ORGANIC SULPHUR QUANTIFICATION USING ROCK-EVAL 7S

1.1.1- Petroleum exploration and production

1.1.1.1- Source rock characterisation

The new method for pyritic sulphur (S^{Pyrite}) and organic sulphur ($S^{Organic}$) quantification using Rock-Eval 7S, by specifically quantifying the amount of organically bound sulphur ($S^{Organic}$) presents in source rocks, gives important information to improve Rock-Eval source rock characterisation (Espitalie *et al.*, 1986; Lafargue *et al.*, 1998; Behar *et al.*, 2001). For instance, the $S^{Organic}$ /TOC ratio can be used, in addition to the classical diagrams for characterisation of source rock kerogen type (HI vs OI or HI vs Tmax), to define type IS (Sinninghe Damsté *et al.*, 1993), type IIS (Orr, 1986) and type IIIS (Sinninghe Damsté *et al.*, 1992) kerogens, which are respectively lacustrine, marine and terrestrial kerogen types presenting high $S^{Organic}$ /TOC ratios.

1.1.1.2- Reservoir characterisation

The new method for S^{Pyrite} and $S^{Organic}$ quantification provides additional information to improve the current Rock-Eval characterisation of reservoir rocks (Espitalie *et al.*, 1986; Lafargue *et al.*, 1998). Indeed, by differentiating the amount of S^{Pyrite} to the amount of $S^{Organic}$, this new method contributes to characterisation of the geochemical and petrophysical attributes of conventional and unconventional reservoir rocks. This method can be helpful, for instance, in the evaluation of the risk of H_2S generation, during steam or hot water injection in reservoir rocks, knowing that reactions which induce H_2S generation, such as aquathermolysis and pyrite oxidation, depend on the availability of S^{Pyrite} and $S^{Organic}$ in reservoirs (Hutcheon, 1998; Lamoureux-Var and Lorant, 2005).

1.1.2- Paleoenvironmental/Paleoclimate reconstruction

Sulphur concentration in sediments and its partitioning between S^{Pyrite} and $S^{Organic}$ is dependent on a host of environmental variables, including dissolve sulphate concentrations, reactive iron availability, redox conditions, and OM quantity and quality (Raiswell and Berner, 1985; Raiswell *et al.*, 1988; Canfield, 1989; Mossmann *et al.*, 1991; Lyons and Berner, 1992; Zaback and Pratt, 1992;

Henneke *et al.*, 1997; Lyons, 1997; Passier *et al.*, 1997; Filley *et al.*, 2002; Werne *et al.*, 2004). And, these environmental variables, allowing S^{Pyrite} and $S^{Organic}$ formation in sediments, potentially provide links with terrestrial environmental and climatic conditions (Russell and Werne, 2009; Zeng *et al.*, 2013). Therefore, this new S^{Pyrite} and $S^{Organic}$ quantification method using Rock-Eval 7S produces very useful data to support the paleoenvironment reconstruction as well as paleoclimate reconstruction. One example application of the using of the new method for S^{Pyrite} and $S^{Organic}$ quantification to help paleoenvironmental reconstruction will be presented in the next chapter.

1.1.3- Coal exploration and production

Despite advances in renewable and gas resources, coal is, and will remain for the foreseeable future, a major source of energy worldwide. Indeed, in U.S., the Energy Information Administration predicts that coal will provide the majority of fuel for the generation of electricity continue up to at least 2035 (Energy Information Administration 2012, 2012).

Like all sedimentary OM, coal contains sulphur in a wide array of forms, solubility, and concentrations, S^{Pyrite} and $S^{Organic}$ being the main constituents (Bauer *et al.*, 2014). The sulphur content and its distribution represent an important parameter in the evaluation of coal resources. Indeed, depending on the way sulphur occurs in energy resources, a strong influence on the operational, environmental, and economic performance of handling and utilizing processes of coal is expected (Bauer *et al.*, 2014). For instance, the knowledge of the sulphur species in coal is required to determine the suitability of a particular coal treatment or cleaning strategy (Machado *et al.*, 2011). Furthermore, process issues such as fouling behaviour in the boiler, deactivation of catalysts, or promotion of high temperature corrosion of equipment may occur and are strongly related to the sulphur speciation (Speight, 2005). Therefore, extension of this new method for S^{Pyrite} and $S^{Organic}$ quantification using Rock-Eval 7S for coal exploration and production will be of great importance and this will require further analytical developments.

1.1.4- Soil pollution

Soil is a prime recipient for sulphur species emitted from power plants, industrial processes, vehicular transport, domestic sources (mainly from the burning of fossil fuels), mining etc. Many sulphur species can exist in soils, including S^{Pyrite} and $S^{Organic}$ (Guo *et al.*, 2015) and they are at the

origin of soil acidification and pollution. For instance, pyrite in soils, and especially those at surface, exposed to atmospheric oxygen and moisture and aided by bacteria, can undergo a series of oxidation and hydrolysis reactions, which produce sulphuric acid solution and mobile metal sulphates penetrating and acidifying the soil profile (e.g. Williamson and Johnson, 1981; Kelly and Wood, 2000), with the consequent risk for groundwater sources (Burgos *et al.*, 2013).The new method for S^{Pyrite} and $S^{Organic}$ quantification using Rock-Eval 7S can be a complementary analysis to other existing analysis for characterisation of soil pollution such as ICP-OES; infrared or gas chromatographic analyses. Indeed, this new method using Rock-Eval 7S will allow rapid screening of a large number of samples, thus helping to identify the samples that are worthy of additional study. However, further analytical development improvements may be needed before the application of this new method for soil characterisation.

1.2- OM PRESERVATION IN MARINE SEDIMENTS: THE LINK TO GEOCHEMICAL PROPERTIES OF CARBON AND SULPHUR

The principal source of OM in marine sediments is phytoplankton. Phytoplankton is composed of unicellular photosynthetic algae, including diatoms and dinoflagellates. Their chemical components are predominantly proteins (long chains of amino-acids), carbohydrates (sugars), and lipids (Baudin *et al.*, 2007). However, it is also possible to find OM from terrestrial sources in marine sediments, brought to the oceans by rivers and wind in either dissolved or particulate form. This terrestrial OM is mainly composed of the remains of vascular plants, pollens and spores, or degradation products from soil OM, which remains a large unknown (Baudin *et al.*, 2007).

1.2.1- Environmental factors controlling OM preservation in marine sediments

A large part of the marine OM produced in the surface ocean is degraded by the metabolic action of bacteria and animals which transform reduced organic carbon into oxidised mineral carbon. The OM that escapes this degradation is buried and preserved in sediments. The factors governing the preservation of OM in marine sediments have been the subject of numerous decades of studies which demonstrate empirical relationships between organic carbon burial and different environmental factors (Demaison and Moore, 1980; Emerson, 1984).

Bottom water oxygen concentration is known to be one principal factor of OM preservation in sediments. Indeed, it is commonly accepted that enhanced preservation of OM in marine sediments is

related to deposition in anoxic/euxinic waters (Demaison and Moore, 1980; Emerson, 1984) compared to oxic waters. The oxic waters corresponding to well oxygenated waters, the anoxic waters being oxygen-depleted to non-oxygenated waters. At the far end of the redox scale are euxinic waters, representing anoxic conditions with free hydrogen sulphide (H_2S) in the water column. The role of bottom water oxygenation on OM preservation can be explained by the fact that the aerobic degradation processes are known to be more efficient than the anaerobic degradation processes (Claypool and Kaplan, 1974; Baudin *et al.*, 2007). However, some studies have not shown any clear-cut and systematic relationship between bottom water concentrations and OM preservation in marine sediments (Betts and Holland, 1991; Calvert and Pedersen, 1992; Canfield, 1994), suggesting that oxygen bottom water concentrations are not necessarily the correct metric to examine OM preservation.

Other evidence supports the conclusion that the primary production of OM in the photic zone is the key factor controlling OM accumulation in marine sediments. For instance, Calvert and Pedersen (1992) suggest that high primary production provides a first-order control on the accumulation of organic-rich facies in sediments.

The rain rate of OM has also been demonstrated to be a factor of OM preservation. Indeed, the study of seafloor recycling of OM in Santa Monica Basin in California shows that the carbon burial rates are primarily controlled by the flux of organic carbon through the water column (Jahnke, 1990).

Finally, according to Müller and Suess (1979), Betts and Holland (1991) and Canfield (1994), another main controlling factor of OM preservation is bulk sedimentation rate. For instance, Canfield (1994) showed that at high rates of deposition, such as near continental margins, little difference is found in preservation despite varying bottom-water oxygen.

A study of Hartnett *et al.* (1998) demonstrated that all these environmental factors (bottom-water oxygen content, primary production rate, rain rate of organic carbon, and overall sedimentation rate) influence the oxygen exposure time of OM at the seafloor adding another direct control on sedimentary organic carbon preservation. Indeed, an increase in either primary production rate or organic carbon rain rate will increase sediment oxygen demand. The consequent steepening of the oxygen gradient will lead to a shallower oxygen penetration depth and decreased oxygen exposure time. Likewise, variations in the mineral sedimentation rate will affect the rate at which material moves through the oxic horizon at/near the sediment surface, further altering oxygen exposure time. Finally, if all other factors remain constant, changes in the bottom-water oxygen concentration will affect oxygen exposure time. The correlation between these other parameters and organic carbon preservation (Jahnke, 1990; Betts and Holland, 1991; Calvert and Pedersen, 1992) probably reflects their individual influence on oxygen exposure time rather than a direct influence on organic carbon burial.

1.2.2- Overview of the different mechanisms of OM preservation in marine environments

1.2.2.1- Degradation-recondensation

The process of degradation-recondensation of OM (Figure 1. 1) is considered to be quantitatively the principal mechanism of OM preservation (Tissot and Welte, 1978; Larter *et al.*, 1979). It includes the degradation of biological polymers (biopolymers) such as proteins and polysaccharides (polymeric carbohydrates), leading to the production of a variety of labile biological monomers, for example amino acids, simple sugars, or fatty acids (Burdige and Gardner, 1998). These labile organic components are then recombined into more refractory compounds by complex condensation reactions. The common condensation reaction is named 'geopolymerisation' or 'humification', a general term for the process by which humic substances form. These humic substances are considered to be amorphous and hydrophilic, and refractory with respect to both chemical and biological degradation (Burdige, 2007). One well-studied example of geopolymerisation is the Maillard reaction. This reaction allows the formation of refractory compounds, known as melanoidins, by a sugar-amino acid condensation reaction (Rashid, 1985), and it has been observed that synthetic melanoidins produced in the laboratory show some similarity to marine humic substances (Frimmel *et al.*, 1988).

1.2.2.2- Selective preservation

This term describes the selective preservation (Figure 1. 1) of part of vascular plants and algae through their production of lignins and highly aliphatic macromolecular material which is insoluble, non-hydrolyzable, and resistant to biological degradation (Leeuw and Largeau, 1993; Gelin *et al.*, 1999). These refractory molecules include (Burdige, 2007)

- Algaenans: algal cell wall components consisting of long-chain aliphatic compounds with hydroxyl or ester functional groups.
- Cutans: nonhydrolyzable components of the cuticles of higher plants.
- Lignins: class of phenolic compounds found exclusively in vascular plants.

They likely represent a very small fraction of the initial biomass produced by marine and terrestrial organisms. However, as they are selectively preserved, they are concentrated in the sedimentary OM pool during diagenesis (Tegelaar *et al.*, 1989).

1.2.2.3- Physical protection of OM

OM can be physically protected by both inorganic and organic matrices. It has been observed in many studies that OM is preferentially associated with fine-grained sediment particles (clay minerals) (Premuzic *et al.*, 1982; Keil *et al.*, 1994; Mayer, 1994). However, the role of these fine-grained sediment particles in OM preservation is not fully understood. Based on observations from different studies (Hedges and Keil, 1995; Ransom *et al.*, 1997; Mayer, 1999; Bock and Mayer, 2000; Arnarson and Keil, 2001; Kennedy and Wagner, 2011; Kennedy *et al.*, 2014), OM-mineral interactions appear to involve physical protection of the OM in small mesopores, either on mineral surfaces or in between mineral grains. For instance, a covariation of mineral surface area (MSA) and TOC across multiple scales of variability was observed by Kennedy and Wagner (2011) and Kennedy *et al.* (2014) suggesting an influence on organic carbon burial by detrital clay minerals controlled MSA. Concerning OM physical protection by organic matrix, it would occur through encapsulation of reactive OM within insoluble, hydrolysis-resistant organic matrices such as algaenans (Knicker, 2004).

In addition to that, Lalonde *et al.* (2012) determined, using an iron reduction method previously applied to soils, the amount of organic carbon associated with reactive iron phases in sediments of various mineralogies collected from a wide range of depositional environments. Their results suggest that associations between organic carbon and iron can promote the preservation of organic carbon in sediments.

1.2.2.4- Natural sulfurization

Natural sulfurization (Figure 1. 1), by creating sulphur-bounds between the organic molecules, leads to the formation of a sulphur rich organic residue that has a lower susceptibility to be degraded (Sinninghe Damste and Leeuw, 1990). It is the chemical process by which organo-sulphur compounds are formed through the incorporation of inorganic sulphur into functionalized lipids and carbohydrates (Aycard *et al.*, 2003). This mechanism is enhanced in marine anoxic-euxinic environments, where the lack of oxygen leads bacteria to use dissolved sulphate (SO_4^{2-}) as electron acceptor to oxidize low molecular weight organic compounds (Canfield, 1994). This process, called bacterial sulphate reduction (BSR), permits the formation of hydrogen sulphide, as illustrated in the following equation involving formaldehyde (CH_2O):

$2CH_2O + SO_4^{2-} \rightarrow H_2S + 2HCO^{3-}$ (Westrich, 1983)

Hydrogen sulphide (H_2S) is the principal sulphide product of BSR, but it is possible to form other sulphides and polysulphides via the partial oxidation of this hydrogen sulphide (Vairavamurthy *et al.*, 1995). In the presence of reactive iron minerals, including oxyhydr(oxides) iron, free sulphide

reacts first with iron to form iron sulphides, such as pyrite. The remaining sulphide is then incorporated into OM to form organo-sulphur compounds. In this classical view, significant sulfurization of OM can only occur if iron minerals have not reacted with all sulphides present (Tribovillard *et al.*, 2015). A direct way of incorporation of dissolved sulphates into OM (assimilatory sulphate reduction) has also been identified. But this process is considered secondary compared to the incorporation of sulphides and polysulphides (Vairavamurthy *et al.*, 1995).

It is interesting to note that, in certain depositional environments, sulfurization can outcompete pyrite formation. Indeed, in the uppermost surface sediments of organic-rich, sulphide-dominated marine sedimentary systems, sulfurization of labile organic compounds, such as humic acids (Francois, 1987; Ferdelman, 1988; Ferdelman *et al.*, 1991), can precede the formation of pyrite (Mossmann *et al.*, 1991; Vairavamurthy *et al.*, 1992; Vairavamurthy *et al.*, 1995; Filley *et al.*, 2002; Werne *et al.*, 2008; Riedinger *et al.*, 2017).

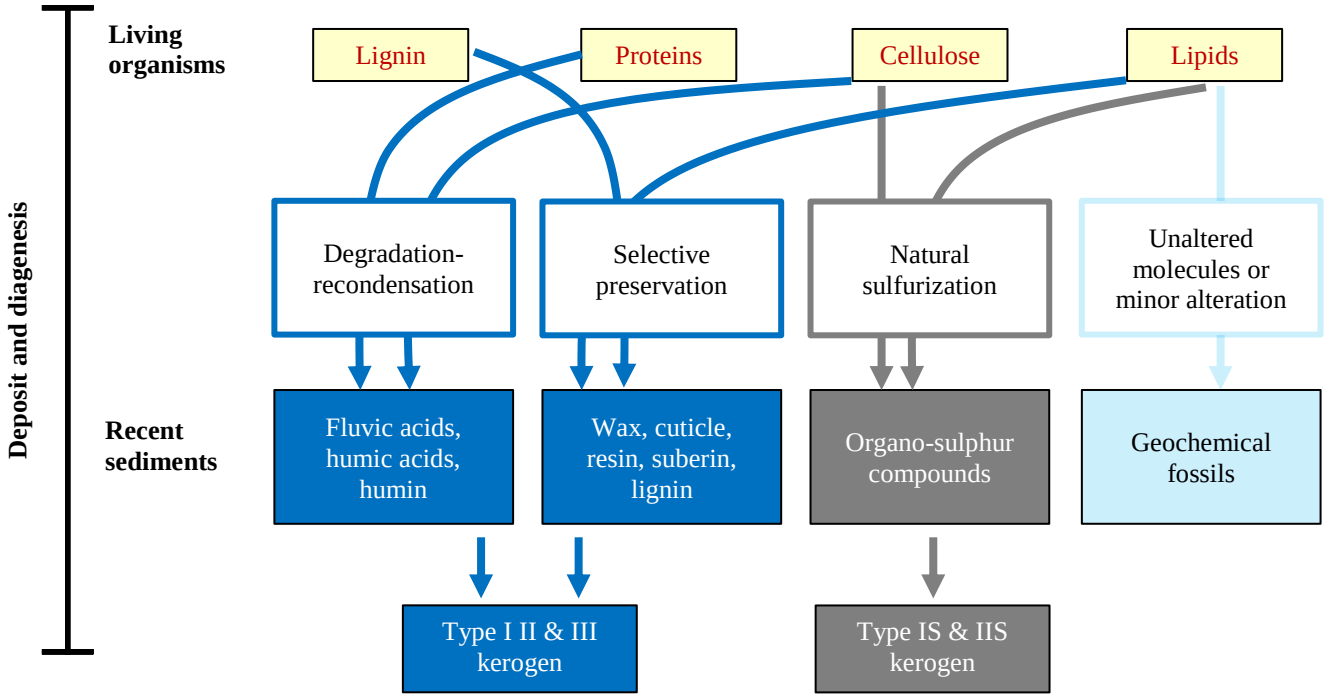

Figure 1. 1 : Conceptual biochemical and geochemical changes undergone by living OM (top) as it is preserved and condensed as kerogen (bottom). Diagram is modified from Curiale and Curtis (2016)

1.2.3- Formation of sulphur species in marine sediments

Marine sediments commonly contain solid-phase sulphur species. This is due to the fact that oceans represent one of the largest reserves of sulphur in the form of dissolved sulphate (SO_4^{2-}) and the principal output of this sulphur, following a range of biogeochemical reactions or evaporation, is sedimentation (Vairavamurthy *et al.*, 1995). Excluding sulphate minerals like gypsum that directly precipitate from evaporating seawater, two principal types of sulphur species are dominant in marine sediments, pyrite and organo-sulphur compounds, both containing sulphur in its reduced form. A diagrammatic representation of the principal processes allowing their formation is presented in Figure 1. 2.

1.2.3.1- Pyrite

Sedimentary pyrite (FeS_2) forms by reaction of reduced sulphur species (HS^-, H_2S) with reactive iron (Berner, 1970; Vairavamurthy *et al.*, 1995; Baudin *et al.*, 2007). The reduced sulphur species are produced by bacterial sulphate reduction (BSR), a process which can only occur under anoxic conditions in marine waters or sediments. Due to the lack of oxygen in the environments, sulphate-reducing bacteria use dissolved sulphate as electron acceptor to oxidize low molecular weight organic compounds, releasing reduced sulphur species (HS^-, H_2S) (Canfield, 1994). Reactive iron or reduced iron is formed via the reduction of iron oxide principally provided from terrigenous supply to the marine environment (Berner, 1984). Two principal types of pyrite particles can be found in marine sediments, framboids and euheudral crystals (Love and Amstutz, 1966). Framboid pyrite formation is generally thought to occur through the formation of metastable iron sulphides, such as greigite (Fe_3S_4) and mackinawite (FeS) (Sweeney and Kaplan, 1973; Morse and Cornwell, 1987; Baudin *et al.*, 2007; Hunger and Benning, 2007), whereas euhedral pyrite would be formed via direct precipitation (Giblin and Howarth, 1984). Pyrite formation, both framboids and euheudral crystals, occurs generally within the sediment during early diagenesis (diagenetic pyrite). Moreover, in euxinic marine basins, pyrite can also form in the water column (syngenetic pyrite) as well as below the sediment-water interface (Raiswell and Berner, 1985; Wilkin and Barnes, 1997). Syngenetic pyrite particles are characteristically smaller and less variable in size relative to diagenetic pyrite particles, reflecting shorter average growth periods due to hydrodynamic instability in the water column (Wilkin and Barnes, 1997).

Other trace metals, such as copper (Cu), lead (Pb), zinc (Zn), can co-precipitate together with iron sulphide minerals or form their own stable metal sulphides during early diagenesis (Jacobs *et al.*, 1985; Huerta-Diaz and Morse, 1990). It is therefore possible to find in marine sediments some traces of other sulphide minerals such as chalco-pyrite ($CuFeS_2$), galena (PbS), or sphalerite ((Zn,Fe)S).

1.2.3.2-Organo-sulphur compounds

The formation of organo-sulphur compounds is the second output of sulphur from the marine column water (Berner and Raiswell, 1983). This process, called natural sulfurization, occurs via two basic pathways, assimilatory and dissimilatory (Vairavamurthy *et al.*, 1995; Werne *et al.*, 2008).

- Assimilatory pathway:

This pathway describes the direct incorporation of dissolved sulphates into the organic matter followed by its reduction to sulphides. This assimilatory sulphate reduction is done by autotrophic organisms, for example, algae in the photic zone of the water column and chemosynthetic bacteria in hydrothermal systems. It is believed that organo-sulphur compounds formed in this way are quantitatively negligible, due principally to the fact that most of the assimilatory sulphur is contained in proteinaceaous substances, which hardly survive degradation to the later stages of diagenesis.

- Dissimilatory pathway:

This more prominent process for organo-sulphur compound formation occurs, like pyrite formation, during early diagenesis and under anoxic-euxinic conditions. This mechanism involves the reduction of dissolved sulphate via BSR. It is commonly assumed that the reduced sulphur species produced (HS^-, H_2S) are firstly used for pyrite formation in the presence of reactive iron minerals, and the remaining reduced sulphur species are incorporated between the organic molecules (intermolecular sulphur incorporation) and into the organic molecules (intramolecular sulphur incorporation) to form organo-sulphur compounds. However, recent works (Mossmann *et al.*, 1991; Vairavamurthy *et al.*, 1992; Vairavamurthy *et al.*, 1995; Filley *et al.*, 2002; Werne *et al.*, 2008; Riedinger *et al.*, 2017) have shown that the generally accepted paradigm of reactive iron minerals outcompeting organic molecules in the presence of dissolved sulphide does not necessarily hold true. As shown by Poulton *et al.* (2004), iron minerals have different reaction half-lives with dissolved sulphide even under ideal, experimental conditions, while some organic molecules are more susceptible to fast sulfurization than previously thought (Raven *et al.*, 2016a).

Different molecular structures of organo-sulphur compounds are found in marine sediment kerogens (Sinninghe Damsté *et al.*, 1988; Uteyev, 2011):

- Sulphides and poly-sulphides: Their formation is related to intermolecular sulfurization which corresponds to the formation of (poly-) sulphide between organic molecules.
- Thiols: Thiols are characterized by the presence of an R-SH functional group in their molecular structure which occurs via intramolecular sulphur incorporation.

❖ Thiophenes: The formation of the thiophene molecular group is due to intramolecular incorporation of sulphur into a cyclic or aromatic organic molecular structure.

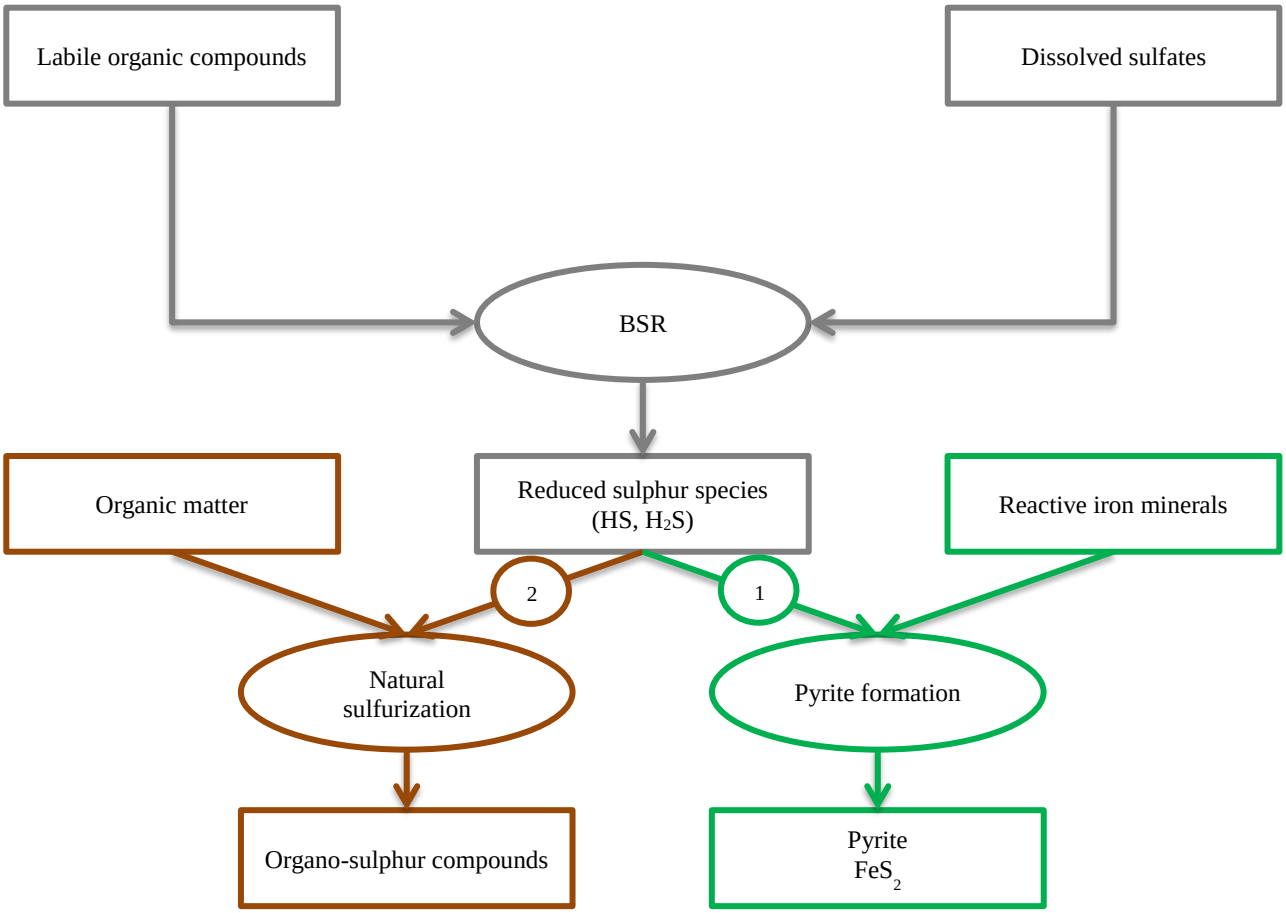

Figure 1. 2 : A diagrammatic representation of the principal processes allowing pyrite (green pathway) and organo-sulphur (red pathway) formation

1.2.3.3-Other sulphur species

- Sulphates:

Sulphate minerals only precipitate in closed basins with a negative water balance, where water input is reduced and the evaporation rate is significant (Vairavamurthy *et al.*, 1995). The common sulphate minerals in marine shale are gypsum ($CaSO_4$, $2H_2O$) and anhydrite ($CaSO_4$) (Jensen *et al.*, 1998), but also barite ($BaSO_4$). Barite is an ubiquitous sulphate mineral in marine sediments which is formed throughout the oceanic water column in association with decaying OM and biogenic debris (Dehairs *et al.*, 1980; Bishop, 1988; Dymond *et al.*, 1992; Arndt *et al.*, 2009). It can also undergo diagenetic redistribution in reducing sediment columns (Von-Breymann *et al.*, 1992; Stamatakis and Hein, 1993; Griffith and Paytan, 2012; Henkel *et al.*, 2012). Syngenetic or diagenetic barium sulphate

can be relatively well-preserved and abundant in marine shales, and can co-occur with pyrite and organic S compounds (Baudin *et al.*, 2007), but it is often concentrated in diagenetic fronts that can be easily recognised (Torres *et al.*, 1996; Riedinger *et al.*, 2006).

- Elemental sulphur:

Elemental sulphur deposits are commonly, but not invariably associated with sulphate minerals. Microbial sulphate reduction is, indeed, considered to be the key process for the precipitation of elemantal sulphur (Davis and Kirkland, 1970; Anadón *et al.*, 1992; Peckmann *et al.*, 1999). Elemental sulphur is not stable in most marine sediments given that it is highly transformed into sulphate or sulphide by organisms such as bacteria (Canfield and Raiswell, 1999; Philippot *et al.*, 2007).

1.2.4- Geochemical properties of carbon and sulphur as descriptors of OM preservation in marine environments

Carbon and sulphur occurrences in marine sedimentary depositional environments can be used as indicators of paleoenvironmental conditions responsible of OM preservation in sediments. Indeed, OM preservation in marine sediments is controlled by numerous environmental factors, such as bottom-water oxygen content, primary production, rain rate of organic carbon and overall sedimentation. Carbon and sulphur relationships have proved useful in the characterisation of marine sedimentary depositional environments. For instance, a relationship between total or pyritic sulphur (S) and organic carbon (C) called “normal marine” sediments (those accumulating under oxygenated water masses) was established in numerous studies (Berner, 1970; Sweeney, 1972; Goldhaber and Kaplan, 1974; Berner, 1982). Their results show that sediments from normal oxygenated waters are characterized by a C/S ratio of 2.8. Samples presenting lower ratios (C/S< 2.8) reflect euxinic environments (Leventhal, 1983; Raiswell and Berner, 1985; Leventhal, 1987). Samples presenting much higher ratios (C/S>5) were found in non-marine freshwater sediments (Berner and Raiswell, 1984).

Many researchers have used C vs. S plots to help characterize ancient depositional environments (Anderson *et al.*, 1987; Leventhal, 1987; Suits *et al.*, 1993; Riboulleau *et al.*, 2003; Rimmer *et al.*, 2004). However, some problems have been noted in using this relationship in iron-poor rocks, such as carbonates and sandstones, where the complete sulfidization of iron may limit the total solid-phase mineral sulphide content of the rock (Berner, 1984; Pratt, 1984). Also, in rapidly accumulating organic-rich sediments, where the amount of dissolved sulphate can become exhausted and limit the formation of pyrite, a linear C vs. S relationship is not always observed (Murray *et al.*,

1978; Devol and Ahmed, 1981). Other problems in the interpretation of C vs. S can arise if the amount of metabolizable organic carbon is limited (Raiswell and Berner, 1985), OM has been lost by heating (Raiswell and Berner, 1986), or unusual water chemistry is present (Tuttle and Goldhaber, 1993).

Organic sulphur occurrences in sediments is indicator of OM sulfurization, an important OM preservation mechanism. Indeed, in marine anoxic-euxinic environments, natural sulfurization can play a significant role in organic carbon preservation (Sinninghe Damsté *et al.*, 1988; Sinninghe Damste and Leeuw, 1990). For instance, Boussafir *et al.* (1995) found, using transmission electron microscopy, that sulfurization of OM does play an important role in the preservation of OM in Kimmeridge Clay Formation sediments (Dorset, UK). The impact of natural sulfurization on OM preservation has been observed by Lückge *et al.* (2002) who show that sulfurization of OM prevents its further decomposition in sediments from the continental margin of Pakistan. The role of natural sulfurization on OM preservation was also observed by Tribovillard *et al.* (2015) in their comparative study of two Jurassic sediment successions (Boulonnais, France). In this study, the enhanced OM preservation of one formation compared to a second has been attributed to differences in natural sulfurization controlled by differences in reactive iron availability. However, other studies, conducted on anoxic sediments from the Cariaco Basin (Venezuela) (Aycard *et al.*, 2003) and on the anoxic formation from Kössen (Hungary) (Vetö *et al.*, 2000), where natural sulfurization is enhanced, show no positive correlation between organo-sulphur compound concentrations and the preservation of OM. In these studies, the OM preservation was not essentially attributed to natural sulfurization but was attributed to the mechanism of degradation-recondensation (Aycard *et al.*, 2003) and to high primary productivity (Vetö *et al.*, 2000).

Carbon and sulphur occurrences in sediments can be indicators of bottom water oxygenation, an important environmental controlling factor of OM preservation, and OM sulfurization, an important OM preservation mechanism. This requires relevant carbon and sulphur parameters, such as: Total Organic Carbon (TOC); Hydrogen Index (HI); Oxygen Index; OM maturity (Tmax); total sulphur (S^{Total}); pyritic sulphur (S^{Pyrite}); and organic sulphur ($S^{Organic}$). These different carbon and sulphur parameters will be determined using Rock-Eval 7S, a new model of Rock-Eval technologies. Indeed, this new facility permits the analysis of sulphur species in addition to organic and inorganic carbon determination. With Rock-Eval 7S, the combined variations of carbon and sulphur parameters in rocks can be quantified rapidly (on average 2 hours) and simultaneously in a large number of samples. The Rock-Eval 7S principles are described in the following section.

1.3- ROCK-EVAL 7S

1.3.1- Rock-Eval 7S principle

Being developed by IFP Energies nouvelles and Vinci-Technologies, the Rock-Eval 7S is the latest model of Rock-Eval technology. It has the same functionalities as the current version (Rock-Eval 6), complemented by a new system adapted for sulphur detection (Figure 1. 3). The Rock-Eval 7S method can be used on a wide range of rock and oil types, such as source rocks, reservoir rocks, recent sediments, crude oils and petroleum distillates. This analytical method can be summarized in two main stages, a pyrolysis followed by an oxidation (Figure 1. 3).

1.3.1.1- Pyrolysis stage

During the pyrolysis stage, the sample is heated under a flux of nitrogen, according to a pre-determined temperature program. The temperature can be raised from 100°C to 800°C at different heating rates, from 1°C/min to 50°C/min. The pyrolysis effluents are separated in three parts. One part is carried to a Flame Ionization Detector (FID) for the quantification of hydrocarbons. Another part is carried to an Infrared detector (IR) for the quantification of CO_2 and CO. The last part passes through a combustion chamber where the reduced sulphur effluents are oxidized into SO_2. This SO_2 effluent is then measured by an Ultra-Violet detector (UV).

1.3.1.2- Oxidation stage

After the pyrolysis stage, the residue of the sample is transferred into an oxidation oven, where it is heated under a flux of air, following a predefined temperature program. The temperature can be raised from 100°C to 1200°C with different heating rates, from 1°C/min to 50°C/min. It is important to note that above 750°C the flux of air is replaced by a flux of nitrogen to initiate sulphate thermal degradation. The released CO and CO_2 are continuously measured using the IR detector. The released sulphur effluents, being already in oxidized form (SO_2), are directly recorded by the UV detector.

1.3.1.3- Rock-Eval parameters

By combining the measurement gathered during pyrolysis and oxidation, the Rock-Eval 7S provides the same peaks for carbon as the Rock-Eval 6, together with additional sulphur peaks:

- S1 and S2 (mg/g rock): The free and the potential hydrocarbons released during the pyrolysis phase.
- S3CO (mg/g rock): The CO from organic sources released during the pyrolysis phase.
- S3'CO (mg/g rock): The CO from organic and mineral sources released during the pyrolysis phase.
- $S3CO_2$ (mg/g rock): The CO_2 from organic sources released during the pyrolysis phase.
- S3'CO_2 (mg/g rock): The CO_2 from mineral sources released during the pyrolysis phase.
- SO_2 pyrolysis (mg/g rock): The SO_2 measured during the pyrolysis phase.
- S4CO (mg/g rock): The CO from organic sources released during the oxidation phase.
- $S4CO_2$ (mg/g rock): The CO_2 from organic sources released during the oxidation phase.
- S5 (mg/g rock): The CO_2 from mineral sources released during the oxidation phase.
- SO_2 oxidation (mg/g rock): The SO_2 measured during the oxidation phase.

From these different signals, various parameters can be defined (Lafargue *et al.*, 1998; Behar *et al.*, 2001). The main parameters are:

- Maturity Index (Tmax):

$$Tmax \rightarrow Temperature\ at\ the\ maximum\ of\ peak\ S2\ (°C)$$

- Production Index (PI):

$$PI = \frac{S1}{(S1 + S2)}$$

- Hydrogen Index (HI):

$$HI = \frac{100 * S2}{TOC}\ (mg\ HC/g\ TOC)$$

- Oxygen Index (IO):

$$OI = \left[\frac{100 * S3CO_2}{TOC}\right](mg\ CO_2/g\ TOC)$$

- Total Organic Carbon (TOC):

$$TOC = PC + RC\ (wt\%)$$

$$PC: Pyrolysed\ organic\ Carbon$$

$$= [(S1 + S2) * 0.083] + \left[(S3CO + \frac{S3'CO}{2}) * \frac{12}{280}\right] + \left[S3CO_2 * \frac{12}{440}\right]$$

$$RC: Remaining\ organic\ Carbon = \left[S4CO_2 * \frac{12}{440}\right] + \left[S4CO * \frac{12}{280}\right]$$

❖ Mineral Carbon (MinC):

$$MinC = PyroMinC + OxiMinC\ (wt\%)$$

$$PyroMinC = \left[S3'CO_2 * \frac{12}{440}\right] + \left[\frac{S3'CO}{2} * \frac{12}{280}\right]$$

$$OxiMinC = \left[S5 * \frac{12}{440}\right]$$

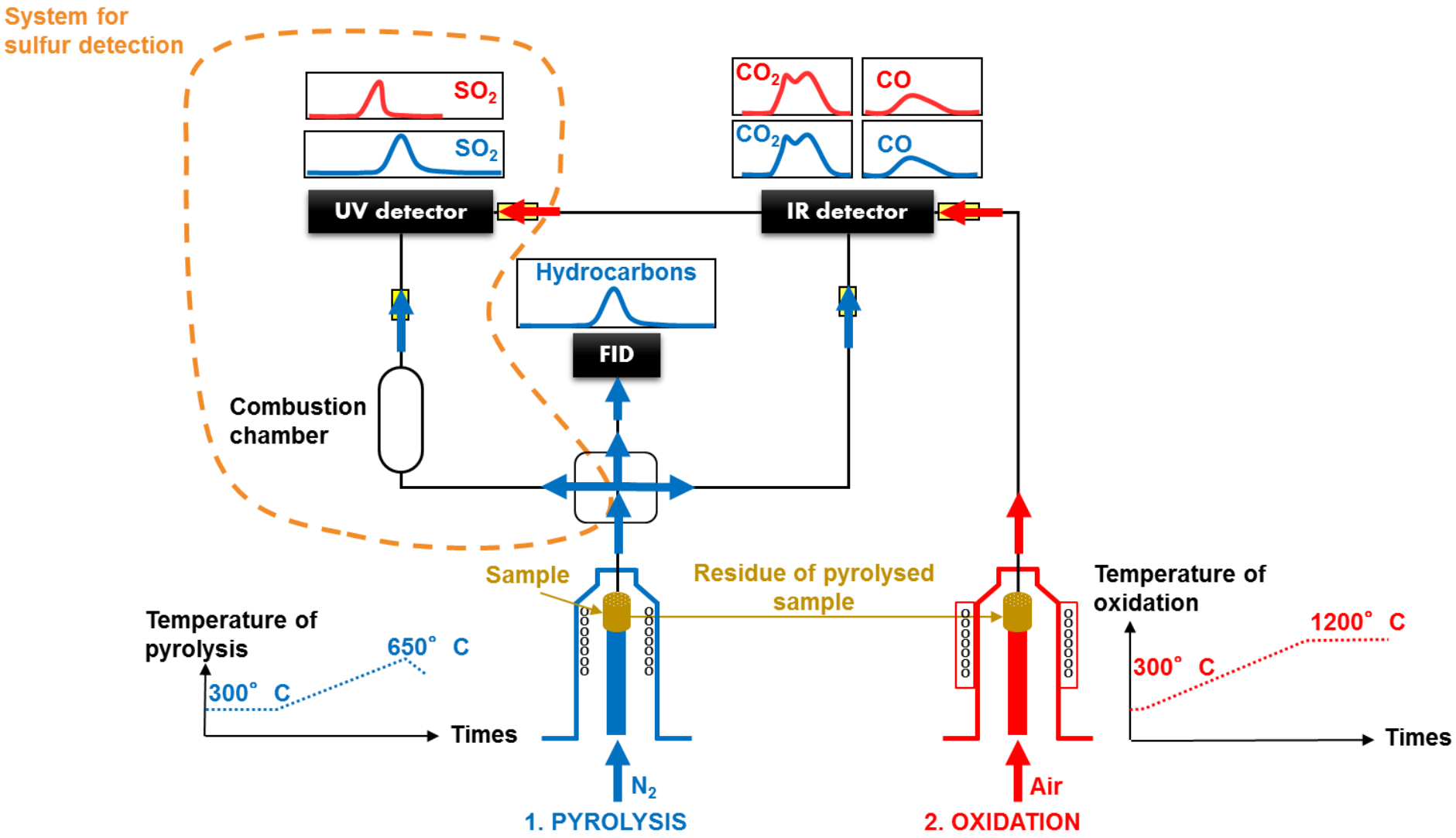

Figure 1. 3 : Rock-Eval 7S principle using the total sulphur temperature program

1.3.2- Rock-Eval 7S sulphur speciation: state of the art

Rock-Eval 7S analysis provides two SO_2 profiles as functions of temperature and time (Figure 1. 4). The first one results from the pyrolysis phase and the second one from the oxidation phase. Combining these two profiles, it is possible to quantify the S^{Total} content of the sample. This technique allows discrimination between various sulphur compounds, such as labile sulphur released during pyrolysis and refractory sulphur released during oxidation. Figure 1. 4 is an example of the SO_2 Rock-Eval 7S signal of a sample from a source rock formation in Limagne (France) where most of the sulphur compounds can be identified:

- $S^{Organic}$: Organic reduced sulphur;
- S^{Pyrite}: Inorganic reduced sulphur (sulphide minerals like pyrite);
- $S^{Sulphates}$: Inorganic oxidised sulphur (sulphates minerals like gypsum).

However, for the complete speciation of all different sulphur compounds in a sample, further improvements must be made, especially for the distinction between $S^{Organic}$ and S^{Pyrite}. Indeed, concerning the SO_2 signal in pyrolysis, it is possible to discriminate $_{Pyrolysis}S^{Organic}$ and $_{Pyrolysis}S^{Pyrite}$ because they generate two distinct peaks (Figure 1. 4). In contrast, in the oxidation phase, $_{Oxidation}S^{Organic}$ and $_{Oxidation}S^{Pyrite}$ are represented within the same SO_2 peak (Figure 1. 4). To quantify the different type of sulphur compounds with Rock-Eval 7S, it is therefore necessary to better resolve the organic-pyritic sulphur peak in the oxidation phase.

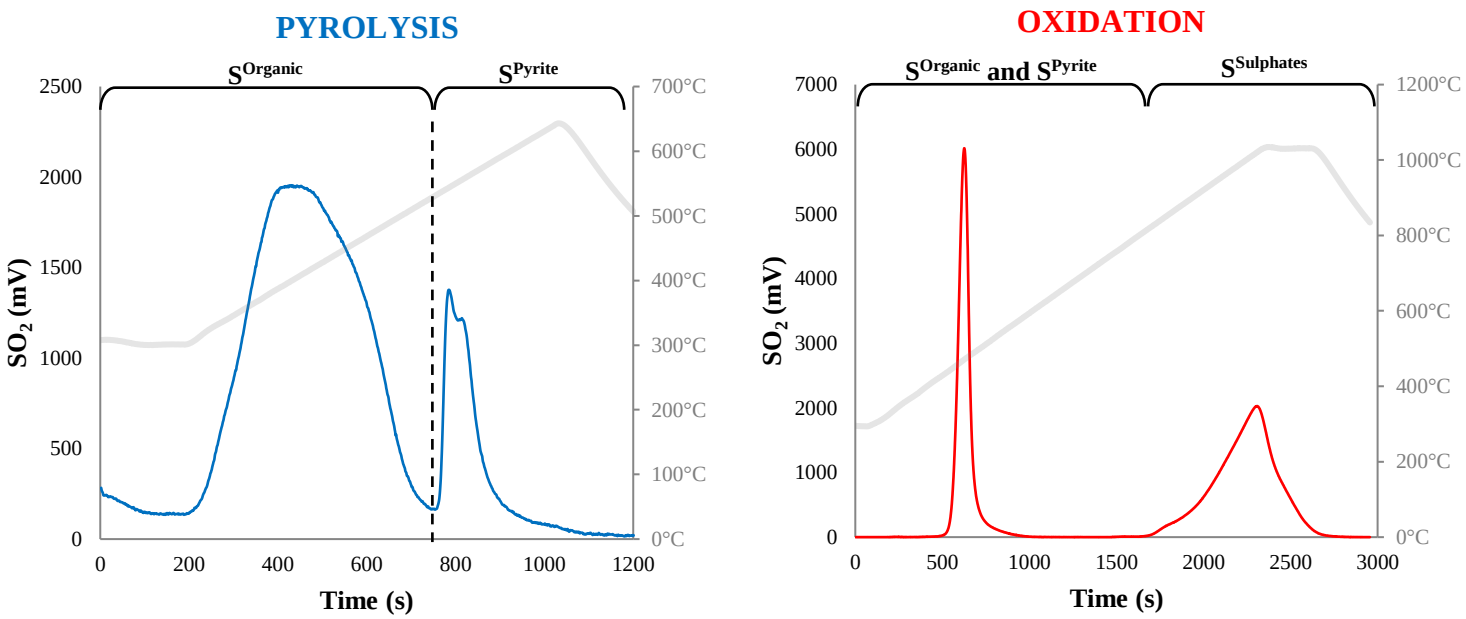

Figure 1. 4 : Example of sulphur detection with Rock-Eval 7S

1.4- PHD OBJECTIVES

This PhD project is in the context of the development of the Rock-Eval 7S, latest model of Rock-Eval technology. Indeed, the main goal of this PhD is developing and validating new analytical methodology on Rock-Eval 7S for sulphur quantification and speciation, to provide key sulphur geochemical variables indicators of paleoenvironmental conditions responsible of OM preservation in marine sediments. A two steps approach has been designed, corresponding to two principal objectives of this PhD project.

1.4.1- First objective: Developing and validating new analytical methodology on Rock-Eval 7S for sulphur quantification and speciation

The new Rock-Eval 7S, in addition to all the functionalities of Rock-Eval 6, has a system for continuous detection of sulphur. Two sulphur (SO_2) profiles are obtained corresponding to the pyrolysis and the oxidation phase of Rock-Eval 7S. These sulphur profiles present different peaks, which can be assigned to different sulphur compounds ($S^{Elemental}$; $S^{Organic}$; S^{Pyrite} and $S^{Sulphates}$). During the pyrolysis phase, ${}_{Pyrolysis}S^{Pyrite}$ and ${}_{Pyrolysis}S^{Organic}$ can be distinguished from each other and quantified separately because they are represented by two distinct SO_2 peaks. However, during the oxidation phase, ${}_{Oxidation}S^{Pyrite}$ and ${}_{Oxidation}S^{Organic}$ are represented by one single peak, making a distinction between these sulphur components impossible. Further challenges arise as chemical reactions occur during the analytical cycle which may modify the original sulphur compounds. This significantly limits quantification of $S^{Organic}$ and S^{Pyrite} using Rock-Eval 7S. It is therefore necessary to develop a new and improved analytical method to quantify $S^{Organic}$ and S^{Pyrite} using Rock-Eval 7S. The strategy applied to reach this objective, and the results obtained, are presented in the next two chapters:

- Chapter 2: Rock-Eval 7S sulphur calibration studies
- Chapter 3: Pyritic and organic sulphur quantification in organic rich marine sediments using Rock-Eval 7S

1.4.2- Second objective: Using Rock-Eval 7S carbon and sulphur parameters as descriptors of OM preservation

The second objective concerns the use of the new Rock-Eval 7S parameters, S^{Pyrite} and $S^{Organic}$, in addition to the classical Rock-Eval 7S carbon and sulphur parameters (TOC; HI; OI; Tmax; MinC; S^{Total}), to help the description of paleo-environmental conditions responsible of OM preservation in various marine environments. To reach this objective, the new Rock-Eval 7S method for S^{Pyrite} and

$S^{Organic}$ quantification has been applied to Jurassic black shales from North Yorkshire, Dorset and Somerset in order to highlight the potential contribution from the new Rock-Eval 7S data in the description of OM preservation. The results obtained are presented in the Chapter 4 of this thesis.

Chapter 2: ROCK-EVAL 7S CALIBRATION STUDIES

2.1- INTRODUCTION

The Rock-Eval 7S, the latest version of the Rock-Eval equipment, has been in development over the last 20 years at IFP Energies Nouvelles - Vinci Technologies. Not only does it allow the same applications as the Rock-Eval 6 in characterizing organic matter in rocks, but it is also equipped with an additional continuous sulphur detection system allowing sulphur characterization in addition to carbon in one single analytical cycle. Indeed, with this new version of Rock-Eval, it is possible to measure the sulphur content of the rocks, split into two sulphur fractions: (a) the pyrolysis sulphur content, corresponding to the sulphur released by the rock under the Rock-Eval pyrolysis; (b) the oxidation sulphur content, corresponding to the sulphur released by the residue of the pyrolyzed rock upon combustion. For that, two SO_2 electric profiles (µV.s) are recorded by the UV sulphur detector, corresponding to the sulphur effluents released during these two phases. The quantification of these two sulphur components, and consequently the quantification of total sulphur (S^{Total}) content, requires calibration of the sulphur response for each phase. Not only calibrating the response of the UV detector by itself is necessary, but more importantly calibrating the response of the whole system. The whole Rock-Eval system, including the ovens, lines and traps, can interact with sulphur effluents, thereby modifying the SO_2 signal recorded by the UV detector. As the sulphur effluent paths for the pyrolysis and the oxidation steps are different, two calibration coefficients, KSO_2 pyrolysis and KSO_2 oxidation, must be defined. This Rock-Eval 7S S^{Total} calibration study constitutes the first part of this chapter (section 2.2). The second part of this chapter (section 2.3), focuses on Rock-Eval 7S identification of the main of sulphur species found in marine sediments to characterise their different Rock-Eval 7S fingerprints.

2.2- ROCK-EVAL 7S S^{Total} CALIBRATION

2.2.1- Samples

2.2.1.1-Reference samples

We selected two reference samples for the Rock-Eval 7S S^{Total} calibration, one sample of elemental sulphur dedicated to the calibration of the pyrolysis phase and one sample of synthetic coal (provided by Sylab, reference: B2323), dedicated to the calibration of the oxidation phase. The elemental sulphur sample appeared promising for this calibration study because it is the simplest natural sulphur species and is chemically well-defined, so its Rock-Eval SO_2 signal should be easy to be measured and interpreted. It was planned to use the elemental sulphur for calibrating both pyrolysis and oxidation. However, due to its high thermal reactivity, elemental sulphur is not well detected and quantified in direct oxidation (Appendix A). Hence, for the calibration of the oxidation phase, the elemental sulphur calibration sample has been replaced by a synthetic coal sample (B2323), which is less thermally reactive.

The calibration involves correlating the sulphur mass (µg) in the samples to their electric SO_2 signal (µV.s). To reach an accurate calibration, it is therefore important to know the precise sulphur mass in the reference samples. For that, two accurate measurements are needed: (a) the masses of the analysed samples, and (b) their sulphur contents. The masses of the reference samples were carefully measured on a precision scale Mettler (reference: MT5), with a balance uncertainty of 2 µg. Concerning the sulphur content, both elemental sulphur and synthetic coal samples were selected because their sulphur contents are already well defined:

- Elemental sulphur sample: The XRD analysis, using PANalytical X'Pert Pro diffractometer, shows no impurities, the sulphur content in this sample was confidently assumed to be 100 wt%.

- Synthetic coal sample (B2323): The coal sample was synthetized to have a sulphur content of precisely 3.42 wt% (organic sulphur) and a carbon content of 63.00 wt%.

2.2.1.2- Validation samples

13 samples from the Whitby Mudstone Fm. (Toarcian, North Yorkshire, UK) (Salem, 2013; Garner, 2014) and 3 samples from the Orbagnoux Fm. (Upper Kimmeridgian, Jura, France) (Mongenot

et al., 1999; Tribovillard *et al.*, 1999; Sarret *et al.*, 2002) were selected for the assessment of Rock-Eval 7S STotal calibration. 3 additional samples obtained by decarbonatation of the 3 Orbagnoux samples, using a modified version of the standard in-house kerogen isolation method (Vandenbroucke and Largeau, 2007) in which only the Hydrochloric acid (6 N HCl) treatment steps were performed, were also selected as validation samples. We chose these samples to cover a wide range of S^{Total} contents from 1wt% to 15wt%, and because they contain the two mains sulphur species S^{Pyrite} and $S^{Organic}$ (Mongenot *et al.*, 1999; Tribovillard *et al.*, 1999; Sarret *et al.*, 2002; Salem, 2013)

2.2.2- Methodology

2.2.2.1- Reference sample weighing

The samples were weighed on a precision scale Mettler (reference: MT5) which works in the milligram weight range. The scale is controlled daily by weighing a certified reference mass of 2000 µg (certificate: 293998). The weighing method provides an uncertainty of ± 2µg, which was deduced from the standard deviation of reproducibility. This uncertainty indicates that a weight value obtained with this method has 90% of probability to be in the range of uncertainty.

$$Standard\ deviation\ of\ reproducibility = 1\mu g$$

$$Uncertainty = 2 * Standard\ deviation\ of\ reproducibility = 2\mu g$$

2.2.2.2- Calibration of the Rock-Eval 7S pyrolysis phase

Different masses of the elemental sulphur sample were analysed using a modified pyrolysis temperature program from 200°C (instead of 300°C) to 650°C with a heating rate of 25°C/min. This temperature program is suitable for the high thermal reactivity of elemental sulphur and completely sufficient to degrade its entire quantity.

Duplicate analyses of 9 different masses, from 100µg to 2000µg, of the elemental sulphur sample were carried out. Given that it consists of 100% elemental sulphur, the sample mass corresponds to the sulphur mass. These different sulphur masses analysed during the Rock-Eval 7S pyrolysis generated different SO_2 peaks. The areas of the peaks put in correlation with the masses of sulphur allowed the determination of the pyrolysis coefficient (KSO_2 pyrolysis).

2.2.2.3- Calibration of the Rock-Eval 7S oxidation phase

A direct Rock-Eval 7S basic oxidation cycle, from 300°C to 850°C with a heating rate of 20°C/min, was applied to analyse different masses of the synthetic coal sample. Duplicate analyses of

five different masses, from 5000µg to 25000µg, were carried out (5000; 10000; 15000; 20000; 25000 µg). The number of analyses was constrained by the relatively low sulphur content of this sample (3.42wt%) compared to its carbon content (63wt%). 5000µg is the minimum mass of sample that delivers a good sulphur signal; 25000µg is the maximum mass of sample to avoid saturation of the carbon detectors; intervals of 5000µg allow the observation of significant differences between the sulphur peaks obtained. The sulphur mass of each aliquot was estimated by multiplying the sample mass and the sulphur content. These different sulphur masses analysed were correlated to the corresponding SO_2 oxidation peaks obtained to derive a calibration coefficient (KSO_2 oxidation).

2.2.2.4- Calculation of the uncertainty on the sulphur mass

Considering the uncertainty of the mass of the samples U[msample] and the uncertainty of their sulphur content U[%S], the uncertainty of their sulphur mass U[mS] can be deduced, according to the following equation:

$$U[mS] = U[msample] * \%S \; + \; msample * U[\%S]$$

This results from the derivation of the following equation:

$$mS = \; msample \times \%S$$

Applied to the elemental sulphur and the coal samples used for the calibration, these equations give the mass of sulphur and its uncertainty in these reference samples (Table 2. 1).

	unit	Elemental sulphur - minimal sulphur mass	Elemental sulphur - maximal sulphur mass	Synthetized coal - minimal sulphur mass	Synthetized coal - maximal sulphur mass
Sample mass msample	µg	100	2000	5000	25000
Uncertainty of sample mass U[msample]	µg	2	2	2	2
Sulphur content %S	µg/µg	1	1	0.342	0.342
Uncertainty of sulphur content U[%S]	µg/µg	0	0	0	0
Sulphur mass mS	µg	100	2000	1710	8550
Uncertainty of sulphur mass U[mS]	µg	2	2	0.684	0.684

Table 2. 1 : Masses of sulphur in reference samples

2.2.2.5-Validation of S^{Total} calibration

To test if the calibration coefficients produce results that are comparable to S contents independently determined for the same samples, we performed duplicate Rock-Eval 7S analyses of the validation samples (section 2.2.1.2). Then, the S^{Total} contents of these selected samples, determined with Rock-Eval 7S using the estimated calibration coefficients, were compared to the S^{Total} contents measured with other sulphur analysis methods:

- LECO: For the Whitby Mudstone samples; analyses performed by Garner (2014) in the context of an MSc project at Newcastle University. The uncertainty for S^{Total} measurement using this method is ±0.2wt% in average for the selected validation samples.

- Infrared (Method MO 240 LA 2008: combustion method similar to LECO): For the Orbagnoux samples; analyses performed by "Groupe SGS France". The uncertainty for S^{Total} measurement using this method is from ±0.1wt% to ±0.3wt% for the range of S^{Total} contents covered by the selected validation samples.

2.2.3- S^{Total} calibration results

2.2.3.1- Determination of the KSO_2 coefficients (Appendix B)

The correlation lines relating the different sulphur masses analysed and their corresponding SO_2 peaks are presented for the two phases of Rock-Eval 7S (pyrolysis and oxidation) in Figure 2. 1. Due to base line issues during the oxidation phase, the sulphur contents of some analyses were under-estimated. Therefore, to establish the oxidation correlation line, only the analyses with a good base line were retained. The calibration coefficients, KSO_2 pyrolysis and KSO_2 oxidation, are the slopes of these correlation lines (Figure 2. 1). This corresponds to the following values:

$$KSO_2\ Pyrolysis = \frac{Pyrolysis\ peak\ areas(\mu V.s)}{100 * sulphur\ mass\ (\mu g)} = \mathbf{21.30}\ \mu \boldsymbol{V.s.}\ \mu \boldsymbol{g^{-1}.10^{-2}}$$

$$KSO_2\ Oxidation = \frac{10000 * sulphur\ mass\ (\mu g)}{Oxidation\ peak\ areas(\mu V.s)} = \mathbf{5.17}\ \mu \boldsymbol{g.10^{4}.}\ \mu \boldsymbol{V^{-1}.s^{-1}}$$

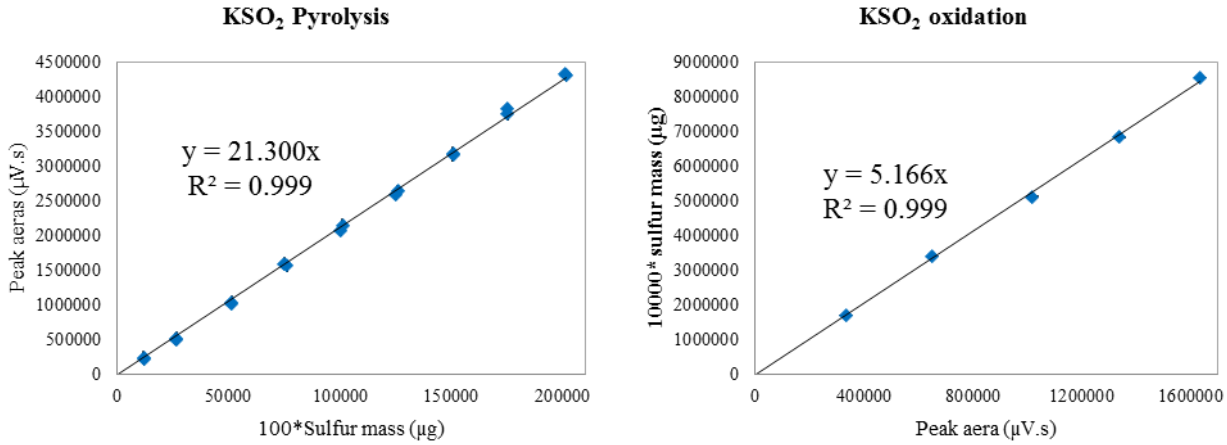

Figure 2. 1: Cross plot of sulphur masses and the corresponding peak areas obtained during pyrolysis and oxidation phases of Rock-Eval 7S

2.2.3.2- Validation of S^{Total} calibration (Appendix C)

We determined, using Rock-Eval 7S analysis with the defined calibration coefficients (KSO_2 pyrolysis and KSO_2 Oxidation), the S^{Total} contents of the selected validation samples. It is obtained by summing ${}_{Pyrolysis}S^{Total}$ and ${}_{Oxidation}S^{Total}$ obtained with these following formulas:

$$_{Pyrolysis}S^{Total}(wt\%) = \frac{Sulphur\ mass\ (mg)}{Sample\ mass\ (mg)} * 100 = \frac{f(Peak\ areas;\ KSO_2\ Pyrolysis)(mg)}{Sample\ mass\ (mg)} * 100$$

$$_{Oxidation}S^{Total}(wt\%) = \frac{Sulphur\ mass\ (mg)}{Sample\ mass\ (mg)} * 100 = \frac{f(Peak\ areas;\ KSO_2\ Oxidation)(mg)}{Sample\ mass\ (mg)} * 100$$

$$\boldsymbol{S^{Total}(wt\%) = {}_{Pyrolysis}S^{Total} + {}_{Oxidation}S^{Total}}$$

The S^{Total} values obtained with Rock-Eval 7S were then compared to those of LECO and Infrared analyses, respectively, in the North Yorkshire and Orbagnoux samples (Figure 2. 2). A linear function passing close the origin and with a slope close to 1 is obtained with very good regression coefficients ($R^2 \geq 0.99$), for the comparison of Rock-Eval 7S with both LECO and Infrared methods. These very good correlation lines allow the validation of the defined calibration coefficients and the confirmation of Rock-Eval 7S sulphur calibration accuracy for S^{Total} quantification. The slight disparity

between S^{Total} values obtained via Rock-Eval 7S and S^{Total} values obtained via the LECO and Infrared can be attributed to combination of analytical errors of the different methods.

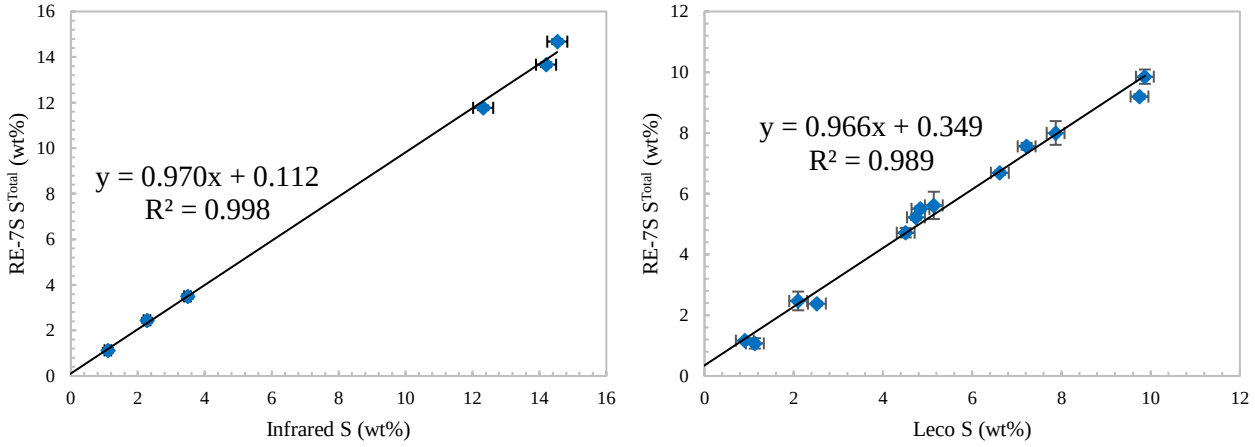

Figure 2. 2: Comparison of the determination of S^{Total} contents: Rock-Eval 7S vs Infrared (Orbagnoux samples) and RE 7S vs LECO (North Yorkshire samples)

2.3- ROCK-EVAL 7S CHARACTERISATION OF THE MAIN TYPES OF SULPHUR SPECIES FOUND IN MARINE SEDIMENTS

2.3.1- Samples and methodology

2.3.1.1-XRD and elemental analysis sample characterisation

We selected samples representing the main types of sulphur species found in marine sediments, to characterize their Rock-Eval 7S specific signals. Before their Rock-Eval 7S analysis, the selected samples were analysed using XRD (PANalytical X'Pert Pro diffractometer) and/or elemental analysis (ICP-AES) to characterize their crystallography/chemical composition and/or to detect possible impurities. Iron sulphide samples, organic-sulphur containing samples, elemental sulphur sample and sulphates samples were thus selected and characterized (Table 2. 2).

- Iron sulphide samples:

❖ Sedimentary pyrite (FeS_2) containing sample: We selected 1 sample from the Whitby Mudstone Formation (Toarcian, North Yorkshire, UK) and isolated its kerogen using a standard in-house kerogen isolation method (Vandenbroucke and Largeau, 2007). The following acids were used sequentially, each being followed by a rinse with hot deionized water: (i) hydrochloric acid; (ii) 1:2 mixture of hydrofluoric acid (40% HF) and hydrochloric acid (6 N HCl); (iii) hydrochloric acid (6 N HCl). Then, knowing that kerogen contains mainly organic sulphur ($S^{Organic}$) and pyritic sulphur (S^{Pyrite}), and assuming that all iron within the kerogen is in pyritic form (FeS_2), we can calculate the kerogen S^{Pyrite} content based on its iron content (Fe) which was measured by direct elemental analysis (ICP-AES at SGS France). From this calculated S^{Pyrite} content and the S^{Total} content determined by Infrared (Method MO 240 LA 2008 at SGS France), we can calculate the $S^{Organic}$ content of the sample. We performed duplicate analyses for each sample. The calculations are as follow:

$$Fe\ in\ kerogen\ (wt\%) = \frac{Fe\ mass\ (g)}{kerogen\ mass\ (g)} * 100$$

$$nFe\ (mol) = \frac{Fe\ mass\ (g)}{MFe\ (g.mol^{-1})}$$

$$\frac{nFe\ (mol)}{kerogen\ mass\ (g)} = \frac{1}{MFe\ (g.mol^{-1})} * \frac{Fe\ mass\ (g)}{kerogen\ mass\ (g)}$$

$$\frac{nFe\ (mol)}{kerogen\ mass\ (g)} = \frac{1}{MFe\ (g.mol^{-1})} * Fe\ in\ kerogen\ (wt\%)$$

$$\frac{n\ pyritic\ S\ (mol)}{kerogen\ mass\ (g)} = \frac{2}{MFe\ (g.mol^{-1})} * Fe\ in\ kerogen\ (wt\%)/100$$

$$\frac{pyritic\ S\ mass\ (mol)}{kerogen\ mass\ (g)} = \frac{2\ MS}{MFe\ (g.mol^{-1})} * Fe\ in\ kerogen(wt\%)/100$$

$$S^{pyrite}\ in\ kerogen\ (wt\%) = \frac{2 * MS}{MFe(g.mol^{-1})} * Fe\ in\ kerogen\ (wt\%)/100$$

$$M: molar\ mass\ (g.mol^{-1})$$

$$S^{organic}\ in\ kerogen\ (wt\%) = S^{total}\ in\ kerogen\ (wt\%) - S^{pyrite}\ in\ kerogen(wt\%)$$

The results of these calculations show that sulphur in kerogen from this Whitby Mudstone Formation sample is mainly bound as pyrite, and organic S compounds are negligible, leading to a S^{Pyrite}/ S^{Total} ratio of around 1 (Table 2. 2)

❖ Igneous iron sulphide samples: Pyrite (FeS_2), marcasite (FeS_2) and pyrrhotite (Fe_7S_8) samples were also selected for this study. Their qualitative XRD analysis, performed at IFP Energies Nouvelles, revealed no secondary phases but only some traces of other minerals (quartz, clays, carbonates and sulphates). Pyrite and marcasite have the same chemical formula but different crystal systems, cubic for pyrite and orthorhombic for marcasite. However, XRD analyses of pyrite and marcasite samples did not show any difference of the crystal systems between these two samples, an apparent inconsistency which cannot be explained.

- <u>Organic-sulphur containing samples:</u>

Three samples from Orbagnoux Formation (Kimmeridgian, France) (Tribovillard *et al.*, 1999) were used to get the signal of organic sulphur compounds. We decarbonated these samples using a modified version of the standard in-house kerogen isolation method (Vandenbroucke and Largeau, 2007) in which the hydrochloric acid (6 N HCl) treatment steps were performed. Indeed just the HCl treatment steps were required here to get pseudo-kerogen samples considering the carbonated matrix of Orbagnoux samples (Tribovillard *et al.*, 1999). Then, we did iron (Fe) and S^{Total} quantification using respectively ICP-AES and Infrared (Method MO 240 LA 2008).

Based on the same calculations as in the previous section about sedimentary pyrite, we can confirm that sulphur in these samples is principally bound to organic matter, leading to a S^{Pyrite}/ S^{Total} ratio close to zero (Table 2. 2).

- Other sulphur species samples:

This part concerns an elemental sulphur sample (S_8) and three sulphate samples, gypsum ($CaSO_4$-$2H_2O$); cupro-gypsum ([Ca, Cu] $[SO_4]2.2H_2O$) and barite ($BaSO_4$). Their qualitative XRD analysis showed no secondary phases and only some traces of other minerals were detected.

Sulphur species	Samples	Suppliers/Formations	Main phase XRD	Trace phases XRD	Iron (wt%)	S^{Pyrite}/S^{Total}
Iron sulphides	Sedimentary pyrite (FeS_2)	Whitby Mudstone Fm.	~	~	30.26	1± 0.1
	Pyrite (FeS_2)	Paris mineral fair	Pyrite	Iron sulphate Clays	~	~
	Marcasite (FeS_2)	Ward's science	Pyrite	Iron sulphate Quartz	~	~
	Pyrrhotite (Fe_7S_8)	Paris mineral fair	Pyrrhotite	Quartz; Carbonate; Clay	~	~
Organic sulphur compounds	9ca-organic sulphur	Orbagnoux Formation	~	~	0.44 ± 0.04	0.04 ± 0.004
	9f-organic sulphur	Orbagnoux Formation	~	~	0.51 ± 0.05	0.04 ± 0.004
	9h-organic sulphur	Orbagnoux Formation	~	~	0.45 ± 0.04	0.04 ± 0.004
Elemental sulphur (S_8)	Elemental sulphur (S_8)	Paris mineral fair	Elemental sulphur	no	~	~
Sulphates	Gypsum ($CaSO_4$-$2H_2O$)	Paris mineral fair	Gypsum	Quartz; Aluminate.	~	~
	Cupro-gypsum ([Ca, Cu][SO_4]2.$2H_2O$)	Paris mineral fair	Gypsum	Quartz; Aluminate.	~	~
	Barite ($BaSO_4$)	Paris mineral fair	Barite	no	~	~

Table 2. 2: XRD and elemental analysis samples characterisation

2.3.1.2-Rock-Eval 7S analysis

As the different sulphur species under study have different thermal reactivities (known from preliminary tests), different Rock-Eval 7S temperature programs were applied. Indeed, elemental sulphur is rapidly degraded at low temperatures during the pyrolysis phase of Rock-Eval 7S analysis,

whereas sulphate thermal degradation requires more energy and so occurs at higher temperature during the last steps of the Rock-Eval 7S oxidation phase. The following temperature programs were used:

- ❖ Iron sulphides and organic sulphur samples: Basic pyrolysis from 300°C to 650°C with a heating rate of 25°C/min; basic oxidation from 300°C to 850°C with a heating rate of 20°C/min.
- ❖ Elemental sulphur sample: Pyrolysis from 200°C to 650°C with a heating rate of 25°C/min.
- ❖ Sulphate samples: Oxidation: from 300°C to 1200°C with a heating rate of 20°C/min.

2.3.2- Rock-Eval 7S characterisation of the main sulphur species found in marine sediments

2.3.2.1- Iron sulphides

During the pyrolysis phase the thermal decomposition of iron sulphides occurs in the range of temperatures from 480 to 650°C, and during the oxidation phase in the range of temperatures from 320 to 580°C (Figure 2. 3). Numerous parameters impact the SO_2 Rock-Eval signals of iron sulphides:

- Chemical composition:

The pyrite (FeS_2) Rock-Eval 7S signal is very different from the pyrrhotite (Fe_7S_8) one. Indeed, pyrite is thermally degraded during the pyrolysis phase whereas pyrrhotite remains stable (Figure 2. 3). As pyrrhotite (Fe_7S_8) is high temperature replacement phase of pyrite (Coats and Bright, 1966; Lambert *et al.*, 1980; Boyabat *et al.*, 2004), its stability during the Rock-Eval 7S pyrolysis phase suggests that the final product of pyrite Rock-Eval 7S pyrolysis could be pyrrhotite. From these observations, the following transformations of pyrite during Rock-Eval 7S analysis can be proposed:

In the pyrolysis oven: Pyrite (s) ➔ **Sulphide effluents (g)** + reduced iron sulphide (pyrrhotite?) (s)

In the oxidation oven: Reduced iron sulphide (pyrrhotite?) (s) ➔ **SO_2(g)** + iron oxide (s)

- Crystal structure:

During the two phases of Rock-Eval 7S analysis, pyrite (FeS_2; cubic crystal system) is degraded later than marcasite (FeS_2; orthorhombic crystal system), showing that pyrite is more thermally resistant (Figure 2. 3). The marcasite signal during the pyrolysis phase is composed of two peaks, a first peak which occurs earlier than the pyrite peak, and a second peak occurring close to the pyrite peak. Therefore, the marcasite sample actually appears to be composed of a mixture of pyrite and marcasite.

This is partially consistent with XRD results of the marcasite sample presenting a pyrite crystal structure.

- Origin:

Sedimentary pyrite (FeS_2) seems less thermally resistant than igneous pyrite (FeS_2) during both pyrolysis and oxidation phases (Figure 2. 3). This may be due to the different formation conditions: Sedimentary pyrite is formed close to the seafloor under early diagenetic temperature and pressures conditions that are much lower than the metamorphic-magmatic conditions under which igneous pyrite is formed. These different pressure and temperature conditions could imply that igneous pyrite is more compacted and denser and consequently more thermally resistant than sedimentary pyrite.

2.3.2.2- Organic sulphur compounds

The Rock-Eval 7S characterization of the Orbagnoux kerogens revealed that during pyrolysis, the thermal decomposition of the organic sulphur compounds occurs in a temperature range of 300 to 500°C (Figure 2. 3). During this phase, some complex organic sulphur molecules would be broken down to form sulphidic effluents, including hydrogen sulphide (H_2S), leaving a refractory sulphur coke:

In the pyrolysis oven: Organic sulphur compounds (s) ➔ **Sulphide effluents (g)** + S-coke(s)

The refractory sulphur coke is then completely degraded during the oxidation phase, releasing principally sulphur dioxide and carbon oxide gases. The thermal decomposition range during this phase is about 350 to 550 °C (Figure 2. 3). The reaction can be expressed as follows:

In the oxidation oven: S-coke(s) + O_2 (g) ➔ **SO_2 (g)** + CO (g)

2.3.2.3- Sulphates

Gypsum, cupro-gypsum and barite are the most thermally resistant sulphur species among those studied here. They are stable in the pyrolysis phase, and during the oxidation phase their thermal degradation occurs between 900 and 1200°C. Under Rock-Eval 7S conditions, barite is not completely decomposed even at 1200°C (Figure 2. 3). This is explained by the fact that sulphates already represent the most oxidized form of sulphur and are therefore difficult to be oxidized by combustion. The reaction of sulphate decomposition during the oxidation phase can be represented as follows:

In the oxidation oven: XSO_4 (s) + O_2 (g) ➔ **SO_2 (g)** + XO (s) + 3/2 O_2 (g)
X: Ca; Mg; Cu; Ba; Fe; Sr…

2.3.2.4- Elemental sulphur

The entire quantity of native sulphur is thermally decomposed into sulphur gas between 200 and 300°C during the pyrolysis phase (Figure 2. 3). This reaction can be represented by the following equation:

In the pyrolysis oven S_8 (s) ➔ **4 S_2 (g)**

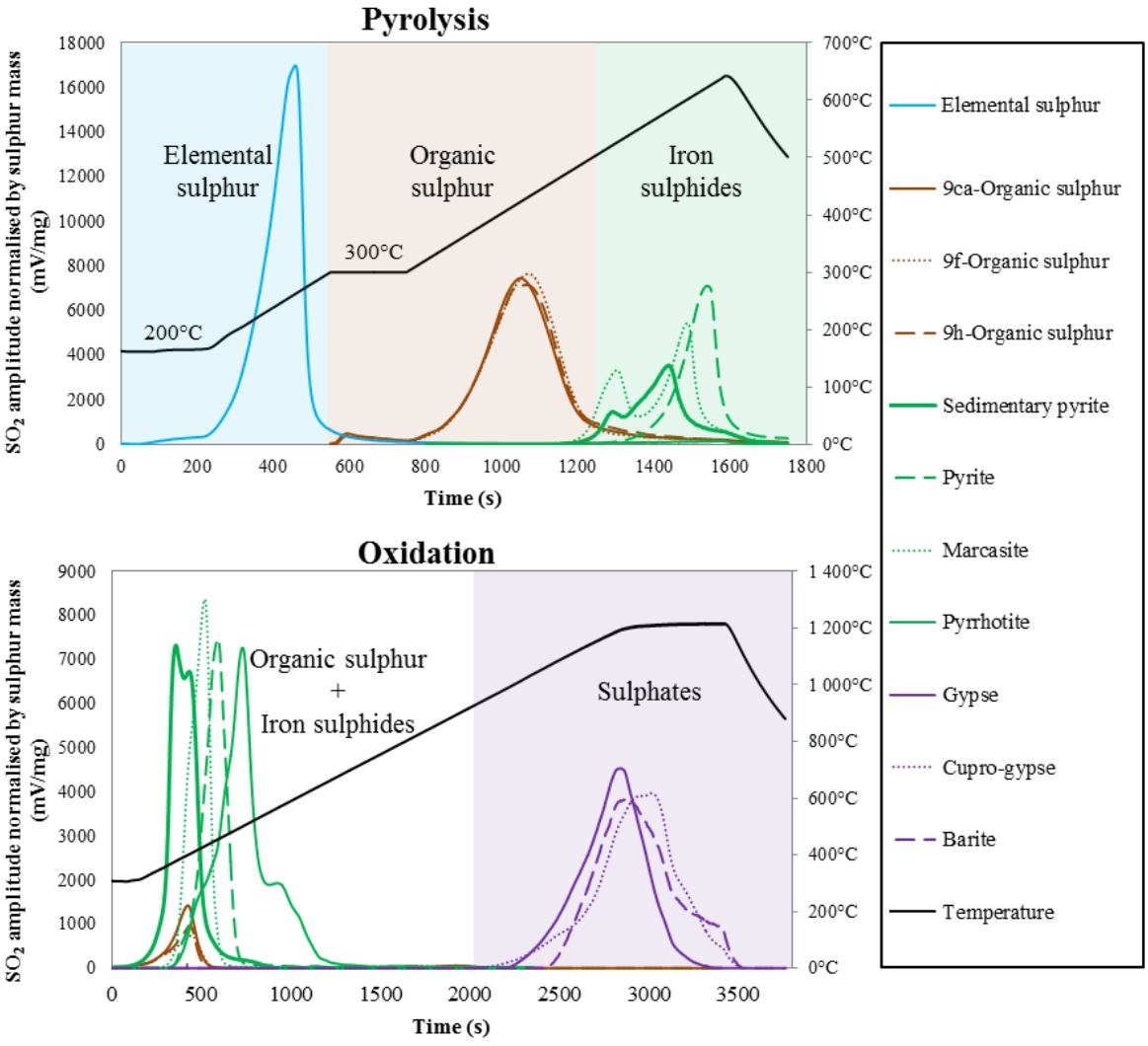

Figure 2. 3: Composite graph presenting a synthesis of Rock-Eval 7S signals of the different types of sulphur species found in marine sediments

2.4- CONCLUSIONS

Rock-Eval 7S was calibrated for S^{Total} quantification by determining two sulphur calibration coefficients, KSO_2 pyrolysis and KSO_2 oxidation, for each phase of the Rock-Eval 7S analysis. The S^{Total} contents of set of sedimentary rock samples were determined with Rock-Eval 7S, using the calculated calibration coefficients, and the results obtained were compared to results from independent sulphur analysis methods (LECO and Infrared spectrometry). The very good correlation lines obtained ($R^2 \geq 0.99$) show that Rock-Eval 7S provides accurate quantification of the S^{Total} content of rock samples.

We then performed Rock-Eval 7S characterisation of the signals of different sulphur species found in marine sediments (S^{Pyrite}; $S^{Organic}$; $S^{Sulphates}$ and $S^{Elemental}$). They decompose at different specific ranges of temperatures, except S^{Pyrite} and $S^{Organic}$, which are degraded at the same temperatures during the oxidation phase (Figure 2. 4). This latter finding is the main reason why in marine sediments it is not possible to completely quantify different sulphur species using the Rock-Eval 7S. Therefore, further analytical development is required to find a method to quantify S^{Pyrite} and $S^{Organic}$ quantification using Rock-Eval 7S. This constitutes the subject of the next chapter.

Chapter 3: PYRITIC AND ORGANIC SULPHUR QUANTIFICATION IN ORGANIC RICH MARINE SEDIMENTS USING ROCK-EVAL 7S

3.1- CHAPTER INTRODUCTION

Methods for pyritic sulphur (S^{Pyrite}) and organic sulphur ($S^{Organic}$) quantification in organic rich sediments are critical for a wide range of applications relevant to petroleum exploration such as characterisation of the type of organic matter (OM) in source rocks. Indeed, by the quantification of $S^{Organic}$ content of source rocks, we can identified type IIS (Orr, 1986), type IS (Sinninghe Damsté *et al.*, 1993) and type IIIS (Sinninghe Damsté *et al.*, 1992) kerogen, corresponding to lacustrine, marine and terrestrial OM, respectively, all characterised by high $S^{Organic}$/TOC ratios. These methods, briefly introduced below, are also of central interest for petroleum production, for instance to evaluate the risk of H_2S production during assisted recovery of oil with thermal processes. It has been shown that some reactions which induce H_2S generation, for instance aquathermolysis and pyrite oxidation, depend on the availability of S^{Pyrite} and $S^{Organic}$ compounds in reservoirs (Hutcheon, 1998; Lamoureux-Var and Lorant, 2005). Methods for S^{Pyrite} and $S^{Organic}$ quantification in sedimentary rocks are not only relevant for petroleum exploration and production but also support paleo-environmental/paleo-climate reconstructions. This recognises that both S^{Pyrite} and $S^{Organic}$ compounds are formed in particular and sometimes extreme depositional environments, such as euxinic environments in which both compounds can be formed in the water column (Raiswell and Berner, 1985; Freeman *et al.*, 1994; Wilkin and Barnes, 1997). S^{Pyrite} formation occurs by reaction of reduced sulphur species (HS, H_2S) with reactive iron (Berner, 1970; Vairavamurthy *et al.*, 1995; Baudin *et al.*, 2007) whereas $S^{Organic}$ compounds are formed by early diagenetic incorporation of reduced sulphur species into kerogen precursors (Vairavamurthy *et al.*, 1995). The formation of S^{Pyrite} and $S^{Organic}$ compounds are therefore competitive processes, with S^{Pyrite} formation as the predominant reaction depending on the availability of reactive iron minerals during times of deposition. The supply of reactive iron in marine settings is dominantly controlled by continental runoff, linking with precipitation, weathering and runoff dynamics in the hinterland, and thus climatic conditions.

Several established techniques are available to quantify S^{Pyrite} and $S^{Organic}$ in sediments, including elemental analysis of kerogens (e.g. Durand, 1980; Vandenbroucke and Largeau, 2007)

chromous chloride pyrite extraction combined with total sulphur combustion analysis (e.g. Canfield *et al.*, 1986; Acholla and Orr, 1993); Sulphur X-ray Absorption Near Edge Structure (S-XANES) (Vairavamurthy *et al.*, 1997; Bolin, 2010; Kelemen *et al.*, 2012; Bolin, 2014); and Electrothermal Vaporization Inductively Coupled Plasma Optical Emission Spectrometry (ETV-ICP OES) (Bauer *et al.*, 2014). However, these methods are often laborious, time-consuming, and none of them directly quantifies S^{Pyrite} and $S^{Organic}$ in the same analytical process. To conclude, up to now there is no quick/efficient and reliable quantitative methodology available to quantify fundamental S variables.

In this chapter, a new and rapid (2 hours per samples) method for S^{Pyrite} and $S^{Organic}$ quantification using Rock-Eval 7S is presented. Subdivided into three sub-chapters, the first one (Section 3.2) presents the development of the new Rock-Eval 7S method, based on pyrite thermal transformation and its interactions with kerogen and minerals during Rock-Eval 7S analysis. The second sub chapter (Section 3.3) presents validation of the new method using organic rich marine sediments, and some sedimentary mixtures. Figure 3. 1 shows a flow chart illustrating the different components of this chapter and the strategy applied in each.

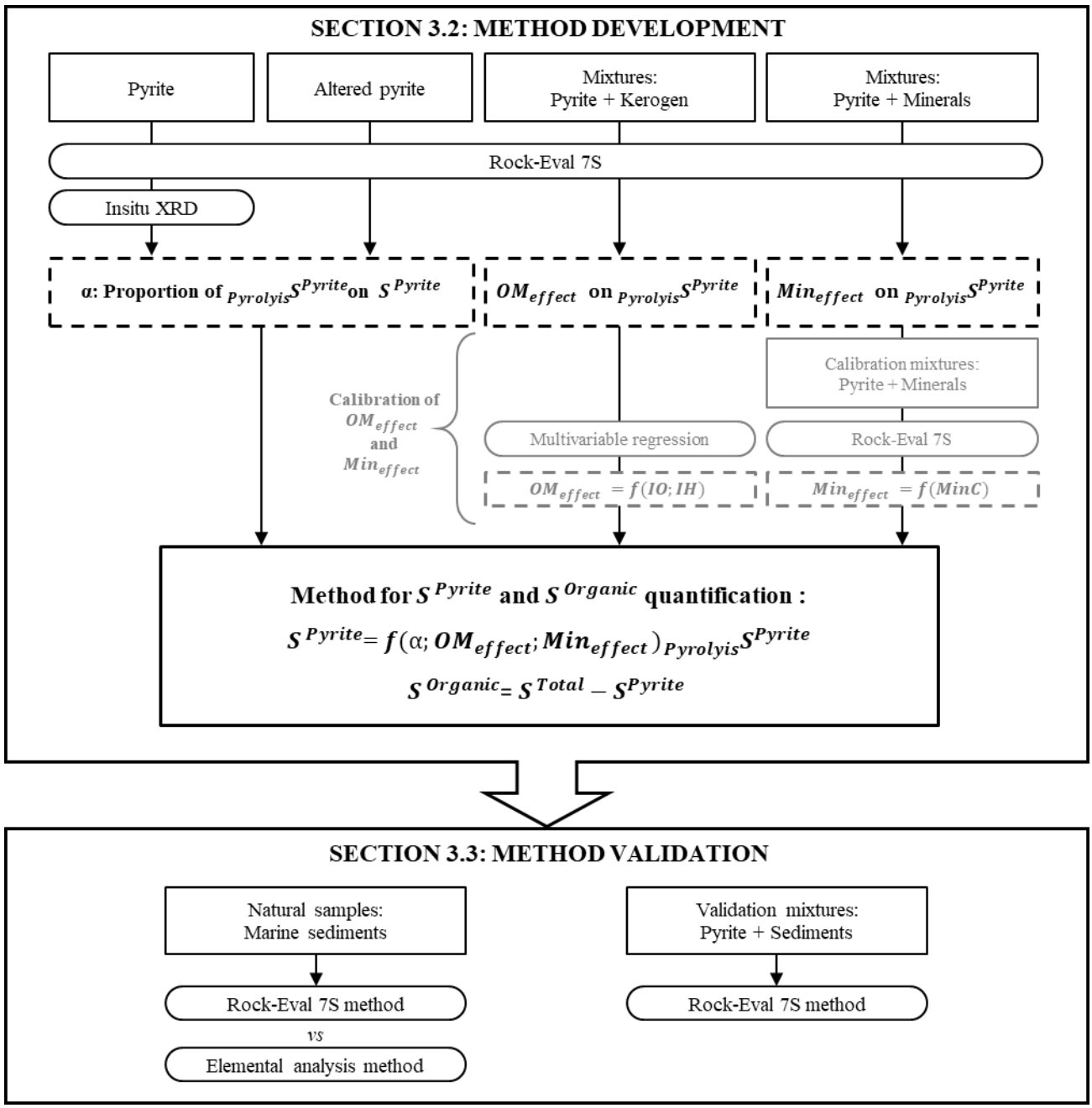

Figure 3. 1: Flow chart presenting the different sections of chapter 3 and the strategy applied in each section. (Pyrite = Pure igneous pyrite)

3.2- DEVELOPMENT OF A NEW METHOD FOR PYRITIC SULPHUR AND ORGANIC SULPHUR QUANTIFICATION USING ROCK-EVAL 7S

3.2.1- Introduction

To enhance its capabilities and applications, the new Rock-Eval-7S is equipped with an additional continuous sulphur detection system, allowing sulphur characterization parallel to carbon in one single analytical cycle. Two sulphur (SO_2) signals are obtained during analysis, corresponding to the pyrolysis and oxidation phases of the analytical cycle. The sulphur (SO_2) signals display several peaks that can be assigned to different sulphur compounds, including elemental sulphur ($S^{Elemental}$), organic sulphur ($S^{Organic}$), pyritic sulphur (S^{Pyrite}) and sulphates ($S^{Sulphates}$) (section 2.3.2). During the pyrolysis phase, ${}_{Pyrolysis}S^{Pyrite}$ and ${}_{Pyrolysis}S^{Organic}$ can be distinguished from each other and quantified separately because they are represented by two distinct SO_2 peaks. However, during the oxidation phase, ${}_{Oxidation}S^{Pyrite}$ and ${}_{Oxidation}S^{Organic}$ are covered by one single peak (section 2.3.2), making a distinction between sulphur components impossible. Further challenges arise as chemical reactions, occurring during the analytical cycle, may modify the original sulphur compounds.

This study presents the development of a novel method that addresses these fundamental issues with the new Rock-Eval 7S system. A four-stage approach was used: (i) To decipher pyrite thermal transformation during analysis, in order to determine the percentage of ${}_{Pyrolysis}S^{Pyrite}$ as part of the total S^{Pyrite} content; (ii) To quantify the effect of organic and mineral species commonly found in organic rich marine sediments based on the amount of ${}_{Pyrolysis}S^{Pyrite}$ released during the pyrolysis stage. (iii) To determine the total S^{Pyrite} content in a sedimentary rock, depending on its ${}_{Pyrolysis}S^{Pyrite}$ content and on its organic and mineral composition. (iv) To deduce the total $S^{Organic}$ content by difference between its S^{Total} and its S^{Pyrite} content. In combination, this new approach aims to provide an accurate speciation of S^{Pyrite} and $S^{Organic}$ in organic-rich marine sediments.

3.2.2- Samples and methods

3.2.2.1- Samples

- <u>Pure igneous pyrite sample</u>:

An igneous pyrite sample was crushed in a zircon oxide ball mill, and then exposed to multiple acid attacks to remove any surface oxides and impurities, consistent with the 5 days in-house

procedures for kerogen isolation at IFP Energies nouvelles (Vandenbroucke and Largeau, 2007). The following acids were used sequentially, each being followed by a rinse with hot deionized water: (i) Hydrochloric acid (6 N HCl); (ii) 1:2 mixture of Hydrofluoric acid (40% HF) and Hydrochloric acid (6 N HCl); (iii) Hydrochloric acid (6 N HCl).

This protocol quantitatively destroys all major mineral impurities in the pyrite sample (carbonates, metal sulphides, sulphate hydroxides, clay minerals, quartz and other silicates), but has been shown not to have a substantial impact on pyrite (Vandenbroucke and Largeau, 2007). After the acid treatment, the remaining pyrite sample was dried at 100°C under nitrogen flow and conserved in a glove box under nitrogen atmosphere to avoid any oxidation. The characterisation of the cleaned igneous pyrite by X-Ray Diffraction (XRD), performed at IFPEN using PANalytical X'Pert Pro diffractometer, revealed no impurities. This cleaned igneous pyrite is named "pure igneous pyrite".

- Altered igneous pyrite sample:

Altered igneous pyrite samples were prepared by surface oxidation of the pure igneous pyrite sample using two techniques:

❖ Chemical oxidation: the pure igneous pyrite powder was treated using a basic aqueous solution (KOH, pH=14) for one week, in ambient atmosphere at 25°C. After this treatment, the altered igneous pyrite sample was rinsed with deionized water and dried at 25°C in ambient atmosphere. This experimental protocol was modified after Karthe *et al.* (1993).

❖ Thermal oxidation: the pure igneous pyrite powder was heated from 200°C to 450°C with a heating rate of 10°C/min, under an air flow of 100mL/min. This thermal oxidation of the pure igneous pyrite sample was performed using the Rock-Eval oxidation oven. The experimental protocol was inspired by Hu *et al.* (2006).

- Mixtures "pure igneous pyrite + kerogens":

We prepared mixtures composed of 2mg of pure igneous pyrite and 4mg of various kerogen samples (Table 3. 1), kerogen isolation being performed using the standard in-house kerogen isolation method (Vandenbroucke and Largeau, 2007). These mixtures "pure igneous pyrite + kerogens" were realised to be as representative of natural organic rich marine sediments as possible, within the technical limitations of the applied methods (e.g. reproducibility and saturation of detectors). All selected kerogen samples are thermally immature or in the early oil window and correspond to the main

existing kerogen types (Table 3. 1). Some of the kerogen samples were artificially oxidized, in a ventilated oven at 140°C during 2, 5 and 11 days, in order to get highly oxidized kerogen samples.

- Mixtures "pure igneous pyrite + minerals":

Mixtures composed of 2mg of pure igneous pyrite and 58mg of different mineral types were prepared (Table 3. 2). Again, these mixtures are realised to mimic natural organic rich marine sediments, within the technical limitations of the applied methods. Various silicate minerals and carbonate minerals were used in this study (Table 3. 2).

Kerogen types	Formations/Wells	Ages	Locations	References
Type I	Green River Shale	Eocene	USA	Ruble *et al.*, 2001
Type II	"Schistes carton"	Toarcian	France	Huc, 1977 Mackenzie *et al.*, 1981
Type II	ODP 959	Coniacian-Santonian	Ivory coast - Ghana	Wagner, 2002
Type IIS	Phosphoria Fm.	Permian	USA	Lewan and Ruble, 2002
Artificially oxidized type II (during 2, 5 and 11 days)	"Schistes carton"	Toarcian	France	Oxidized following Landais *et al.*, 1991
Type III	Calvert Bluff Fm.	Palaeocene	USA	Behar *et al.*, 2008
Artificially oxidized type III (during 2 and 5 days)	Calvert Bluff Fm.	Palaeocene	USA	Oxidized following Landais *et al.*, 1991
Mixtures Type II and type III	"Schistes carton" - Calvert Bluff Fm.	Toarcian - Paleocene	France - USA	Mackenzie *et al.*, 1981 Behar *et al.*, 2008

Table 3. 1: Kerogen samples used in mixtures of "2mgpure igneous pyrite+ 4mgkerogen"

	Minerals	Locations/References
Silicate minerals	Quartz	Fontainebleau sand, France
	Kaolinite	Reference: CMS KGa 1b
	Illite	Decarbonated "Clay of Velay", France
	Smectite	Reference: Mx80
Carbonates minerals	Calcite	Pillot *et al.*, 2013
	Dolomite	
	Siderite	

Table 3. 2: Mineral samples used in mixtures of "pure igneous pyrite+ minerals"

3.2.2.2- Rock-Eval 7S analyses

Rock-Eval 7S analysis allows the quantification of S^{Total} contents of samples, calculated as the sum of ${}_{Pyrolysis}S^{Total}$ and ${}_{Oxidation}S^{Total}$ (section 2.2), using the "total sulphur" temperature program:

- Pyrolysis: 300°C to 650°C, with a heating rate of 25°C/min, under nitrogen flow of 150mL/min;
- Oxidation: 300°C to 1200°C, with a heating rate of 20°C/min, under air flow of 100mL/min.

We performed duplicate or triplicate Rock-Eval 7S analyses of the different selected samples. In a first step, the pure igneous pyrite sample was analysed to determine the proportion of sulphur released from pyrite during the pyrolysis phase (${}_{Pyrolysis}S^{Pyrite}$) on its total S^{Pyrite} content. In a second step, each altered igneous pyrite sample was analysed to determine the proportion of ${}_{Pyrolysis}S^{Pyrite}$ released from altered pyrite during the pyrolysis phase on its total S^{Pyrite} content. In a third step, the mixtures "pure igneous pyrite + kerogens" and "pure igneous pyrite + minerals" were analysed in the same way to study, respectively, the organic matter effects (OM_{effect}) and mineral effects (Min_{effect}) on the amount of ${}_{Pyrolysis}S^{Pyrite}$ released during the pyrolysis.

3.2.2.3- In-situ XRD analyses

In-situ X-ray diffraction (*in-situ* XRD) is a technique to monitor changes in crystal structure or crystal phase transformations, resulting from a determined temperature program and under controlled atmospheric conditions. Here, we performed an *in-situ* XRD analysis on the pure igneous pyrite sample using PANalytical X'Pert Pro diffractometer. This aims to characterise pyrite crystal phase transformations during a basic Rock-Eval 7S cycle:

- Pyrolysis: 300°C to 650°C, with a heating rate of 25°C/min, under nitrogen flux of 150mL/min;
- Oxidation: 300°C to 850°C, with a heating rate of 20°C/min, under air flux of 100mL/min.

The goal of this *in-situ* XRD analysis was to verify the accordance between the amount of sulphur released from pyrite during the pyrolysis and oxidation phases of Rock-Eval 7S, and the pyrite crystal phase transformations. The crystal phase identification was realized using the crystallography interpretation software AXCore, using the Crystallography Open Database (COD).

3.2.3- Results

3.2.3.1- Pure igneous pyrite thermal transformation during Rock-Eval 7S analysis

The SO_2 signals gathered from the Rock-Eval 7S analysis of different masses of pure igneous pyrite are shown in Figure 3. 2. Two peaks corresponding to the pyrite thermal transformation are observed, one during the pyrolysis phase, between 610°C - 650°C, and a second during the oxidation phase, at around 400°C - 420°C. An artefact peak is identified at 300°C during the pyrolysis phase which is not present in the Rock-Eval 7S pyrolysis signal of bulk pyrite sample (Figure 2.3). This peak which represents about 1 to 2 wt.% of pyrite total sulphur content is likely related to the presence of labile sulphur compounds, such as elemental sulphur, which have an identical Rock-Eval fingerprint (section 2.3.2). It is assumed that these labile sulphur compounds have been formed by acid treatment when purifying the igneous pyrite sample prior to Rock-Eval analysis.

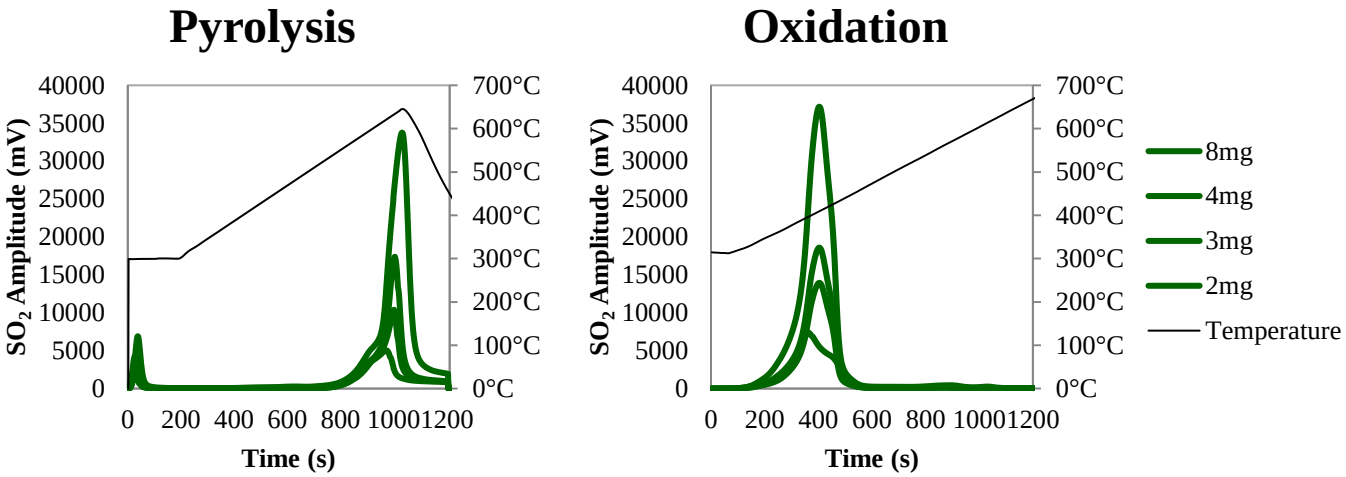

Figure 3. 2: Rock-Eval 7S SO_2 signals of different masses of pure igneous pyrite

Results from Rock-Eval 7S analyses of different masses of the pure igneous pyrite sample show linearity between the area of the SO_2 peaks and the sample mass of pyrite, both during the pyrolysis phase and the oxidation phase (Figure 3. 3). From the areas of the SO_2 peak in the pyrolysis and the oxidation phases, using a phase-specific calibration coefficient (section 2.2), the sulphur content was independently calculated ($_{Pyrolysis}S^{Pyrite}$ and $_{Oxidation}S^{Pyrite}$). The sulphur content from both phases represents the mass of sulphur released during each phase divided by the total mass of the sample. The total S^{Pyrite} content was calculated by summing the $_{Pyrolysis}S^{Pyrite}$ and the $_{Oxidation}S^{Pyrite}$ contents, representing the total mass of sulphur divided by the total mass of the sample.

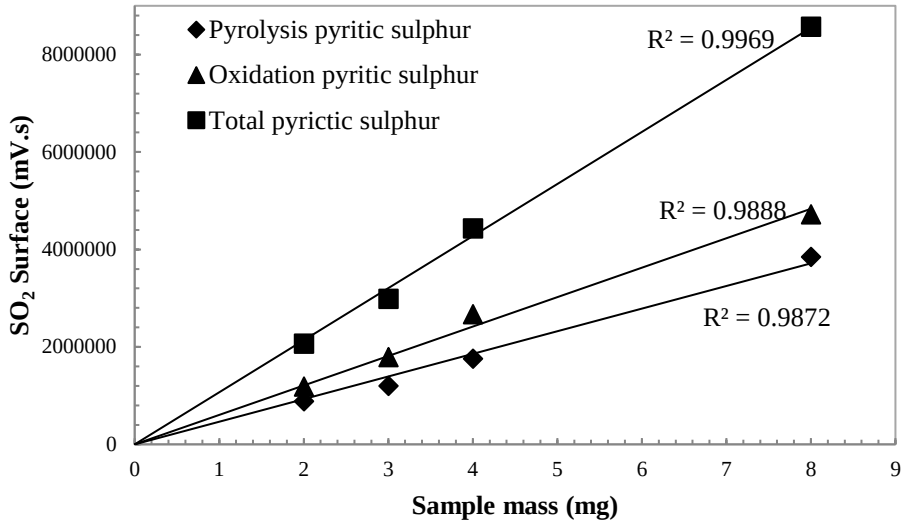

Figure 3. 3: Rock-Eval 7S response linearity between the areas of the SO_2 peak and the sample mass of pyrite

Table 3. 3 summarises the Rock-Eval 7S sulphur results of different masses of the pure igneous pyrite sample. The average ${}_{Pyrolysis}S^{Pyrite}$ content is 23wt% ± 2wt%. The artefact peak observed during the pyrolysis phase has been accounted for in the calculation of pyrolysis sulphur content, recognising that sulphur mass balances show that it is a part of the original ${}_{Pyrolysis}S^{Pyrite}$ content. The average ${}_{Oxidation}S^{Pyrite}$ content of the pure igneous pyrite sample is 31wt% ± 1wt%. This adds up to an average total S^{Pyrite} content of 54wt% ± 2wt%, which corresponds to weight percentage of sulphur in pyrite and confirms that pyrite released all its sulphur during analysis. From these results, it is possible to calculate the proportion of ${}_{Pyrolysis}S^{Pyrite}$ released during the pyrolysis phase and the proportion of ${}_{Oxidation}S^{Pyrite}$ released during the oxidation phase from the total S^{Pyrite}, as follows:

$$\%Pyrolysis\ pyritic\ sulphur\ on\ the\ total\ pyritic\ sulphur = \left(\frac{{}_{Pyrolysis}S^{Pyrite}}{S^{Pyrite}}\right) * 100$$

$$\%Oxidation\ pyritic\ sulphur\ on\ the\ total\ pyritic\ sulphur = \left(\frac{{}_{Oxidation}S^{Pyrite}}{S^{Pyrite}}\right) * 100$$

These calculations indicate that the proportion of ${}_{Pyrolysis}S^{Pyrite}$ on the total S^{Pyrite} is 42% ± 2%, with the remaining 58% ± 2% being mobilized during the oxidation phase (Table 3. 3).

									Average	Standard deviation
Sample mass (mg)	2	2	2	3	3	3	4	8	~	~
$_{Pyrolysis}S^{Pyrite}$ (wt%)	22	25	23	24	21	20	22	24	**23**	**2**
$_{Oxidation}S^{Pyrite}$ (wt%)	31	31	33	30	31	31	33	30	**31**	**1**
S^{Pyrite} (wt%)	53	55	56	54	51	51	55	54	**54**	**2**
Proportion of $_{Pyrolysis}S^{Pyrite}$ on S^{Pyrite} (%)	41	45	41	45	41	39	40	45	**42**	**2**
Proportion of $_{Oxidation}S^{Pyrite}$ on $_{Pyrolysis}S^{Pyrite}$ (%)	59	55	59	55	59	61	60	55	**58**	**2**

Table 3. 3: Rock-Eval 7S results of sulphur content of the pure igneous pyrite sample

The *in-situ* XRD analysis of the pure igneous pyrite allows the observation of pyrite (FeS_2) crystal phase transformation into pyrrhotite (Fe_7S_8) during the pyrolysis phase, followed by the oxidation of the newly formed pyrrhotite (Fe_7S_8) into hematite (Fe_2O_3) during the oxidation phase (Figure 3. 4). These reactions are represented by the following chemical equations, the stoichiometric coefficients of which are constrained by the molecular formula:

Pyrolysis: $FeS_2(s) \rightarrow {}^{1}/_{7}\ Fe_7S_8\ (s) + {}^{3}/_{7}\ S_2\ (g)$

Oxidation: ${}^{1}/_{7}\ Fe_7S_8\ (s) + {}^{53}/_{14}\ O_2\ (g) \rightarrow {}^{1}/_{2}\ Fe_2O_3\ (s) + {}^{8}/_{7}\ SO_2\ (g)$

Accordingly, during pyrolysis, 1 mole of pyrite (FeS_2) releases ${}^{3}/_{7}$ moles of S_2 (0.8571 moles of S) corresponding to 42.86% of the total S^{Pyrite}. During the oxidation phase, the remaining sulphur content of pyrite ${}^{8}/_{7}$ moles of SO_2 (1.1428 moles of S) is released, corresponding to 57.14% of the total S^{Pyrite}.

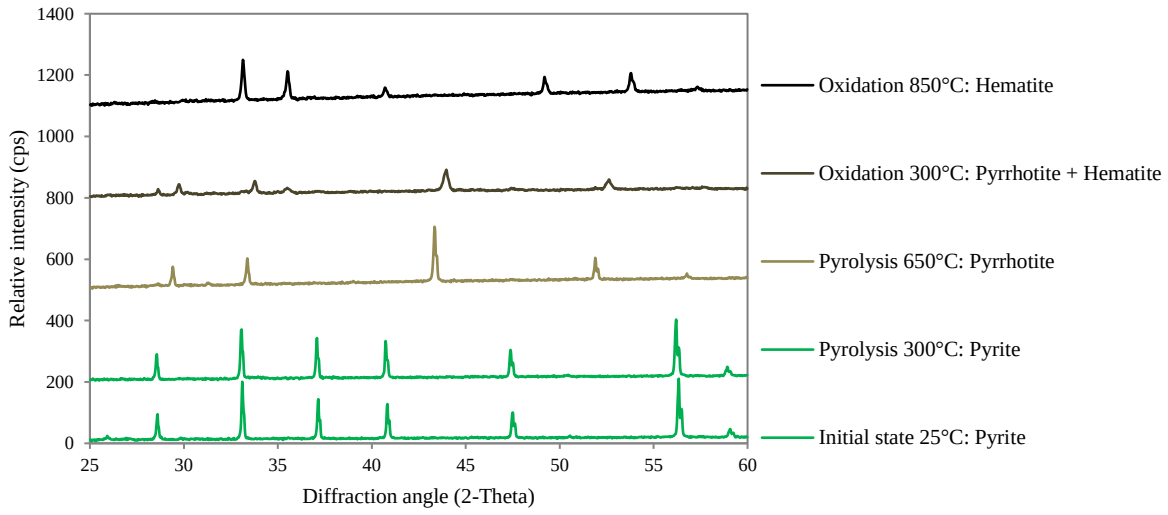

Figure 3. 4: *In-situ* XRD analyses of a pure igneous pyrite sample simulating the conditions created during Rock-Eval 7S analysis

These results from the in-situ XRD and Rock-Eval 7S analyses are highly consistent, building confidence that there is thermal transformation of pyrite (FeS_2) into pyrrhotite (Fe_7S_8), during the Rock-Eval 7S pyrolysis phase, releasing about 43% of its total sulphur, and during the oxidation phase the newly formed pyrrhotite (Fe_7S_8) is transformed into hematite (Fe_2O_3) releasing the remaining 57% of pyrite total sulphur content.

3.2.3.2- Altered pyrite thermal transformation during Rock-Eval 7S pyrolysis

The Rock-Eval 7S sulphur results of the different altered pyrite samples are summarized in Table 3. 4. The total S^{Pyrite} content is 23wt% for the thermally altered pyrite sample and 35wt% ± 1wt% for the chemically altered pyrite sample, while the S^{Pyrite} content of the original, unaltered pyrite (stoichiometrically, and as determined by Rock-Eval 7S) is about 54wt% ± 2wt%. These results confirm that the surface oxidation/alteration experiments lead to lower the original sulphur contents of pyrite.

During pyrolysis, altered pyrite samples are degraded before the normal pyrite sample (Appendix D). This could be related to the fact that the different oxidation technics result to weaken the crystal structure of pyrite particles, leading to altered pyrite samples more thermally reactive than the normal pyrite sample (Appendix D).

The proportion of ${}_{Pyrolysis}S^{pyrite}$ as part of the total S^{Pyrite} were calculated for each altered pyrite sample (Table 3. 4). It represents 35% ±1% for the thermally altered pyrite sample and 40% ±1% for the chemically altered pyrite sample, while it is 42% ±2% for the original, unaltered pyrite. The results show that the proportions of ${}_{Pyrolysis}S^{Pyrite}$ released from the altered pyrite samples during pyrolysis as part of their total S^{Pyrite} (34% to 41%) is distinct from the proportion of ${}_{Pyrolysis}S^{Pyrite}$ released from the unlatered pyrite sample as part of its total S^{Pyrite} (40% to 44%). This indicates that the level of pyrite alteration can have a considerable impact (up to 23%) on the pyrolysis results.

	${}_{Pyrolysis}S^{Pyrite}$ (wt%)	**S^{Pyrite} (wt%)**	**${}_{Pyrolysis}S^{Pyrite}$ / S^{Pyrite} (%)**
Thermally altered pyrite	8 ± 0	23 ± 0	35 ± 1
Chemically altered pyrite	14 ± 1	35 ± 1	40 ± 1
Unaltered pyrite	23 ± 2	54 ± 2	42 ± 2

Table 3. 4: Rock-Eval 7S results of sulphur content of the altered pyrite samples *vs* the unaltered pyrite sample

3.2.3.3- Interactions between pyrite and kerogens during Rock-Eval 7S pyrolysis

The Rock-Eval 7S analysis of different mixtures "pure igneous pyrite + kerogen" aims to study interactions of both compounds during the pyrolysis phase. Two principal behaviours are observed. (i) The pyrolysis sulphur signals of mixtures "pure igneous pyrite + type I, II and IIS kerogens", presented in Table 3. 1, represent a proportionate combination of the pure igneous pyrite signal and of the kerogen signal. One example of this behaviour is shown for the mixture "pyrite + type II kerogen" in Figure 3. 5a. In these cases, there is no significant interaction between pyrite and kerogen during pyrolysis. (ii) Different from that, the pyrite peaks of the other mixtures "pure igneous pyrite + kerogen", presented in Table 3. 1, show lower amplitude than the expected sulphur signal of pure igneous pyrite sample, as shown for the mixture "pyrite + type III kerogen" (Figure 3. 5b). Pyrite peak temperature of mixtures "pyrite + kerogen" (Figure 3. 5b) are in the same range as those of pure igneous pyrite (610°C-650°C), suggesting that pyrite thermal transformation into pyrrhotite also occurs in "pyrite + kerogen" mixtures. This implies that part of the amount of sulphur released from pyrite thermal transformation during pyrolysis is trapped and incorporated in the kerogen char. Indeed, as kerogen is being thermally degraded at much lower temperature than pyrite (Appendix E) (Figure 3. 5b), it seems possible that active carbon sites in the kerogen fraction trap sulphur released from pyrite pyrolysis as newly formed and strongly bound organic sulphur compound. These newly formed organic sulphur compounds, transferred from stable pyrite, are only degraded during the oxidation phase, leading to a disproportionate and unexpectedly high residual peak during the oxidation stage (Figure 3. 5b). Effectively, this thermochemical process during pyrolysis transfers sulphur from an inorganic to an organic form, thus biasing the results of the Rock-Eval 7S analysis.

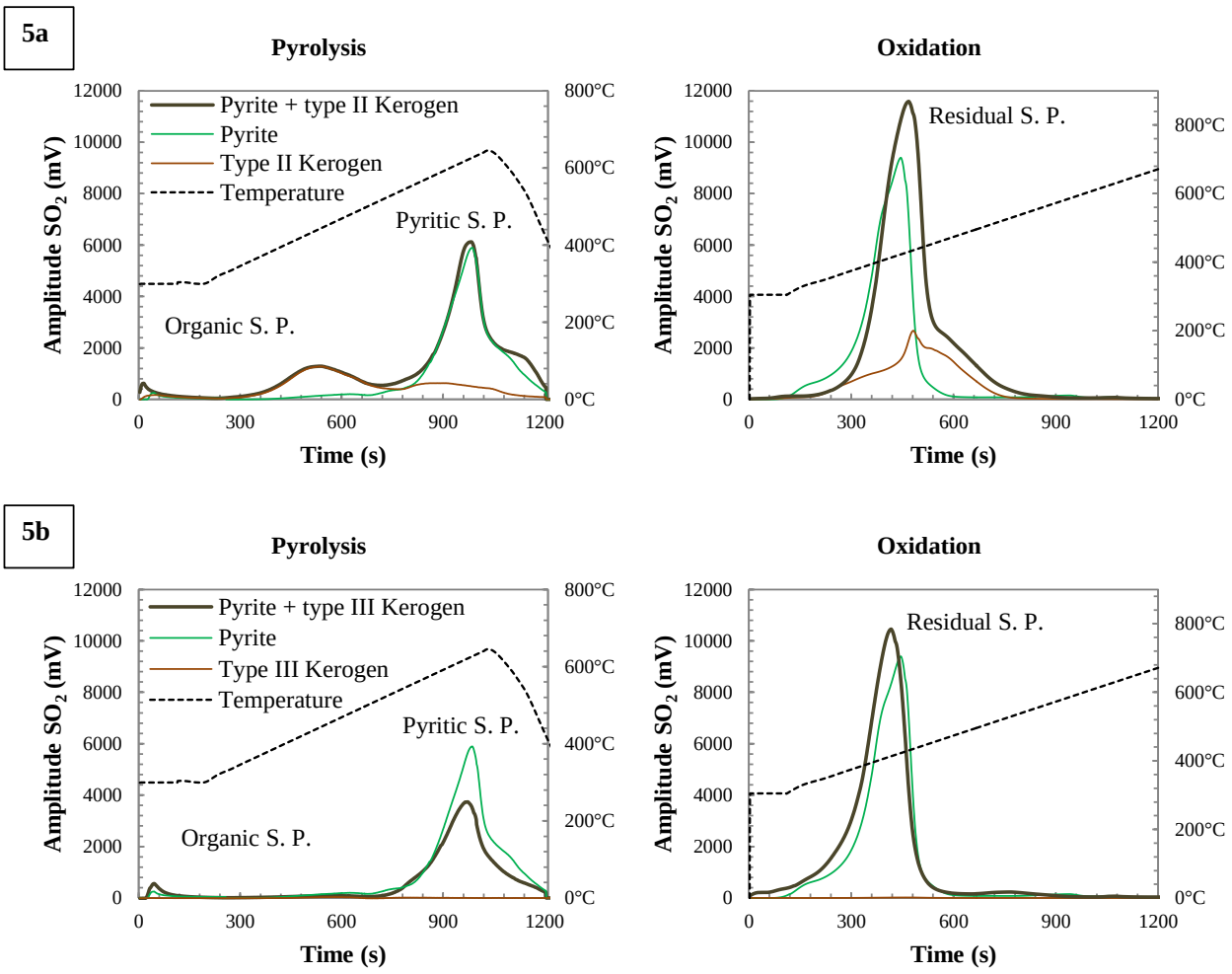

Figure 3. 5: 5a) Rock-Eval 7S sulphur signals of mixtures (pure igneous pyrite + type II kerogen), of the pure igneous pyrite and of type II kerogen sample. 5b) Rock-Eval 7S sulphur signal of mixtures (pure igneous pyrite + type III kerogen), of the pure igneous pyrite and of type III kerogen sample. S. P.: sulphur peaks

We name this behaviour "OM_{effect}", representing the percentage of ${}_{Pyrolysis}S^{Pyrite}$ trapped by the kerogen matrix during the pyrolysis phase. The OM_{effect} can be calculated using the following formula (Appendix F and G):

$$\boldsymbol{OM_{effect}}\,(\mathbf{wt\%}) = \left(\frac{\boldsymbol{Expected\ S_{pyrolysis}^{mixtures\ "pyrite+kerogen"}} - \boldsymbol{Obtained\ S_{pyrolysis}^{mixtures\ "pyrite+kerogen"}}}{\boldsymbol{Expected\ S_{pyrolysis}^{mixtures\ "pyrite+kerogen"}}}\right) * \mathbf{100}$$

$\boldsymbol{Expected\ S_{pyrolysis}^{mixtures\ "pyrite+kerogen"}}$: *Pyrolysis sulphur content of mixtures "pyrite + kerogen" expected if there is no interactions between pyrite and kerogen samples during the pyrolysis phase. It is obtained by adding proportionally the pyrolysis sulphur content of the pyrite sample alone and the pyrolysis sulphur content of the kerogen sample alone.*

$\boldsymbol{Obtained\ S_{pyrolysis}^{mixtures\ "pyrite+kerogen"}}$ *: Pyrolysis sulphur content of the mixtures "pyrite + kerogen" obtained by Rock-Eval 7S analysis.*

Figure 3. 6 shows the OM_{effect} of each studied kerogen type as a function of their respective Hydrogen Index (HI) and Oxygen Index (OI). A negative trend between OM_{effect} and HI, and a marked positive trend between OM_{effect} and OI is observed, showing that the OM_{effect} on the amount of ${}_{Pyrolysis}S^{Pyrite}$ transferred into organic sulphur compounds is more pronounced for kerogen with low HI and high OI, and ranges from 0wt.% to about 40wt.%.

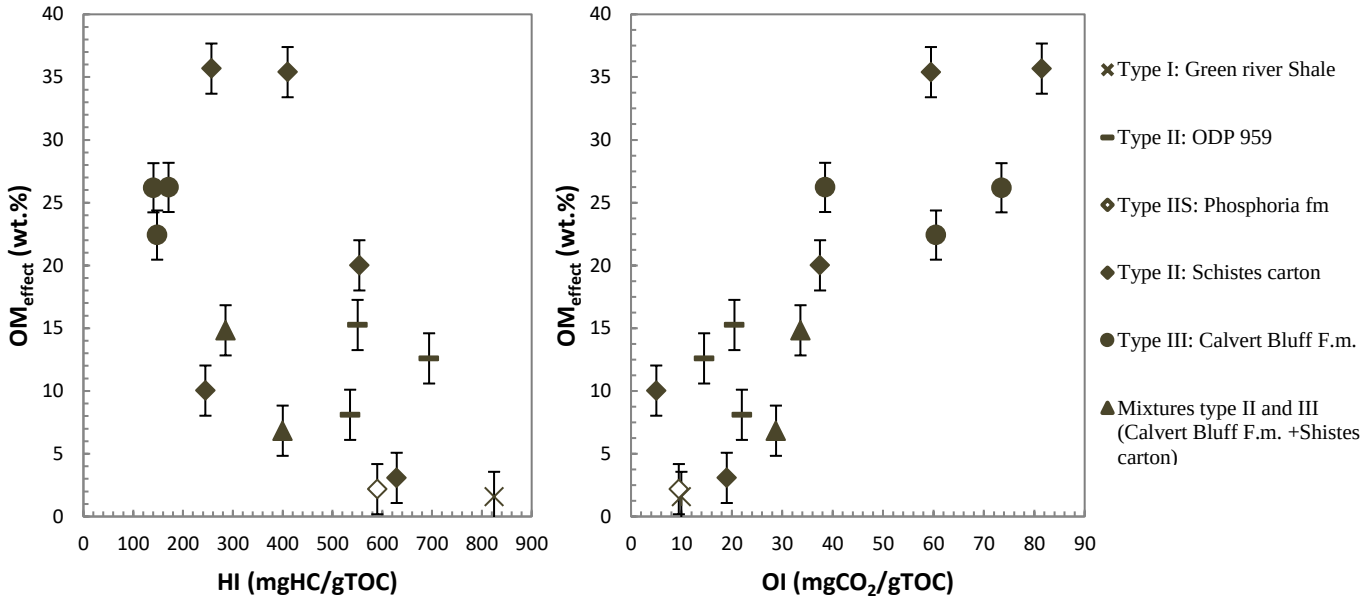

Figure 3. 6: Evolution of the OM_{effect} in function of the Hydrogen Index (HI) and in function of the Oxygen Index (OI)

3.2.3.4- Interactions between pyrite and minerals during Rock-Eval 7S pyrolysis

The interactions between pyrite and minerals during the pyrolysis phase were studied by comparing the pyrolysis sulphur signal of the pure igneous pyrite sample to pyrolysis sulphur signals of the different "pure igneous pyrite + mineral" mixtures. The Rock-Eval 7S sulphur signals of the different "pure igneous pyrite + mineral" mixtures are illustrated in Figure 3. 7, for silicate minerals and for carbonate minerals in Figure 3. 8.

During pyrolysis, mixtures "pyrite + silicates" present almost the same signal amplitude as the reference analysis of pyrite. An exception is the mixture "pyrite + smectite" (Figure 3. 7), where the pyrolysis sulphur signal is lower than expected. Pyrite peak temperatures of mixture "pyrite + smectite" (Figure 3. 7) are in the same range as recorded for pure igneous pyrite (610°C-650°C), suggesting that pyrite thermal transformation into pyrrhotite occurs just as for pure igneous pyrite. We therefore

suggest that part of the sulphur released from pyrite thermal transformation is trapped by smectite minerals. The oxidation sulphur signal of mixture “pyrite + smectite” reveals refractory sulphur peaks presenting similar fingerprint as sulphate minerals (sulphate peaks) (section 2.3.2), and which have not been identified in the pure pyrite or smectite samples (Figure 3. 7).

The presence of carbonate minerals, during the pyrolysis phase, considerably reduces the sulphur signal amplitude of pyrite (Figure 3. 8). Indeed, as for smectite minerals, part of the sulphur released from pyrite thermal transformation seems to get trapped by carbonate minerals. The following oxidation signals of mixture “pyrite + carbonate minerals” (Figure 3. 8) present new sulphate peaks in the case of calcite and dolomite, and higher sulphate peaks in the case of siderite which already contain some sulphur impurities.

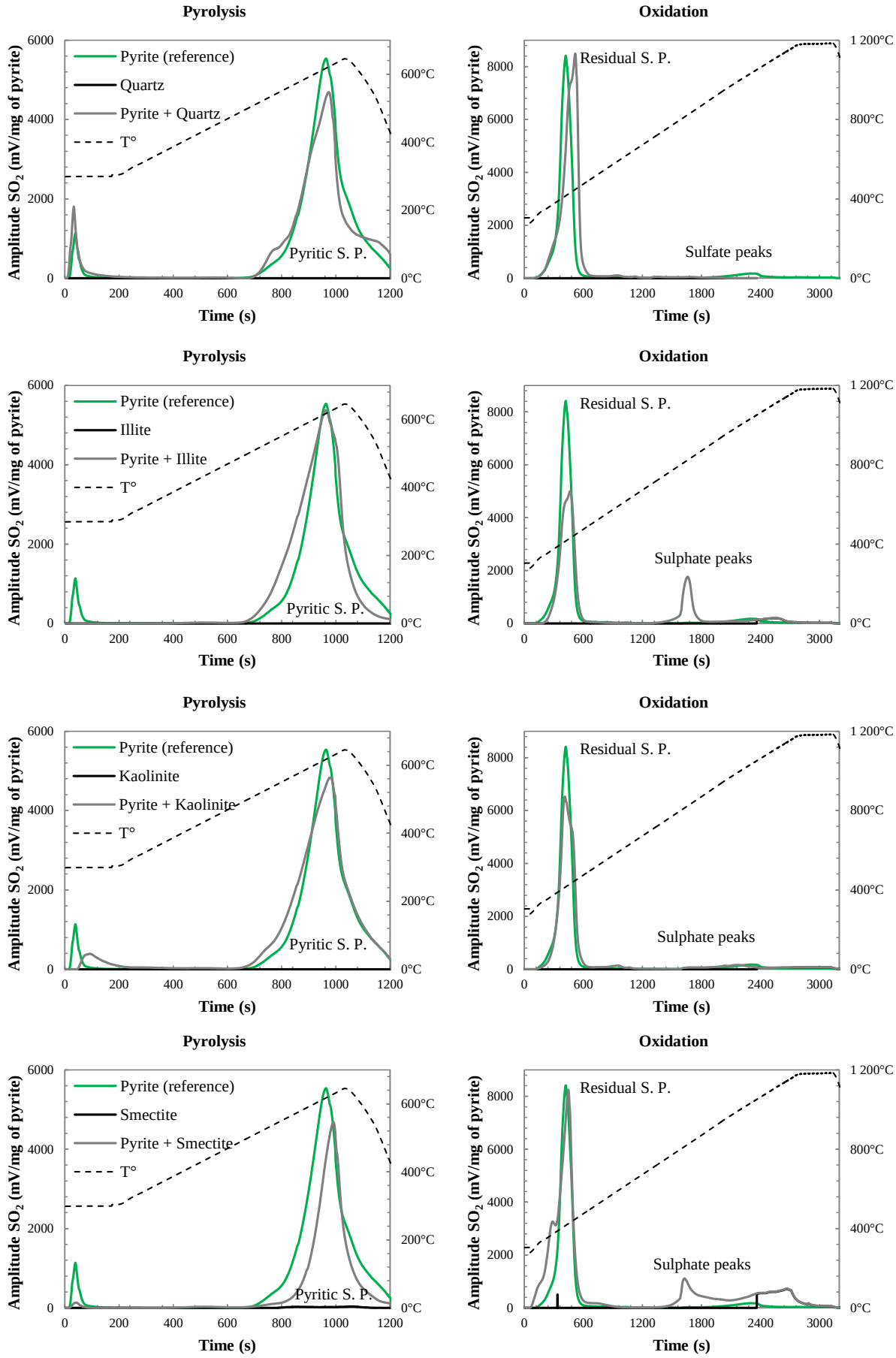

Figure 3. 7: Rock-Eval 7S sulphur signal of pyrite sample and sulphur signal of mixtures pure igneous pyrite + silicate minerals. S. P. (sulphur peaks)

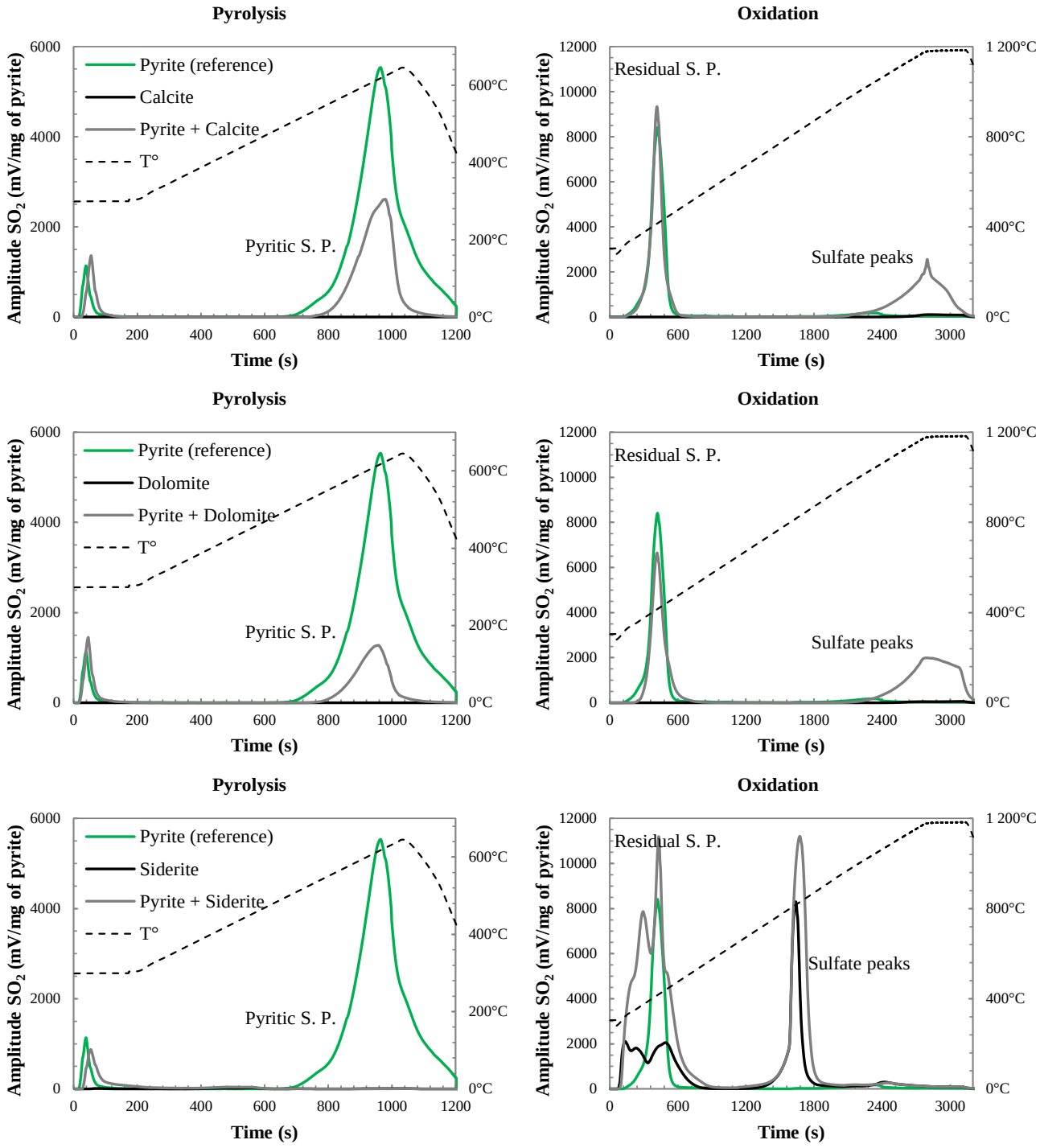

Figure 3. 8: Rock-Eval 7S sulphur signal of pyrite sample and sulphur signal of mixtures pure igneous "pyrite + carbonate minerals". S. P. (sulphur peaks)

Consistent with the OM_{effect}, we define the Min_{effect} as the percentage of ${}_{Pyrolysis}S^{Pyrite}$ transferred into the mineral residues during the Rock-Eval 7S pyrolysis, calculated as below (Appendix H):

$$\boldsymbol{Min_{effect}}\,(\mathbf{wt.\%}) = \left(\frac{\boldsymbol{Expected\ S_{pyrolysis}^{mixtures\ "pyrite+mineral"}} - \boldsymbol{Obtained\ S_{pyrolysis}^{mixtures\ "pyrite+mineral"}}}{\boldsymbol{Expected\ S_{pyrolysis}^{mixtures\ "pyrite+mineral"}}}\right) * \mathbf{100}$$

$\boldsymbol{Expected\ S_{pyrolysis}^{mixtures\ "pyrite+mineral"}}$: *Pyrolysis sulphur content of mixtures "pyrite + mineral" expected if there is no interactions between pyrite and mineral samples during the pyrolysis phase. It is obtained by adding proportionally the pyrolysis sulphur content of the pyrite sample alone and the pyrolysis sulphur content of the mineral sample alone.*

$\boldsymbol{Obtained\ S_{pyrolysis}^{mixtures\ "pyrite+mineral"}}$ *: Pyrolysis sulphur content of the mixtures "pyrite + mineral" obtained by Rock-Eval 7S analysis.*

Figure 3. 9 show the Min_{effect} of each mineral type. As already observed, silicate minerals do not show a significant Min_{effect}, except for smectite, which reduces the amount of ${}_{Pyrolysis}S^{Pyrite}$ released during Rock-Eval 7S pyrolysis by about 40% relative to the pure ${}_{Pyrolysis}S^{Pyrite}$ amount. In contrast, carbonate minerals show a strong effect on the amount of ${}_{Pyrolysis}S^{Pyrite}$ expected to be released during pyrolysis, varying according to the carbonate mineral type between ~ 60% for calcite, ~79% for dolomite and ~95% for siderite.

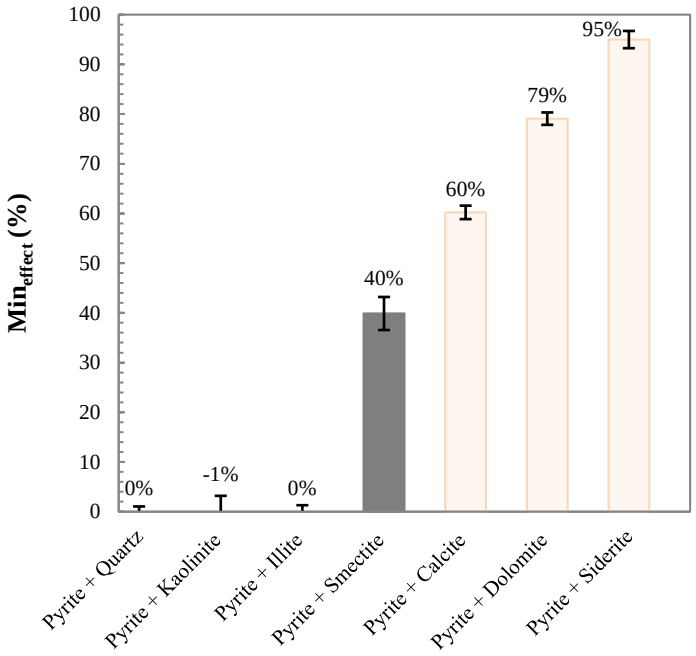

Figure 3. 9: Min_{effect} on the amount of ${}_{Pyrolysis}S^{Pyrite}$ released during Rock-Eval 7S pyrolysis phase for each mineral

3.2.4- Discussions

3.2.4.1- Pyrite thermal transformation during Rock-Eval 7S pyrolysis and its interaction with organic and mineral species commonly found in organic rich marine sediments

Results from Rock-Eval 7S and *in-situ* XRD analyses of the pure igneous pyrite sample show that during the Rock-Eval 7S pyrolysis phase there is thermal transformation of pyrite (FeS_2) into pyrrhotite (Fe_7S_8) releasing about 43% of the pyrite's original total sulphur content. This principle transformation process is consistent with findings of earlier pyrolysis experiments (Coats and Bright, 1966; Lambert *et al.*, 1980; Boyabat *et al.*, 2004). It must be noted, however, that different factors impact the degree of pyrite thermal transformation during pyrolysis, including gas flow rate, reaction temperature, duration time, and the pyrite particle size (Boyabat *et al.*, 2004). For Rock-Eval 7S pyrolysis, gas flow rate, reaction temperature and duration time are fixed, and the pyrite particle size can also be fixed by a fine crushing of sample (<200µm), as recommended by Espitalie *et al.*, 1985. This suggests that pyrite will always present the same degree of thermal transformation during a basic Rock-Eval pyrolysis phase.

The pure pyrite sample studied has an igneous origin and formed under high temperatures and pressures, whereas pyrite in organic rich marine sediments is typically formed in the water column or during low-temperature diagenesis, raising the question if these two types of pyrite have identical thermal reactivity. Kelemen *et al.* (2012) and Bolin (2014) in their pyrolysis experiments show also that sedimentary pyrite (FeS_2) is transformed into pyrrhotite (Fe_7S_8) and troilite (FeS) at an equivalent maturity of Ro = 2.4%, which translates to conditions established at the end of the Rock-Eval pyrolysis phase. The fraction of pyrrhotite formed ranges from 100% to 49% and the fraction of troilite from 0% to 51%. Using these results, the proportion of sulphur released from sedimentary pyrite during similar conditions has been calculated to be between 43% and 47%. We observe that the proportion of sulphur released from sedimentary pyrite during pyrolysis (Kelemen *et al.*, 2012; Bolin, 2014) is very close to the proportion of sulphur released during pyrolysis from igneous pyrite (43% - 47% *vs* 40% - 44%, respectively). The slight difference can easily be attributed to different experimental protocols. Igneous pyrite thermal transformation during the pyrolysis phase of Rock-Eval 7S therefore seems to be representative of sedimentary pyrite thermal transformation.

In organic-rich marine sediments, at least a fraction of the pyrite particles is likely to be altered, for example, through oxidative loss of sulphur during surface weathering (Raiswell and Berner, 1986). Weathering or other alteration processes often lead to formation of oxic rims (Fe_3O_4) on pyrite grains (Fruit *et al.*, 1995; Brothers *et al.*, 1996). The alteration experiments performed in this study aimed to generate oxic rims on pyrite particles (Karthe *et al.*, 1993; Hu *et al.*, 2006), to verify if their presence

has a detectable effect on the proportion of sulphur released from pyrite during pyrolysis. The results obtained show that the presence of oxic rims on altered pyrite grains lead to a potentially significant reduction (up to 23%) of the proportion of sulphur released from pyrite during the pyrolysis stage. However, this reduction percentage represent a maximun pyrite alteration effect in cases were all pyrite particles are highly alterred. And, this is not representative of the majority of marine sediments.

Results from Rock-Eval 7S analysis of mixture "pure igneous pyrite + kerogen" highlight the fact that the OM content of marine sediments can trap sulphur released during pyrite pyrolysis. This observation is consistent with other studies which show that sulphur from pyrite thermal transformation, under closed or restricted pyrolysis conditions, can be incorporated into solid macromolecular OM char resulting in the formation of new organic sulphur compounds (Cleyle *et al.*, 1984; Gryglewicz and Jasieńko, 1992; Ibarra *et al.*, 1994; Yperman *et al.*, 1995; Chen *et al.*, 2000). However, these earlier studies that support incorporation and retention of sulphur from pyrite thermal transformation into the OM of kerogen chars have been obtained under closed or restricted pyrolysis conditions, which are not the same as for Rock-Eval open pyrolysis. Bolin (2014) used open system pyrolysis conditions, similar to Rock-Eval, and reported a lack of incorporation and retention of sulphur from pyrite thermal transformation into kerogen chars which is not consistent with the results from this study. One reason of this could be differences in reaction times of Bolin (2014) pyrolysis *vs* Rock-Eval 7S pyrolysis. Indeed, compared to the pyrolysis reaction time applied in Bolin's study (1 s at 630°C), the Rock-Eval pyrolysis reaction time is slower (from 300°C to 650°C with a heating rate of 25°C/min) and so more suitable for chemical interactions. Furthermore, a sulphur mass balance was not made in Bolin's works, so a firm conclusion concerning the lack of incorporation of sulphur from pyrite thermal transformation into kerogen chars has not been made.

The OM_{effect} on the amount of sulphur released from pyrite during pyrolysis is more important for kerogens with high OI and low HI (i.e., types III and IV), suggesting that the abundance of oxygen combined with the lack of hydrogen seems to govern OM reactivity, with sulphur released from pyrite during pyrolysis. This conclusion was also made by Chen *et al.* (2000) who suggest that the lack of the indigenous hydrogen as well as the presence of oxygen in the organic matrix are dominant factors determining the incorporation of sulphur from pyrite pyrolysis in the OM chars during pyrolysis.

The mineral content of organic rich marine sediments can also reduce the proportion of sulphur released from pyrite during pyrolysis. Indeed, the results obtained from analysis of mixtures "pure igneous pyrite + mineral" confirm that sulphur gas from pyrite pyrolysis can be retained by the mineral matrix. This Min_{effect} depends of the mineral type. Our results indicate that silicate minerals, except smectite, do not show significant Min_{effect}. Smectite properties, in particular its high surface area, high

cation exchange capacity, and interlayer surfaces with unusual hydration characteristics (Odom, 1983) are likely reasons why this mineral retains sulphur gas from pyrite pyrolysis. Moreover, findings from Volzone (2007) support our results by showing that natural smectite acts as a better and more solid adsorbent of sulphur gas than natural illite and kaolinite.

Carbonate minerals show the highest Min_{effect} on the amount of sulphur gas released from pyrite pyrolysis. The reactions between sulphur gas (hydrogen sulphide) and carbonate minerals, such as calcite and dolomite, has been a subject of many studies (Attar and Dupuis, 1979; Efthimiadis and Sotirchos, 1992; Yrjas *et al.*, 1996; Hartman *et al.*, 2002). These studies conclude that carbonate minerals indeed directly react with hydrogen sulphide. This direct reaction is known to be very slow (Yrjas *et al.*, 1996) and follows the equation:

XCO_3 (s) + H_2S ⟷ XS (s) + CO_2 + H_2O
X: Ca; Mg; Fe…

A more rapid reaction of hydrogen sulphide removal has been observed in presence of calcined carbonates, the oxide compounds form by carbonate thermal degradation (e.g. : CaO, MgO; FeO) (Attar and Dupuis, 1979; Efthimiadis and Sotirchos, 1992; Yrjas *et al.*, 1996; Hartman *et al.*, 2002). This reaction usually involves the prior thermal degradation of carbonates:

XCO_3 (s) ⟷ XO (s) + CO_2
XO (s) + H_2S ⟷ XS (s) + H_2O
X: Ca; Mg; Fe…

Knowing that during Rock-Eval pyrolysis some carbonate minerals, for instance Siderite ($FeCO_3$), are thermally degraded into FeO (Lafargue *et al.*, 1998; Pillot *et al.*, 2013), before releasing sulphur gas from pyrite thermal transformation, this second and rapid reaction could also be responsible for the retention of sulphur gas from pyrite thermal transformation. The main products of these reactions between carbonate minerals and sulphur gases from pyrite during Rock-Eval 7S pyrolysis are sulphide minerals (XS) which would then be stabilised into sulphate minerals during the oxidation phase (Figure 3. 8), and CO_2 as shows the CO_2 signals of mixtures “pyrite + carbonates” (Appendix I).

The main complex reactions occurring between sulphur gas from pyrite thermal transformation and minerals during the Rock-Eval 7S pyrolysis phase have been shown to lead to the formation of new sulphate minerals. It is therefore important to be aware that during Rock-Eval 7S analysis of a rock sample, the presence of sulphate peaks can be representative of the original sulphate content of the samples (native sulphate) or document neoformed sulphates. These neoformed sulphates cover a wide range of temperatures from 700°C to 1200°C (Figure 3. 7; Figure 3. 8) while native sulphates occur

only from 900°C to 1200°C (section 2.3.2). Therefore, additional works are needed to better decipher the Rock-Eval 7S sulphate peaks.

3.2.4.2-Towards a new and calibrated methodology for S^{Pyrite} and $S^{Organic}$ quantification using Rock-Eval 7S

The study of pyrite thermal transformation during Rock-Eval 7S pyrolysis and its interaction with organic and mineral species commonly found in organic rich marine sediments, support the establishment of a new methodology for accurate S^{Pyrite} and $S^{Organic}$ quantification using Rock-Eval 7S. This method can be directly performed on bulk sedimentary rock samples, without any chemical preparation. It consists in Rock-Eval 7S quantification of the total sulphur content of the sample as well as other sulphur parameters in two hours of analysis (section 2.2). Then, the sulphur parameters obtained with Rock-Eval 7S are used to quantify S^{Pyrite} and $S^{Organic}$ as follows:

$$\boldsymbol{S^{Pyrite} = \frac{(1+\beta+\gamma)}{\alpha} \cdot {}_{Pyrolysis}S^{Pyrite}}$$

$$\boldsymbol{S^{Organic} = S^{Total} - S^{Pyrite}}$$

$\boldsymbol{{}_{Pyrolysis}S^{Pyrite}}$: Rock-Eval 7S parameter representing the pyritic sulphur released during the pyrolysis phase.
$\boldsymbol{S^{Total}}$: Rock-Eval 7S parameter representing the total sulphur content, i.e. the total sulphur released during the pyrolysis and the oxidation phases.
***α**: Proportion of $\boldsymbol{{}_{Pyrolysis}S^{Pyrite}}$ on the total $\boldsymbol{S^{Pyrite}}$. It was demonstrated in this study that the representative value of this factor α is 43% corresponding stoichiometrically to the thermal transformation of pyrite into pyrrhotite.*
***β**: Correction factor of the $\boldsymbol{OM_{effect}}$ on the amount of pyritic sulphur released during Rock-Eval 7S pyrolysis ($\boldsymbol{{}_{Pyrolysis}S^{Pyrite}}$:).*
***γ**: Correction factor of the $\boldsymbol{Min_{effect}}$ on the amount of pyritic sulphur released during Rock-Eval 7S pyrolysis ($\boldsymbol{{}_{Pyrolysis}S^{Pyrite}}$:).*

- Calibration of OM_{effect}:

To calibrate the OM_{effect}, a multi-variable regression was performed using different Rock-Eval parameters. The best regression was obtained using HI and OI values of the different kerogen samples studied. This enables the prediction of the OM_{effect} on the amount of ${}_{Pyrolysis}S^{Pyrite}$ released during pyrolysis, using the following formula:

$$\boldsymbol{OM_{effect\ predicted}(wt.\%) = 0.37 * OI - 0.006 * HI + 5.74}$$

We observed a statistically relevant trend (R^2=0.77) between values of OM_{effect} predicted ($OM_{effect\ predicted}$) and values of OM_{effect} obtained by the analysis of mixtures "pyrite + kerogen" (OM_{effect}) (Figure 3. 10). It must be noted that this formula is only calibrated for thermally immature or early oil window samples, reflecting the range of maturity used in this study.

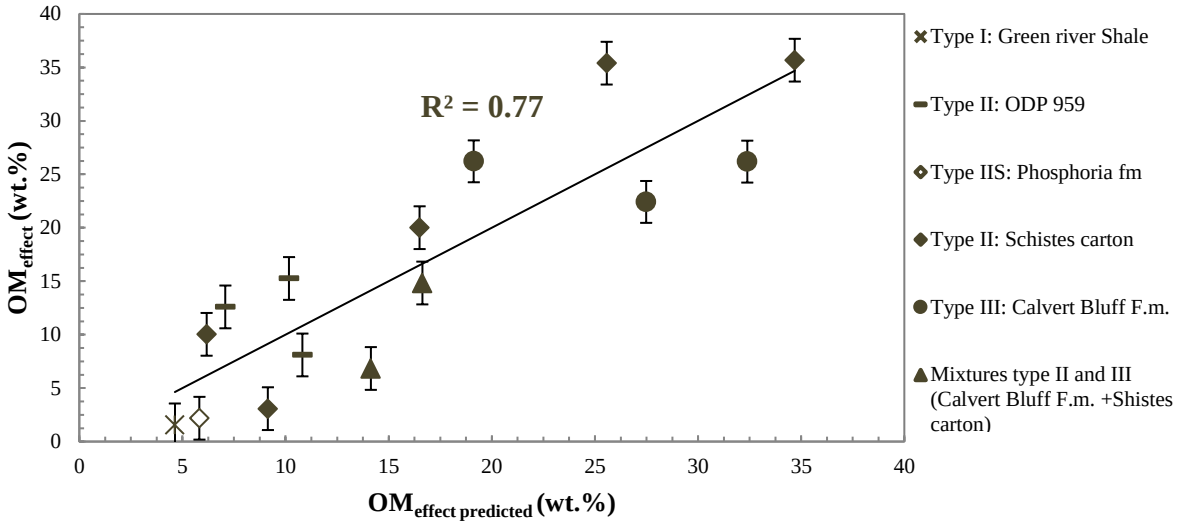

Figure 3. 10: The OM_{effect} obtained by the analysis of mixtures "pyrite + kerogen" vs $OM_{effect\ predicted}$ from HI and OI

The OM_{effect} correction factor is β. This factor aims to consider the amount of ${}_{Pyrolysis}S^{Pyrite}$ trapped in the organic matrix during pyrolysis that we named $CorrOM_{effect}$:

$$\boldsymbol{CorrOM_{effect} = {}_{Pyrolysis}S^{Pyrite\ expected} - {}_{Pyrolysis}S^{Pyrite}}$$

In this formula, ${}_{Pyrolysis}S^{Pyrite}$ represents the pyritic sulphur released during the pyrolysis phase, and ${}_{Pyrolysis}S^{Pyrite\ expected}$ is the amount of pyritic sulphur that would be released during pyrolysis if there was no OM_{effect}. Therefore, $CorrOM_{effect}$ and consequently β can be deduced from the OM_{effect} as follows:

$$OM_{effect} = \frac{{}_{Pyrolysis}S^{Pyrite\ expected} - {}_{Pyrolysis}S^{Pyrite}}{{}_{Pyrolysis}S^{Pyrite\ expected}}$$

$$1 - \frac{{}_{Pyrolysis}S^{Pyrite}}{{}_{Pyrolysis}S^{Pyrite\ expected}} = OM_{effect}$$

$$\frac{{}_{Pyrolysis}S^{Pyrite}}{{}_{Pyrolysis}S^{Pyrite\ expected}} = 1 - OM_{effect}$$

$$\frac{1}{{}_{Pyrolysis}S^{Pyrite\ expected}} = \frac{1 - OM_{effect}}{{}_{Pyrolysis}S^{Pyrite}}$$

$$_{Pyrolysis}S^{Pyrite\ expected} = \frac{_{Pyrolysis}S^{Pyrite}}{1 - OM_{effect}}$$

$$CorrOM_{effect} = \frac{_{Pyrolysis}S^{Pyrite}}{1 - OM_{effect}} - {}_{Pyrolysis}S^{Pyrite}$$

$$CorrOM_{effect} = {}_{Pyrolysis}S^{Pyrite}\left(\frac{1}{1 - OM_{effect}} - 1\right)$$

$$CorrOM_{effect} = {}_{Pyrolysis}S^{Pyrite} * \left(\frac{OM_{effect}}{1 - OM_{effect}}\right)$$

$$CorrOM_{effect} = {}_{Pyrolysis}S^{Pyrite} * \beta$$

$$\boldsymbol{\beta = \left(\frac{OM_{effect}}{1 - OM_{effect}}\right)}$$

- <u>Calibration of Min_{effect}:</u>

Calibration mixtures composed of "pure igneous pyrite + 0 to 100% silicate minerals + 0 to 100% carbonate minerals" were analysed with Rock-Eval 7S in order to calibrate Min_{effect} (Appendix H):

- ❖ Minimal Min_{effect} calibration mixtures: Mixtures presenting the minimum retention effect on the amount of $_{Pyrolysis}S^{Pyrite}$ "pure igneous pyrite + kaolinite + calcite";
- ❖ Mean Min_{effect} calibration mixtures: Mixtures presenting the average retention effect on the amount of $_{Pyrolysis}S^{Pyrite}$ "pure igneous pyrite + all silicate minerals + all carbonate minerals";
- ❖ Maximal Min_{effect} calibration mixtures: Mixtures presenting the maximum retention effect on the amount of $_{Pyrolysis}S^{Pyrite}$ "pure igneous pyrite + smectite + siderite".

Min_{effect} for each type of calibration mixtures is plotted versus their mineral carbon content (MinC), representing the carbonate content of each mixtures (Figure 3. 11). An increase in the Min_{effect} as a function of carbonate is observed for each type of calibration mixtures. The obtained calibration curves (Figure 3. 11) can be divided into three sedimentary formation groups according to the carbonate content:

- ❖ Clays: 0wt% ≤ Carbonate content < 30wt% (0wt% ≤ MinC< 3.6wt%);
- ❖ Marls: 30wt% ≤ Carbonate content < 70wt% (3.6wt% ≤ MinC< 8.4wt%);

❖ Carbonates: 70wt% ≤ Carbonate content < 100wt% (8.4wt% ≤ MinC≤12wt%).

Each sedimentary formation defined here present large variability of Min_{effect}. Clay rich formations, for example, show Min_{effect} from 0wt% to 88wt%, for marl formations they range from 35wt% to 92wt% and for carbonate formations from 42wt% to 99wt%. An average Min_{effect} for each sedimentary formation has been defined using the mean Min_{effect} calibration curve which is obtained by analysis the "mean Min_{effect} calibration mixtures" (Figure 3. 11). It is 38wt% for clays, 78wt% for marls and 90wt% for carbonates.

The correction factor of Min_{effect} is γ. This factor aims to consider the amount of ${}_{Pyrolysis}S^{Pyrite}$ trapped in the mineral matrix during pyrolysis. As for β the correction factor of OM_{effect}, γ the correction factor of Min_{effect} can be written as the following formula:

$$\gamma = \left(\frac{Min_{effect}}{1 - Min_{effect}}\right)$$

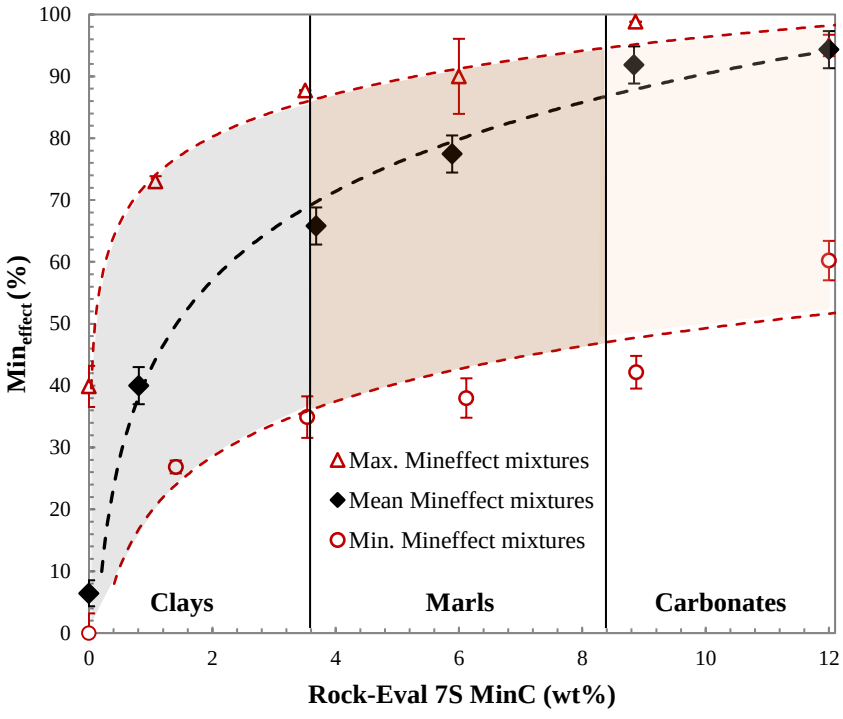

Figure 3. 11: Min_{effect} *vs* MinC calibration curves corresponding to minimal, mean and maximal Min_{effect} calibration mixtures

- Method limitations:

We observed that, during Rock-Eval 7S analysis, interactions between sulphur gas from pyrite pyrolysis and minerals can result formation of new sulphate minerals (neoformed sulphates) during Rock-Eval 7S analysis. And, these neoformed sulphates can present the same Rock-Eval 7S signal as native sulphates. This limits the application of the Rock-Eval 7S method introduced here to sedimentary rocks containing mainly S^{Pyrite} and $S^{Organic}$ compounds. Indeed this new Rock-Eval 7S method can only be applied on samples from most of marine depositional environments where the total sulphur content of organic rich marine sediments is essentially composed of S^{Pyrite} and $S^{Organic}$ species (Berner and Raiswell, 1983; Garrels and Lerman, 1984; Vairavamurthy *et al.*, 1995). However, this new Rock-Eval 7S method does not directly apply to rock samples from limited evaporitic environments which can contain high amount of native sulphate minerals (Vairavamurthy *et al.*, 1995). Indeed, a preliminary sulphate removing operation, using chemical treatments for instance, is required before applying this new Rock-Eval 7S method to rock samples containing sulphates.

OM_{effect}, an important parameter of this method was only calibrated for thermally immature or early oil window kerogen samples. Therefore, further analytical development is required before the application of this new method on mature samples.

Ideally, the Rock-Eval 7S method has to be performed on fresh sedimentary rock samples. Because, we have seen in this study that altered pyrite grains lead to a potentially significant reduction (up to 23%) of α, the proportion of sulphur released from pyrite during the pyrolysis stage, which is an important parameter of this method.

3.2.5- Conclusions

Pyrite thermal transformation during Rock-Eval 7S pyrolysis and its interaction with OM and minerals commonly found in organic rich marine sediments were studied here. The results obtained show that during the pyrolysis phase, pyrite (FeS_2) is thermally transformed into pyrrhotite (Fe_7S_8), releasing about 43% of its total S^{Pyrite} content. The sulphur gas released from pyrite pyrolysis can directly react with OM and mineral, providing efficient trapping mechanisms. This implies that the presence and nature OM and mineral types can reduce the fraction of $_{Pyrolysis}S^{Pyrite}$ as part of the total S^{Pyrite}. These observations form the basis to propose an improved methodology for accurate S^{Pyrite} and $S^{Organic}$ quantification in organic rich marine sediments, using Rock-Eval 7S:

$$S^{Pyrite} = \frac{(1+\beta+\gamma)}{\alpha} \cdot {}_{Pyrolysis}S^{Pyrite}$$

$$S^{Organic} = S_{total} - S^{Pyrite}$$

The factor α is the percentage of ${}_{Pyrolysis}S^{Pyrite}$ of the total S^{Pyrite} (43%). The factors β and γ are correction factors of the OM_{effect} and the Min_{effect} on the amount of ${}_{Pyrolysis}S^{Pyrite}$ released during pyrolysis, respectively. These correction factors aim to take into account the amount of ${}_{Pyrolysis}S^{Pyrite}$ trapped in the OM and in the mineral matrix during the pyrolysis phase.

3.3- VALIDATION OF THE NEW ROCK-EVAL 7S METHODOLOGY FOR PYRITIC SULPHUR AND ORGANIC SULPHUR QUANTIFICATION ON ORGANIC RICH SEDIMENTS

3.3.1- Introduction

The recent development of the next generation of the Rock Eval pyrolysis system, the Rock-Eval 7S, opens a new opportunity to fill this critical gap in analytical capability, and widens the application of routine carbon and sulphur analyses to a broad range of research and industry areas, from petroleum geochemistry to environmental and soil sciences.

Recognising the potential of the new Rock-Eval 7S, a new and advanced methodology for S^{Pyrite} and $S^{Organic}$ quantification, was developed using Rock-Eval 7S. The development of this method was presented in the first part of this chapter (Section 3.2). In this second part of the chapter, we present validation of this new Rock-Eval 7S methodology for S^{Pyrite} and $S^{Organic}$ quantification on two types of sediments: (i) Organic rich marine sediments where the new Rock-Eval 7S methodology was tested against the elemental analysis method. (ii) Sedimentary mixtures with defined amounts of S^{Pyrite} and $S^{Organic}$.

3.3.2- Samples and methods

3.3.2.1-Samples

- Organic rich marine sediments:

The organic rich marine sediment samples selected to validate the Rock-Eval 7S method for S^{Pyrite} and $S^{Organic}$ quantification are all immature or in the early oil window (Tmax from 413°C to 435°C), they present a wide range of TOC content (0.7 to 36.9wt%), HI (131 to 759 mgHC/gTOC), OI (12 to 44 $mgCO_2$/gTOC) and MinC (0.1 to 11.2wt%) (Table 3. 5). Therefore, the selected samples cover most of organic rich marine sediments. They are from the following formations:

- Grey Shale Member: The Grey Shale Member constitutes the base of the Whitby Mudstone Formation in the Cleveland Basin (North Yorkshire, UK). Placed within the Toarcian, this interval is characterised by marine mudstones named “grey shale” intercalated with three distinct layers of organic and sulphur rich shales (~10-60 cm thick), named the ‘sulphur bands’

(Chowns, 1966; Hallam, 1981; Jenkyns, 1985; Salem, 2013). The kerogen content in this formation has a mixed type II and type III composition (Salem, 2013). A set of 13 samples from the sulphur bands and from the under/overlying grey shale were collected from Grey Shale Member outcrop at North Yorkshire (Garner, 2014). These samples fall within the scope of the Rock-Eval 7S method given that they do not contain sulphate minerals (XRD characterisation: Appendix M), their OM maturation level is generally below the oil window (Tmax from 422°C to 435°C), and knowing that particular attention was taken to selected fresh unaltered samples (Garner, 2014).

- Kimmeridge Clay Formation (KCF): Tithonian-Kimmeridgian marine rock samples from the KCF in Dorset were selected. The studied section consists of alternating beds of carbonates and shales, which range from organic-poor to very organic-rich, and exhibit HI values indicative of type II OM (Huc *et al.*, 1992). Sediments with high organic content (high TOC values) also have the greatest contents of S^{Total} with a dominance of $S^{Organic}$ over S^{Pyrite} (Lallier-Vergès *et al.*, 1993). We selected 8 organic-poor to organic rich carbonate and shale samples from shale and carbonate beds of core material from the Swanworth Quarry 1, drilled at the type locality of the KCF in Dorset. These samples fall within the scope of the Rock-Eval 7S method given that they contain small amount of sulphate minerals (Lallier-Vergès *et al.*, 1993), their OM maturation level is generally below the oil window (Tmax from 413°C to 429°C), and these samples were assumed to be fresh as retrieved from core material in 2014.

Formation	Sample names	Tmax (°C)	TOC (wt%)	HI (mgHC/gTOC)	OI (mgCO2/gTOC)	MinC (wt%)
Grey Shale Member	GR-3	432	0.7	131	17	0.1
	SB-9	422	1.5	255	16	0.2
	SB-10	422	3.7	421	14	0.3
	SB-11	423	3.4	397	13	0.3
	SB-12	422	4.1	450	12	0.4
	SB-13	423	3.0	337	15	0.3
	SB-14	426	1.3	133	28	0.2
	GR-15	435	0.8	145	24	0.2
	GR-17	433	1.1	154	28	0.2
	SB-18	428	3.1	421	13	0.5
	GR-40	434	0.9	141	15	0.5
	GR-44	433	1.9	261	14	0.3
	GR-50	425	2.5	208	21	0.2
Kimmeridge Clay Formation	SSK52130	414	2.4	632	44	11.2
	SSK52132	413	26.8	703	17	3.4
	SSK52133	422	6.6	488	19	0.4
	SSK52134	417	36.9	731	12	1.5
	SSK52135	421	9.5	607	19	2.6
	SSK52137	429	1.5	411	40	8.0
	SSK52138	414	6.7	759	21	10.1
	SSK52139	425	18.6	704	15	2.6

Table 3. 5: Basic Rock-Eval parameters of the selected samples

- Sedimentary mixtures:

Validity of the new Rock-Eval 7S method for S^{Pyrite} and $S^{Organic}$ quantification was further assessed using sedimentary mixtures with defined amounts of S^{Pyrite} and $S^{Organic}$. To obtain these mixtures, different amounts of the pure igneous pyrite were added to sedimentary rock samples which are known, from preliminary Rock-Eval 7S and literatures, to be immature (Tmax 407°C from to 419°C) and to contain mainly $S^{Organic}$. These sedimentary rock samples are from the Orbagnoux Fm. (Mongenot *et al.*, 1999; Tribovillard *et al.*, 1999; Sarret *et al.*, 2002); the Phosphoria Fm. (Lewan *et al.*, 1986; Price and Wenger, 1992); and the Limagne Fm. (Barrabe, 1932). Their total sulphur contents were determined using the new Rock-Eval 7S method described in the previous sub-chapter.

In a second step, the S^{Total}, S^{Pyrite} and $S^{Organic}$ contents were calculated for each of the sedimentary mixtures. Table 3. 6 presents the different sedimentary rocks studied as well as the experimental protocol defining the different mixtures.

Formations	**Orbagnoux**				**Phosphoria**	**Limagne**
Ages	Kimmeridgian				Permian	Oligocene-Eocene
Locations	France				USA	France
References	Mongenot *et al.*, 1999; Tribovillard *et al.*, 1999; Sarret *et al.*, 2002				Lewan *et al.*, 1986; Price and Wenger, 1992	Barrabe, 1932
Samples	O-9m	O-9ka	O-9cb	O-9ca	P-43	L-S18-2
Rock weight (mg)	60±0.02	60±0.02	60±0.02	30±0.02	30±0.02	60±0.02
Tmax (°C)	408	409	407	408	415	419
Rock-Eval 7S TS of the rock samples (wt%)	0.3±0.03	0.7±0.03	0.7±0.03	1.21±0.03	1.8±0.03	0.4±0.03
Pyrite weight (mg)	1±0.02 2±0.02 3±0.02 4±0.02	1±0.02 2±0.02 3±0.02 4±0.02	1±0.02 2±0.02 3±0.02 4±0.02	1±0.02 2±0.02	1±0.02 2±0.02	1±0.02 2±0.02 3±0.02 4±0.02
Rock-Eval 7S TS of the pyrite sample (wt%)	54±2	54±2	54±2	54±2	54±2	54±2

Table 3. 6: Sedimentary rock samples used in mixtures "sedimentary rocks + pyrite", their weights and total sulphur contents. Pyrite weights used in the mixtures "sedimentary rocks + pyrite" and its total sulphur content.

3.3.2.2-Methods

- Rock-Eval 7S:

We performed duplicate quantification of S^{Pyrite} and $S^{Organic}$ contents of the selected organic rich marine sediments and the sedimentary mixtures using the new Rock-Eval 7S method (Aboussou *et al.*, 2017; Aboussou *et al.*, 2018). This method involves rapid analysis (2 hours per sample) of a rock sample with Rock-Eval 7S using total sulphur temperature program, followed by data processing of key parameters in order to quantify S^{Pyrite} and $S^{Organic}$:

$$S^{Pyrite} = \frac{(1+\beta+\gamma)}{\alpha} \cdot {}_{Pyrolysis}S^{Pyrite}$$
$$S^{Organic} = S^{Total} - S^{Pyrite}$$

${}_{Pyrolysis}S^{Pyrite}$ *: Rock-Eval 7S parameter representing the pyritic sulphur released during the pyrolysis phase.*
S^{Total} *: Rock-Eval 7S parameter representing the total sulphur content, i.e. the total sulphur released during the pyrolysis and the oxidation phases.*
α *: Proportion of* ${}_{Pyrolysis}S^{Pyritic}$ *on* S^{Pyrite}
β *: Correction factor of the* OM_{effect} *on* ${}_{Pyrolysis}S^{Pyrite}$
γ *: Correction factor of the* Min_{effect} *on* ${}_{Pyrolysis}S^{Pyrite}$

- Elemental analysis:

Duplicate S^{Pyrite} and $S^{Organic}$ quantification using a routine elemental analysis method (Durand, 1980; Vandenbroucke and Largeau, 2007) was conducted on the organic rich marine sediment samples. This consisted in two stages: (i) Isolation of kerogen: kerogen was isolated from the dominant mineral phases of the rock by a series of chemical attacks with hydrochloric and hydrofluoric acids destroying the mineral matrix, i.e., the carbonate and silicate minerals. Pyrite (FeS_2), as well as some minor oxides including iron oxides, being resistant to this treatment, remained preserved in the kerogen residue obtained. (ii) Elemental analysis of kerogen: the total iron content of kerogen (${}_{Kerogen}Fe^{Total}$) was quantified by Inductively Coupled Plasma Atomic Emission Spectrometry (ICP-AES) and the total sulphur content (${}_{Kerogen}S^{Total}$) by Infrared spectrometry.

It is assumed that the iron content in the kerogen is exclusively composed of pyrite (Durand, 1980; Vandenbroucke and Largeau, 2007). Therefore, by determining the iron content of the kerogen (${}_{Kerogen}Fe^{Total}$), the ${}_{Kerogen}S^{Pyrite}$ content can be calculated stoichiometrically. The ${}_{Kerogen}S^{Organic}$ content can be then deduced by the difference between ${}_{Kerogen}S^{Total}$ content and the obtained ${}_{Kerogen}S^{Pyrite}$ content. The entire data set acquired on kerogen samples (${}_{Kerogen}S^{Total}$, ${}_{Kerogen}S^{Pyrite}$ and ${}_{Kerogen}S^{Organic}$ content) was then extrapolated to the bulk rock, using the weight loss during kerogen isolation. The following equations were used:

$${}_{Kerogen}S^{Pyrite} = \frac{(2*32.1)}{55.8} * {}_{Kerogen}Fe^{Total}$$
$${}_{Kerogen}S^{Organic} = {}_{Kerogen}S^{Total} - {}_{Kerogen}S^{Pyrite}$$

$$S^{Total} = {}_{Kerogen}S^{Total} * p$$
$$S^{Pyrite} = {}_{Kerogen}S^{Pyrite} * p$$
$$S^{Organic} = {}_{Kerogen}S^{Organic} * p$$

${}_{Kerogen}Fe^{Total}$ *: Total iron content of kerogen quantified by ICP-AES*
${}_{Kerogen}S^{Total}$ *: Total sulphur content of kerogen quantified by Infrared spectrometry*
p *: Proportion of kerogen in bulk rock sample obtained using the weight loss during kerogen isolation*

3.3.3- Results and discussions

3.3.3.1- Organic rich marine sediments (Appendix J and K)

Both methods, Rock-Eval 7S and elemental analysis, were applied to the organic rich marine sediment samples. We then compared S^{Total}, S^{Pyrite} and $S^{Organic}$ contents obtained from the two independent methods.

Regarding S^{Total} contents, both techniques result in an excellent linear correlation (Figure 3. 12) with R^2=0.98. Elemental analysis seems to slightly underestimate the S^{Total} content in bulk rock sample sets essentially in samples from the Grey Shale Member and not in samples from KCF in Dorset. This could be due to the fact that the elemental analysis method was performed on kerogen samples in which a small fraction of the original total sulphur content, from sulphate minerals and/or acid volatile sulphide minerals (FeS), could have been be removed by the chemical pre-treatment (Canfield *et al.*, 1986; Vandenbroucke and Largeau, 2007). Knowing from XRD characterisation (Appendix M) that Grey Shale Member samples do not contain sulphate minerals, we assumed that acid volatile sulphide minerals were removed during the kerogen isolation chemical treatment (Canfield *et al.*, 1986; Vandenbroucke and Largeau, 2007) leading to the underestimation of the S^{Total} contents of the Grey Shale Member samples via the elemental analysis method.

For the S^{Pyrite} content, both methods show an excellent linear correlation (R^2=0.96) (Figure 3. 13). A slight disparity between the Rock-Eval 7S method and the elemental analysis method is observed. Concerning the elemental analysis method, two factors can lead to a miss-quantification of S^{Pyrite}: (i) The loss of some labile S^{Pyrite} compounds, such as acid volatile sulphide (FeS), during the acid treatment, which would lead to an underestimation of the elemental analysis method, as observed in some samples mostly from the Grey Shale Member. (ii) Such a minor disparity of the elemental analysis method may be expected as S^{Pyrite} quantification using elemental analysis is based on the assumption that all the iron content of the kerogen samples is related to pyrite particles, which may not be strictly correct (Vandenbroucke and Largeau, 2007). Indeed, other iron containing minerals, such as iron oxides, could remain in the kerogen samples, false the assumption that all the iron content of the kerogen samples is related to pyrite particles, and so lead to an overestimation of the S^{Pyrite} quantification, as observed here in some samples. Concerning the Rock-Eval 7S method, the extrapolation used in the calibration of the OM_{effect} and Min_{effect} correction factors (Section 3.2) could explained a slight miss-quantification of the S^{Pyrite}. Indeed, by using mean/extrapolated values for the OM_{effect} and Min_{effect}, we don't consider complexity of natural samples, and this could lead to minor disparity of the Rock-Eval 7S method.

The comparison between Rock-Eval 7S and elemental analysis concerning the quantification of $S^{Organic}$ content is presented in Figure 3. 14. The correlation is not as good as for S^{Total} content and for S^{Pyrite} content, i.e. R^2<0.90. Two reasons may contribute to explain this scatter: (i) The fact that estimation of $S^{Organic}$ based on elemental analysis was done by a combination of two different techniques (ICP-AES and Infrared), which may increase the uncertainty of elemental results. (ii) The fact that the final $S^{Organic}$ quantification, as deduced from S^{Total} and S^{Pyrite}, combines analytical errors of the two methods for S^{Total} and S^{Pyrite} quantification. This potential bias can be tested by removing from $S^{Organic}$ scatter plot all samples which do not show good agreement between both methods for S^{Total} and S^{Pyrite} quantification (samples presenting y/x < 0.85 and y/x>1.15). Indeed, without these 'inconsistent' samples, the match between both methods for $S^{Organic}$ quantification further increases from R^2= 0.84 (n=21) to R^2=0.97 (n=12) (Figure 3. 15).

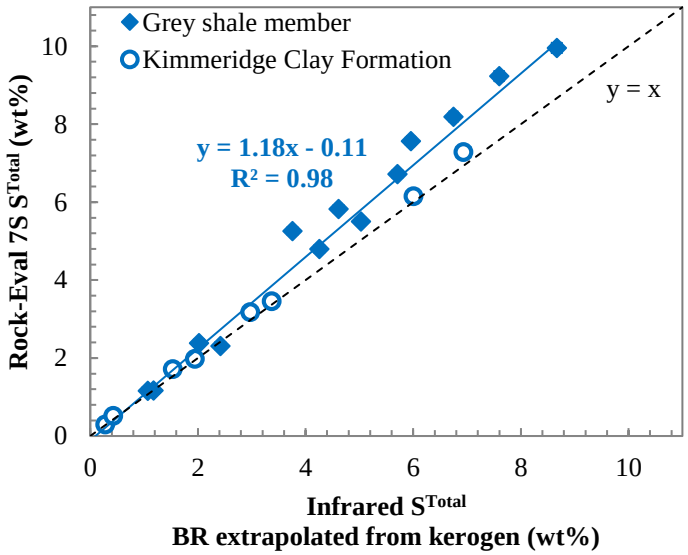

Figure 3. 12: Comparison of Rock-Eval 7S and elemental analysis in the quantification of the S^{Total} content of the organic rich marine sediment samples

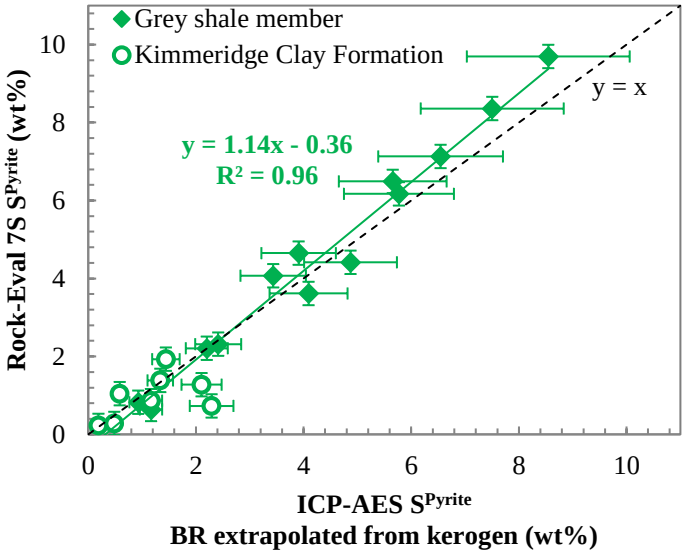

Figure 3. 13: Comparison of Rock-Eval 7S method and elemental analysis method in the quantification of the S^{Pyrite} content of the organic rich marine sediment samples

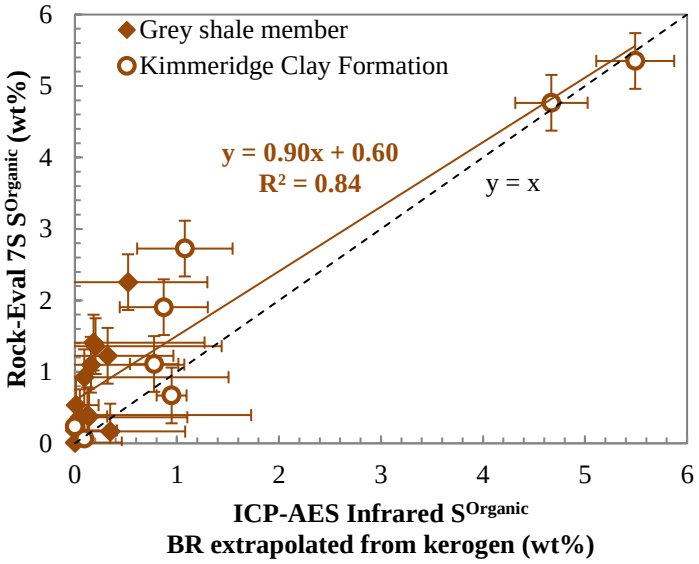

Figure 3. 14: Comparison of Rock-Eval 7S method and elemental analysis method in the quantification of the $S^{Organic}$ content of the organic rich marine sediment samples

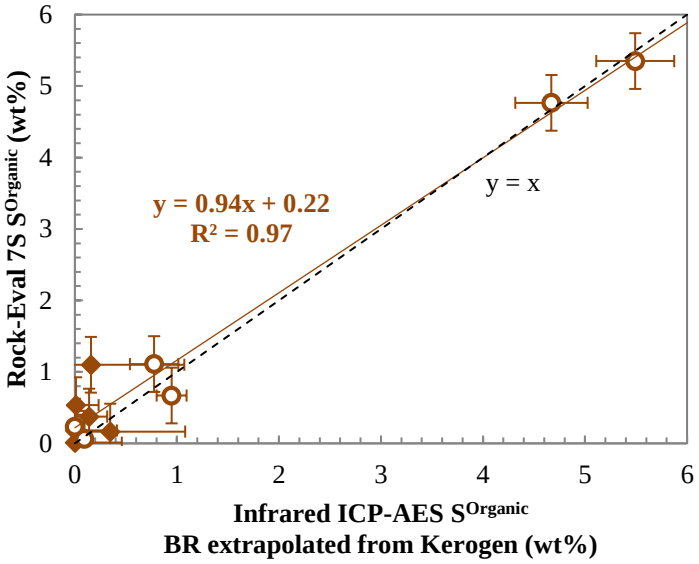

Figure 3. 15: Comparison of Rock-Eval 7S method and elemental analysis method in the quantification of the $S^{Organic}$ content of the organic rich marine sediment samples without samples presenting misscorrélation between both method for S^{Total} and S^{Pyrite} sulphur quantification

3.3.3.2- Sedimentary mixtures (Appendix J and L)

Like any analytical technique, the elemental analysis method may induce errors in the quantification of S^{Total}, S^{Pyrite} and $S^{Organic}$ contents as performed on kerogen samples then extrapolated to bulk rock samples using the weight loss during kerogen isolation, and as based on the assumption that the iron content in the kerogen is exclusively composed of pyrite which is not always true (Durand, 1980; Vandenbroucke and Largeau, 2007). Consequently, this method does not strictly allow for a correct evaluation of the Rock-Eval 7S method, which have also its own limitation and biases. To better constrain and quantify these methodological biases, we applied the Rock-Eval 7S method to sedimentary mixtures with known S^{Pyrite} and $S^{Organic}$ contents.

We realised sedimentary mixtures composed of sedimentary rocks containing mainly $S^{Organic}$ and different amount of the pure igneous pyrite. The selected sedimentary rocks were firstly characterised using Rock-Eval 7S (Figure 3. 16). Their pyrolysis sulphur signals present mainly of organic sulphur peaks with very low or no pyrite peaks. Their oxidation signals show residual organic sulphur peaks, sulphate peaks from 600°C to 1000°C which have the same signature as neoformed sulphates (section 3.2.3.4), and sulphate peaks, occurring between 1000°C to 1200°C and present essentially on Orbagnoux Fm., which can be neoformed or native (Section 2.3.2 and Section 3.2.3.4). However, results from Tribovillard *et al.* (1999) show that there is no sulphate minerals in the different unit of Orbagnoux Fm. This suggests that the sulphate peaks observed in Orbagnoux samples are

mainly neoformed during the Rock-Eval 7S analysis. Therefore, all the selected samples contain mainly organic sulphur compounds.

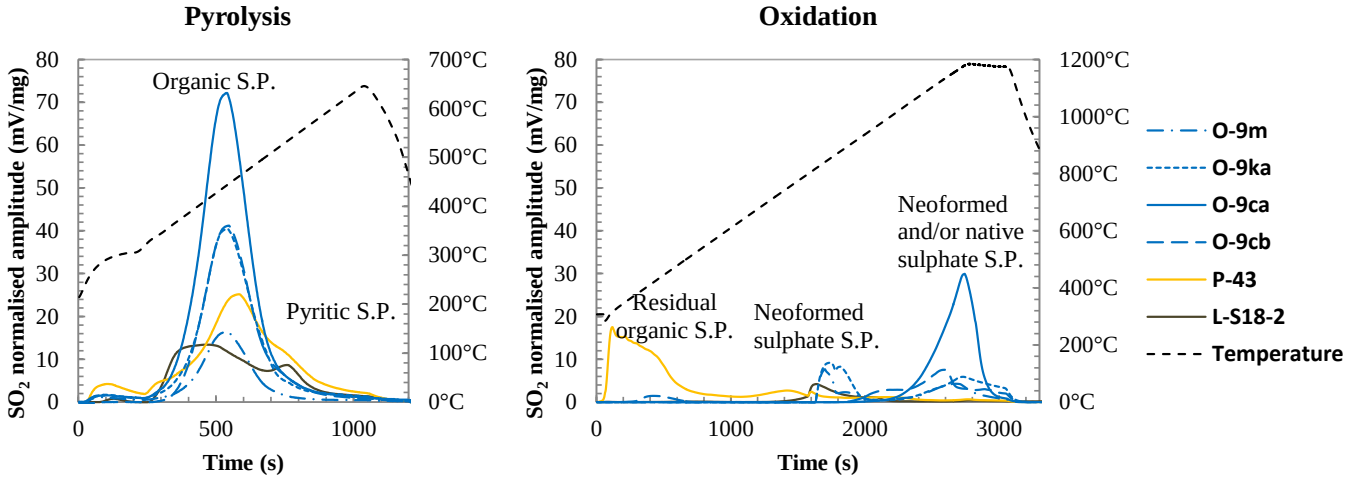

Figure 3. 16: Rock-Eval 7S sulphur signals of the selected sedimentary rocks from Orbagnoux Fm. (O), Phosphoria Fm. (P) and Limagne Fm. (L). S.P.: Sulphur peak

Strong linear correlations, with $R^2 \geq 0.9$, slopes close to 1, and intercepts close to 0, were obtained when directly comparing the Rock-Eval 7S results with known values of S^{Total}, S^{Pyrite} and $S^{Organic}$ in the different sedimentary mixtures (Figure 3. 17; Figure 3. 18; Figure 3. 19). These obtained results from the sedimentary mixtures analysis show that the Rock-Eval 7S method provides accurate quantification of S^{Total}, S^{Pyrite} and $S^{Organic}$. A slight dispersivity and underestimation of the S^{Pyrite} content, which leads to a slight dispersivity and overestimation of the $S^{Organic}$ content of about 10%, is observed for the Rock-Eval 7S method. This slight dispersivity and underestimation of S^{Pyrite} is probably due to the fact that the OM_{effect} and Min_{effect} were calibrated using common OM types and minerals found in marine sediments, so their calibrations do not consider the huge variability of marine sedimentary rocks. In addition, OM_{effect} and Min_{effect}, were calibrated separately while it is possible that OM and minerals have an additional combined impact on the amount of $_{Pyrolysis}S^{Pyrite}$ released during pyrolysis. Therefore, further studies are needed to improve calibration of OM_{effect} and Min_{effect}, as well as to understand and quantify the potentially combined effects of OM and minerals.

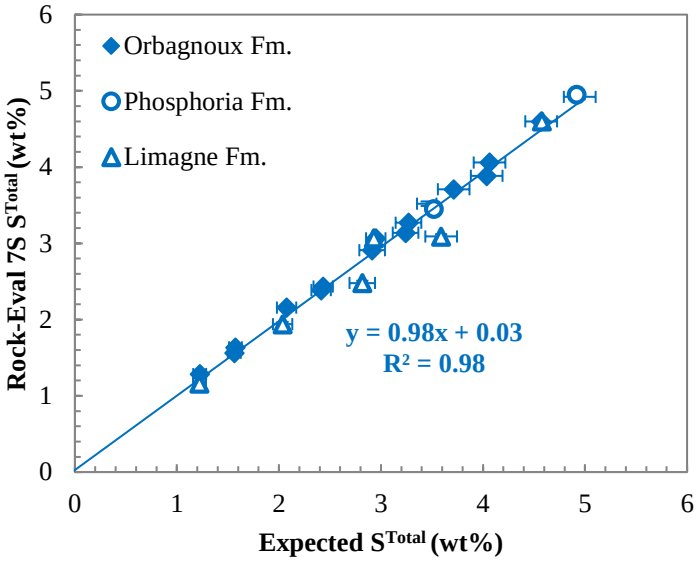

Figure 3. 17: Comparison between S^{Total} content of the mixtures "sedimentary rocks + pyrite" obtained with Rock-Eval 7S and the expected S^{Total} content.

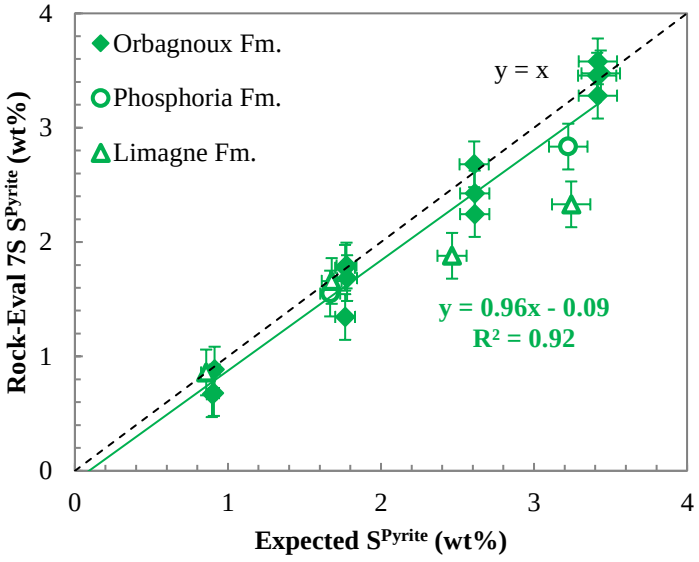

Figure 3. 18: Comparison between S^{Pyrite} content of the mixtures "sedimentary rocks + pyrite" obtained with the Rock-Eval 7S method and the expected S^{Pyrite} content.

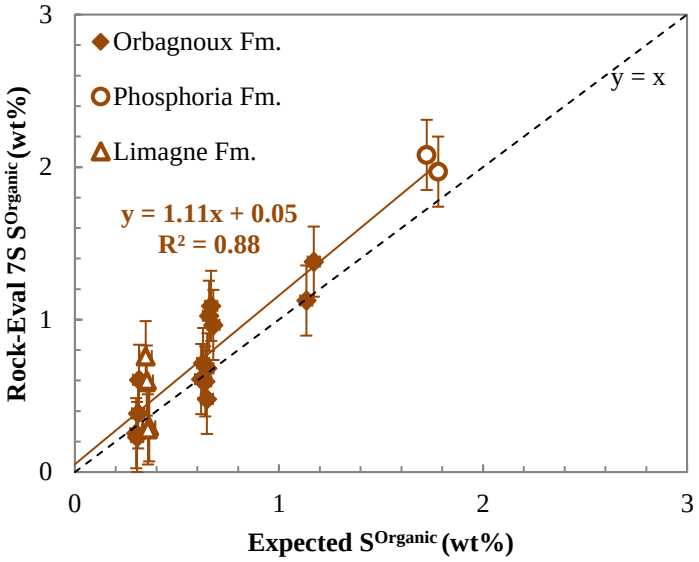

Figure 3. 19: Comparison between $S^{Organic}$ content of the mixtures "sedimentary rocks + pyrite" obtained with the Rock-Eval 7S method and the expected $S^{Organic}$ content.

3.3.4- Conclusions

By testing the new Rock-Eval 7S method (introduced in section 3.2) on a set of organic rich marine sediment samples against well-established elemental analysis (ICP-AES and Infrared spectrometry), we observe a good agreement between both methods for S^{Pyrite}, but not for $S^{Organic}$. We recognise that the elemental analysis is not the perfect reference method as it uses kerogen samples, with a series of unconstrained potential alterations during acid treatment, and works on the assumption that the iron content measured in kerogen only represents iron in pyrite (FeS_2), which is an oversimplification (Vandenbroucke and Largeau, 2007). To minimise or avoid these biases and to evaluate the Rock-Eval 7S method for S^{Pyrite} and $S^{Organic}$ quantification, we applied the method to mixtures with known S^{Pyrite} and $S^{Organic}$ contents (sedimentary rocks containing only $S^{Organic}$ + pyrite). A good correlation ($R^2 \geq 0.9$) between results from the Rock-Eval 7S method and the expected values of S^{Pyrite} and $S^{Organic}$ content has been observed, building confidence that the new Rock-Eval 7S method provides accurate quantification of both S^{Pyrite} and $S^{Organic}$. A slight overestimation (~10%) of the $S^{Organic}$ relative to pyrite sulphur is observed. This would be linked to calibration of OM_{effect} and Min_{effect}, two important parameters of the Rock-Eval 7S method. Therefore, one outlook will be to study the effect of the OM and minerals on the amount of pyritic sulphur released during pyrolysis in more detail, to improve calibration of OM_{effect} and Min_{effect}.

3.4- CHAPTER CONCLUSIONS

The study of pyrite thermal transformation during Rock-Eval 7S pyrolysis and its interaction with OM and minerals commonly found in organic rich marine sediments, allowed the development of an improved method for accurate S^{Pyrite} and $S^{Organic}$ quantification in organic rich marine sediments, using Rock-Eval 7S:

$$S^{Pyrite} = \frac{(1+\beta+\gamma)}{\alpha} \cdot {}_{Pyrolysis}S^{Pyrite}$$

$$S^{Organic} = S_{total} - S^{Pyrite}$$

In these formulas, the factor α is the percentage of ${}_{Pyrolysis}S^{Pyrite}$ on the total S^{Pyrite}. The factors β and γ are correction factors of the OM_{effect} and Min_{effect}, which aim to consider the amount of ${}_{Pyrolysis}S^{Pyrite}$ trapped in the OM and in the mineral matrix during the pyrolysis phase.

This new Rock-Eval 7S method for S^{Pyrite} and $S^{Organic}$ quantification was assessed and validated on a set of organic rich marine sediment samples, and on sedimentary mixtures with known S^{Pyrite} and $S^{Organic}$ contents (sedimentary rocks containing only $S^{Organic}$ + pyrite). The results obtained show that the new Rock-Eval 7S method provides an accurate quantification of both S^{Pyrite} and $S^{Organic}$. We observed, nevertheless, a slight disparity of the Rock-Eval 7S method which can be linked to the calibration of the OM_{effect} and Min_{effect}, two important parameters of the Rock-Eval 7S method. Therefore, the next analytical development of this method will be to improve calibration of these two parameters, OM_{effect} and Min_{effect}, by studying for instance their combined effect.

The potential applications and opportunities of this new method are numerous. Indeed, this advanced and rapid method for S^{Pyrite} and $S^{Organic}$ quantification can provide useful data for a wide range of studies including petroleum exploration and production, paleoenvironmental/paleoclimate reconstruction, coal exploration and production and soil pollution. However, given that this method was developed here for ancient organic rich marine sediments, further analytical development is required before the using of this method on other type of samples (e.g., recent sediments, coals, soils…).

Chapter 4: APPLICATION OF ROCK-EVAL 7S TO THE DESCRIPTION OF OM PRESERVATION OF JURASSIC BLACK SHALES FROM NORTH YORKSHIRE, DORSET AND SOMERSET

4.1-INTRODUCTION

One important application of the new Rock-Eval 7S method for pyritic sulphur (S^{Pyrite}) and organic sulphur ($S^{Organic}$) quantification can be to help description of OM preservation in marine sediments, by providing information for the reconstruction of paleo-environmental conditions based on the relative abundance of both sulphur compounds. Indeed, S^{Pyrite} and $S^{Organic}$ formation are competitive processes in marine settings that potentially provide direct links with environmental and climatic conditions on land. S^{Pyrite} formation occurs by reaction of reduced sulphur species (HS^-, H_2S) with reactive iron minerals (Berner, 1984; Vairavamurthy *et al.*, 1995; Baudin *et al.*, 2007). This process is inherently linked to OM remineralisation, as the reduced sulphur species are produced during OM oxidation via bacterial sulphate reduction, and the reduced iron is derived from the reduction of iron (oxyhydr)oxides by either reduced sulphur species or by dissimilatory iron reduction. Iron (oxyhydr)oxides in marine settings are dominantly supplied through continental runoff, directly linking the formation of pyrite in marine sediments with precipitation, weathering and runoff dynamics in the hinterland (Berner, 1984). According to general consensus, the formation of S^{Pyrite} precedes the formation of $S^{Organic}$ in marine sediments. Only when the pool of iron (oxyhydr)oxides in the sediments is exhausted and reduced sulphur species continue to be generated, $S^{Organic}$ compounds are formed by incorporation of the excess reduced sulphur into kerogen precursors (Vairavamurthy *et al.*, 1995). However, recent studies (Mossmann *et al.*, 1991; Vairavamurthy *et al.*, 1992; Vairavamurthy *et al.*, 1995; Filley *et al.*, 2002; Werne *et al.*, 2008; Riedinger *et al.*, 2017) point out the fact that $S^{Organic}$ formation can be faster than commonly thought and even can precede S^{Pyrite} formation. Indeed, sulphur can be incorporated into OM on a timescale of days, while some reactive iron phases react are preserved in sulfidic sediments for hundreds of years (Poulton *et al.*, 2004).

OM preservation in marine sediments can be described using the S^{Pyrite} *vs* TOC relationship, which has proved useful in the reconstruction of past bottom water oxygenation (Anderson *et al.*, 1987; Leventhal, 1987; Suits *et al.*, 1993; Riboulleau *et al.*, 2003; Rimmer *et al.*, 2004), an important factor

of OM preservation in sediments (Demaison and Moore, 1980; Emerson, 1984). The use of S^{Pyrite} *vs* TOC ratios as indicator of bottom water oxygenation is based on the observation that modern, fine-grained normal marine (oxygenated overlying water with normal ocean salinity) siliciclastic sediments exhibit a reasonably well-defined linear relationship between TOC and S^{Pyrite} with a mean TOC/S^{Pyrite} = 2.8 ± 0.8 (Berner, 1970; Sweeney, 1972; Goldhaber and Kaplan, 1974; Berner, 1982). Lower TOC/S^{Pyrite} ratios are attributed to sediments accumulating under euxinic bottom waters (Raiswell and Berner, 1985). However, in iron-poor rocks, such as carbonates and sandstones where the availability of iron limits S^{Pyrite} formation in the rock (Berner, 1984; Pratt, 1984), problems arise when using the TOC *vs* S^{Pyrite} relationship as indicator of bottom water oxygenation. Also, in rapidly accumulating organic-rich sediments, where the amount of dissolved sulphate can become exhausted and limit the formation of S^{Pyrite}, the TOC *vs* S^{Pyrite} relationship may deviate from the expected 'normal' ratio (Murray *et al.*, 1978; Devol and Ahmed, 1981). Other problems in TOC *vs* S^{Pyrite} interpretations can arise if the amount of metabolizable organic carbon is limited (Raiswell and Berner, 1985), if OM has been lost by heating/maturity (Raiswell and Berner, 1986), or if unusual water chemistry is present (Tuttle and Goldhaber, 1993).

The OM preservation in marine sediments can also be described using the amount of $S^{Organic}$ which informs about the degree of OM sulfurization, an important mechanism of OM preservation (section 1.1.2). Indeed, positive relationships between TOC and $S^{Organic}$ were observed in numerous studies (Boussafir *et al.*, 1995; Boussafir and Lallier-Vergès, 1997; Lückge *et al.*, 2002; Tribovillard *et al.*, 2015), confirming the positive impact of OM sulphurisation on OM preservation. However, other studies, conducted on anoxic sediments from the Cariaco Basin (Venezuela) (Aycard *et al.*, 2003) and on the anoxic formation from Kössen (Hungary) (Veto *et al.*, 2000), where natural sulfurization is enhanced, show no positive correlation between organo-sulphur compound concentrations and the OM preservation. In this context, it is important to note that many studies looking at $S^{Organic}$ in OM-rich sediments in the past, focused on identifying and quantifying specific sulphurised organic compounds (Sinninghe Damsté *et al.*, 1989; Sinninghe Damsté *et al.*, 1998; Petsch *et al.*, 2000; Kolonic *et al.*, 2006; Amrani, 2014), while the presented Rock-Eval 7S method allows for a cumulative quantification of all sulphurised OM compounds, arguably a better measure of overall OM sulphurisation.

The present study focusses on the application of the new Rock-Eval 7S parameters S^{Pyrite} and $S^{Organic}$ defined in Chapter 3, in addition to the classical Rock-Eval 7S carbon and sulphur parameters (TOC; HI; OI; Tmax; MinC; S^{Total}), to describe OM preservation in Jurassic sediments. The goal of this section is to highlight the value of Rock-Eval 7S analyses in supporting paleo-environmental interpretation.

4.2- METHODOLOGY

Only Rock-Eval 7S analysis was performed here. The Rock-Eval 7S has the same functionalities as the former version (Rock-Eval 6) (Lafargue *et al.*, 1998; Behar *et al.*, 2001) complemented by a new system adapted for sulphur detection (section1.2). Indeed, this novel and powerful screening tool allows, in ~2 hours of analysis per sample, the quantification of numerous carbon and sulphur parameters, including the basic Rock-Eval 7S parameters (TOC; HI; OI; Tmax; MinC; S^{Total}) as well as the new Rock-Eval 7S parameters (S^{Pyrite}; $S^{Organic}$) based on the new method introduced in Chapter 3.

Samples from three different Jurassic sedimentary sections in the UK (Dorset, Yorkshire and Somerset), all deposited in shallow epicontinental seas, were analysed here to highlight the contribution that Rock-Eval 7S data can make to improve our understanding of OM preservation in marine sediments. The different studied sections are introduced in the following paragraphs.

4.2.1- Dorset section: Kimmeridge Clay Formation

The Kimmeridge Clay Formation (KCF) in Dorset was deposited in the Wessex Basin during Late Jurassic times (Kimmeridgian-Tithonian). The studied section consists of alternating beds of carbonates and shales and contains bands particularly rich in OM (TOC > 7wt%) (Herbin *et al.*, 1995; Morgans-Bell *et al.*, 2001; Jenkyns *et al.*, 2002; Tribovillard *et al.*, 2004). These organic-rich intervals are separated by sedimentary deposits with relatively lower TOC contents (typically 1–7 wt%) (Morgans-Bell *et al.*, 2001; Tribovillard *et al.*, 2004; Piper and Calvert, 2009). The Hydrogen Index (HI) of these samples exhibits an average of 608 mgHC/gTOC, a value indicative of marine OM (type II), but ranges from 200 up to 850 mgHC/gTOC (Huc *et al.*, 1992).

The TOC variations in the KCF section have been assessed in numerous studies which mainly suggest two models of OM preservation: Either OM accumulation driven by higher primary productivity followed by an establishment of anoxic-euxinic conditions (e.g. Gallois, 1976; Bertrand and Lallier-Vergès, 1993; Lallier-Vergès *et al.*, 1993; Tribovillard *et al.*, 1994) or variations in OM preservation primarily driven by anoxic bottom water condition variations unrelated to primary productivity changes (e.g. Tyson *et al.*, 1979; Oschmann, 1988; Wignall and Myers, 1988; Matthews *et al.*, 2004; Weedon *et al.*, 2004). In addition to these two models, Boussafir *et al.* (1995) used transmission electron microscopy and found a potential impact of OM sulphurisation on OM preservation in the Dorset section. Finally, a recent study by Armstrong *et al.* (2016) suggested that

orbitally paced fluctuations in rainfall intensity ultimately controlled fluctuations in the burial of OM in the KCF.

For this study, we selected 8 samples covering the range of organic-rich to organic-poor in the shale and carbonate beds of core material from the Swanworth Quarry 1, drilled at the type locality of the KCF in Dorset. The same samples were also previously used to validate the Rock-Eval 7S method (section 3.3).

4.2.2- North Yorkshire section: Grey Shale Member

The Grey Shale Member is situated at the base of the Whitby Mudstone Formation in the Cleveland Basin (North Yorkshire, UK). It was deposited during the marine transgression (major basin subsidence) that marks the boundary between the Pliensbachian and Toarcian Stages of the Early Jurassic in most areas of North-West European epicontinental basins (Hallam, 1981; Jenkyns, 1985; Powell, 2010). Placed within the Toarcian and overlain by the Jet Rock Formation (Toarcian Oceanic Anoxic Event, T-OAE, the Grey Shale Member is characterised by organic poor marine mudstones named “grey shale” intercalated with three distinct layers of organic and sulphur rich shales (~10-60 cm thick), named ‘sulphur bands’ (Chowns, 1966; Salem, 2013).

Salem (2013) conducted a detailed multi-proxy geochemical study on the Grey Shale Member to reconstruct its redox history. These results show that the Grey Shale Member overall records a gradual transition from oxic to anoxic-euxinic bottom waters. Within this trend, generally oxic conditions, during which the organic-poor grey shale was deposited, were intercalated by several brief episodes of anoxic-euxinic bottom water conditions preceding the global T-OAE and allowing formation of the organic-rich sulphur bands. Indeed, Salem (2013) suggested that OM preservation in the Grey Shale Member was linked to redox conditions. Concerning their kerogen characterisation, Salem (2013) showed that OM in the grey shale as well as the sulphur bands has a mixed marine (type II) and terrestrial (type III) composition.

For this study, we selected 13 samples at the base of the Grey Shale Member covering the range of organic poor sediments in the “grey shale” to organic rich sediments in the “sulphur bands”. We selected samples within the sulphur bands and in the grey shale directly above and below the sulphur bands. The same samples were also used to validate the Rock-Eval 7S method (section 3.3).

4.2.3- Somerset section: Blue Lias

The Hettangian-Sinemurian boundary sequence (upper part of the *Angulata* zone and lower part of the *Bucklandi* zone) situated on the coast of west Somerset, near East Quantoxhead, was selected for

this study. This section is part of the Blue Lias Formation in the Bristol Channel basin. The Blue Lias Formation comprises rhythmic interbeds of laminated organic-rich shale, pale and dark marl, and limestone (Hesselbo and Jenkyns, 1995; Warrington and Ivimey-Cook, 1995). It was deposited in an epicontinental marine environment influenced by eustatic and regional sea-level fluctuations and a warm, predominantly humid climate (Hallam, 1975; Hallam and Sellwood, 1976). According to the wide range of HI values (55 to 728 mg HC/g TOC), the OM of the Blue Lias Formation is distributed between type II (marine OM) and type IV (altered or mixed OM) (Deconinck *et al.*, 2003).

OM preservation in this section, as suggested by Sellwood (1970) and Hesselbo *et al.* (2004); seems to be linked to bottom water oxygenation which has varied significantly through the deposition of the Blue Lias Formation. Indeed, they observed that the more carbonate-rich beds reflect in general well-oxygenated conditions, whereas the organic-rich facies represent anoxic conditions at the sea floor.

We sampled the Blue Lias Fm. across the *Angulata-Bucklandi* boundary of the Somerset section. We selected 50 samples ranking from organic-poor to organic-rich. Unlike the Dorset and North-Yorkshire samples, the Somerset samples were not previously used to validate the Rock-Eval 7S method. However, these samples fall within the scope of the Rock-Eval 7S method given that they do not contain sulphate minerals (as indicated by XRD characterisations: Appendix M) and their OM maturation level is below the oil window (Tmax from 421°C to 434°C) (Deconinck *et al.*, 2003).

4.3- ROCK EVAL 7S RESULTS

The Tmax values of all selected samples are between 413°C and 435°C confirming that OM in the studied sections is immature to upper oil window. This suggests that the OM in these samples is primarily representative of the different supply and preservation mechanisms, and not heavily overprinted by thermal maturation and/or late diagenesis.

The OM kerogen type in each studied section can be deduced using HI *vs* OI diagram (Figure 4. 1). Samples from the Dorset section present HI and OI values which indicate type II OM, as observed by (Huc *et al.*, 1992), with some samples showing type I OM characteristics. Samples from the North-Yorkshire section, in contrast, contain a mix of type II and type III OM, as observed by Salem (2013). Finally, the OM in the Somerset section is mainly type II and type IV kerogen according to the wide range of HI and OI values, as observed by Deconinck *et al.* (2003). Fourteen Somerset samples presenting OI values > 100 mg CO_2/g TOC were removed, firstly because their TOC content is

assumed to be highly affected by oxidative processes and secondly because the new method for S^{Pyrite} and $S^{Organic}$ applied here was calibrated for OI values ranging from 0 to 90 mg CO_2/gTOC (section 3.2).

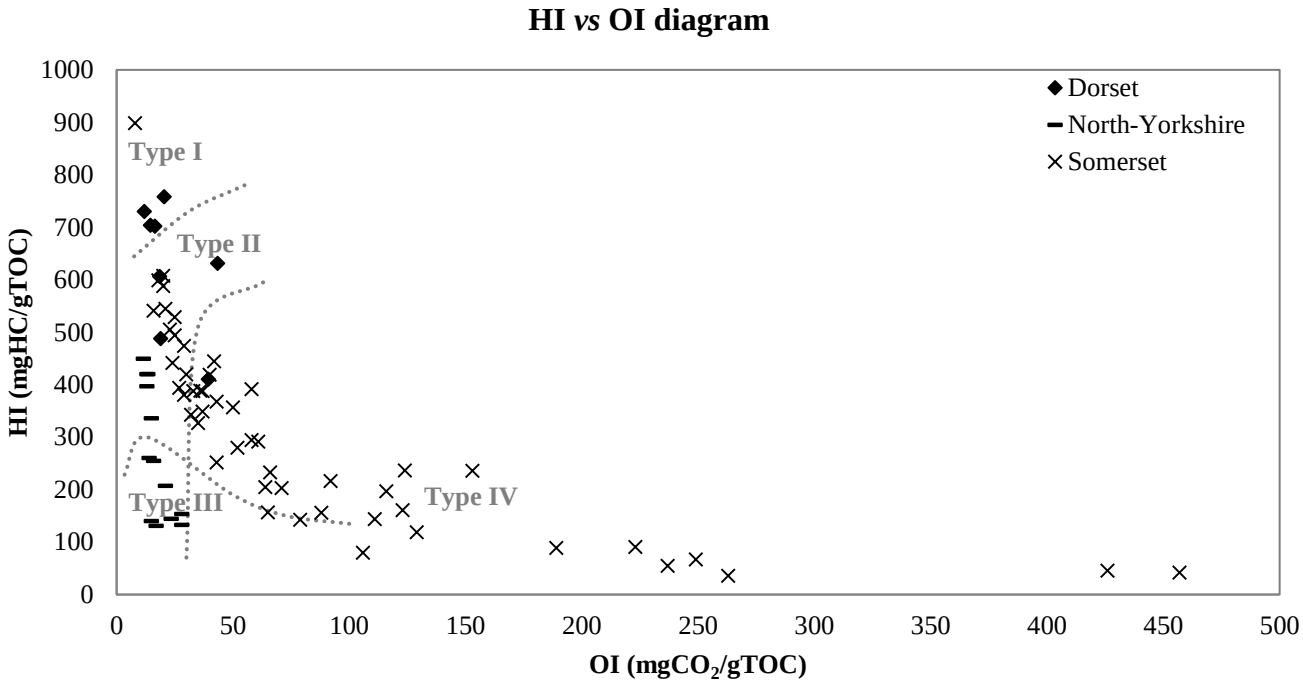

Figure 4. 1: HI vs IO diagram (Espitalie *et al.*, 1986) allowing characterisation of OM type in the different studied sections

The Rock-Eval 7S Mineral Carbon content (MinC) of the studied samples helps to define the general sample lithology and carbonate content using a modified Pettijohn (1957) classification:

- Clays: 0wt% ≤ Carbonate content < 30wt% (0wt% ≤ MinC< 3.6wt%);
- Marls: 30wt% ≤ Carbonate content < 70wt% (3.6wt% ≤ MinC< 8.4wt%);
- Carbonates: 70wt% ≤ Carbonate content < 100wt% (8.4wt% ≤ MinC≤12wt%).

The obtained MinC values indicate that samples are clay to carbonate-rich in the Dorset section (0.4 wt% ≤ MinC ≤ 11.2 wt%), clay-rich in the North-Yorkshire section (MinC ≤ 0.5 wt%) and are essentially marls with variable contributions of clay and carbonate in the Somerset section (3.3 wt% ≤ MinC ≤ 7.3 wt%).

In the following, the relationship between sulphur parameters, obtained using the new Rock-Eval 7S method described in Chapter 3, and TOC concentration is presented for each studied section.

4.3.1- Dorset section: Kimmeridge Clay Formation (Appendix J and N)

In the Dorset section, there is a positive correlation (R^2>0.9) between TOC and the total amount of reduced sulphur (S^{Total}) (Figure 4. 2a). This indicates that the intensity of bacterial sulphate reduction allowing formation of reduced sulphur species (HS^-, H_2S) was enhanced during deposition of the organic-rich samples.

We observe that carbonate-rich samples have relatively lower TOC and S^{Total} contents than clay rich samples (Figure 4. 2a). This suggests a dilution of both OM and terrigenous clay input by carbonate.

S^{Pyrite} contents of the studied samples are low compared to their S^{Total} contents, scattering around 1-2 wt% for most samples (Figure 4. 2b). This suggests that the pyritization process was limited by the concentration of of reactive iron, i.e. reactive iron minerals were not sufficiently abundant compared to the amount of reduced sulphur species produced by sulphate reduction. As the pyritization process would have been limited under these conditions, the S^{Pyrite} *vs* TOC relationships cannot be used as indicator of the overlying water oxygenation in the KCF at Dorset (Berner, 1984; Pratt, 1984). These Rock-Eval 7S results are consistent with Lallier-Vergès *et al.*, 1993 results of the same Dorset section of the Kimmeridge Clay Formation. Therefore, this confirm the validity of the new Rock-Eval 7S method for S^{Pyrite} quantification.

A strong, positive correlation (R^2>0.9, intercept close to zero) between $S^{Organic}$ and TOC is observed in the Dorset section (Figure 4. 2c), suggesting that OM sulfurization processes played an important role for OM preservation. These Rock-Eval 7S results are consistent with Lallier-Vergès *et al.*, 1993 results of the same Dorset section of the Kimmeridge Clay Formation. Therefore, this confirm the validity of the new Rock-Eval 7S method for $S^{Organic}$ quantification.

In Figure 4. 2d, 2e and 2f, we observe that for samples presenting TOC contents < 7 wt%, the S^{Total} is low and is mostly represented by S^{Pyrite}. For samples with higher TOC contents, the S^{Total} is relatively high and mostly occurs as $S^{Organic}$, with S^{Pyrite} remaining fairly constant. This shows that the reactive of reactive iron into the depositional environment must have been limited, and the increasing excess of reduced sulphur was incorporated into kerogen precursors to form $S^{Organic}$ compounds. It is interesting to note that this was the case for all samples of this section, independent of the relative contribution of carbonate or clay to their overall lithology.

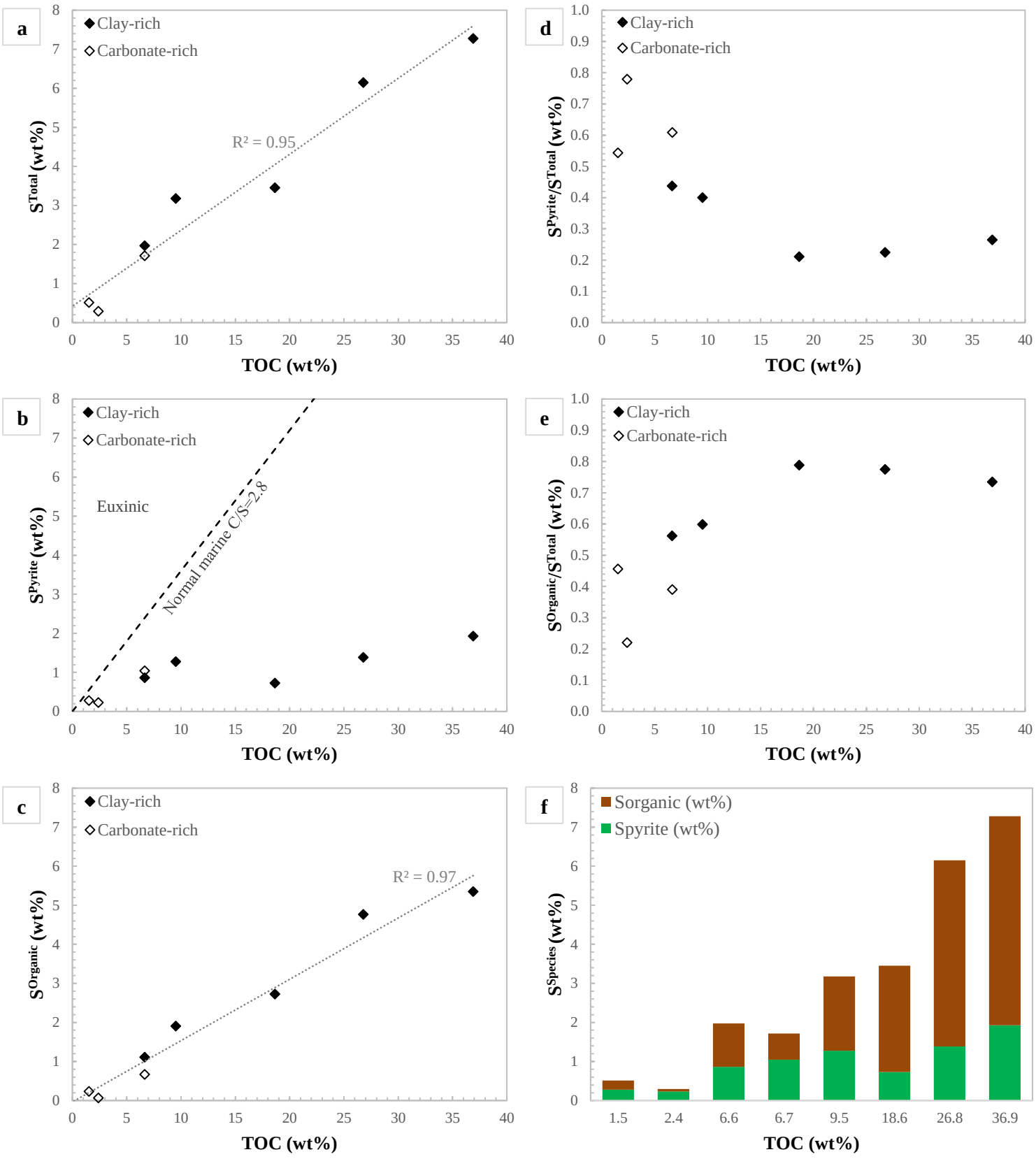

Figure 4. 2: Rock-Eval 7S sulphur parameters *vs* TOC for the Dorset section. Dashed line: Normal marine C/S relationship (Berner, 1982)

4.3.2- North Yorkshire section: Grey Shale Member (Appendix J and N)

In the North Yorkshire section, we observe a positive trend between TOC and S^{Total} with R^2=0.78 (Figure 4. 3a). This suggests that the intensity of bacterial sulphate reduction allowing formation of reduced sulphur species (HS^-, H_2S) was enhanced during deposition of the organic-rich samples compared to the organic poor samples.

We also observe a positive trend for S^{Pyrite} *vs* TOC (Figure 4. 3b) with R^2=0.69, similar to S^{Total} *vs* TOC (Figure 4. 3a), indicating that the depositional environment was not limited in reactive iron. Therefore, in this section, the S^{Pyrite} *vs* TOC relationships can be used as an indicator of the overlying water oxygenation given that this relationship is only valid in siliciclastic environments where S^{Pyrite} formation is not limited. The North Yorkshire section is characterised by organic-poor marine mudstones ("grey shale") which are intercalated with three distinct layers of organic- and sulphur-rich shales, the "sulphur bands". Our results show that the grey shale samples present TOC/S^{Pyrite} ratios ranking from values close to the dashed line representing TOC vs S^{Pyrite} relationship for normal marine sediments (Berner, 1982) to values corresponding to anoxic-euxinic bottom water condition. Samples from the sulphur bands present relatively lower TOC/S^{Pyrite} ratios compared to grey shale samples, indicative of anoxic-euxinic bottom water conditions (Figure 4. 3b).

We do not observe any direct relationship between $S^{Organic}$ and TOC in the North Yorkshire section (Figure 4. 3c), and in Figure 4. 3d, 3e and 3f, we observe that the formation of S^{Pyrite} clearly predominates over $S^{Organic}$. Therefore, with the new Rock-Eval 7S data we do not observe a direct link between OM preservation and OM sulfurization at this study site which presents lower TOC values compared to the Dorset section where the role of natural sulfurization was highlighted.

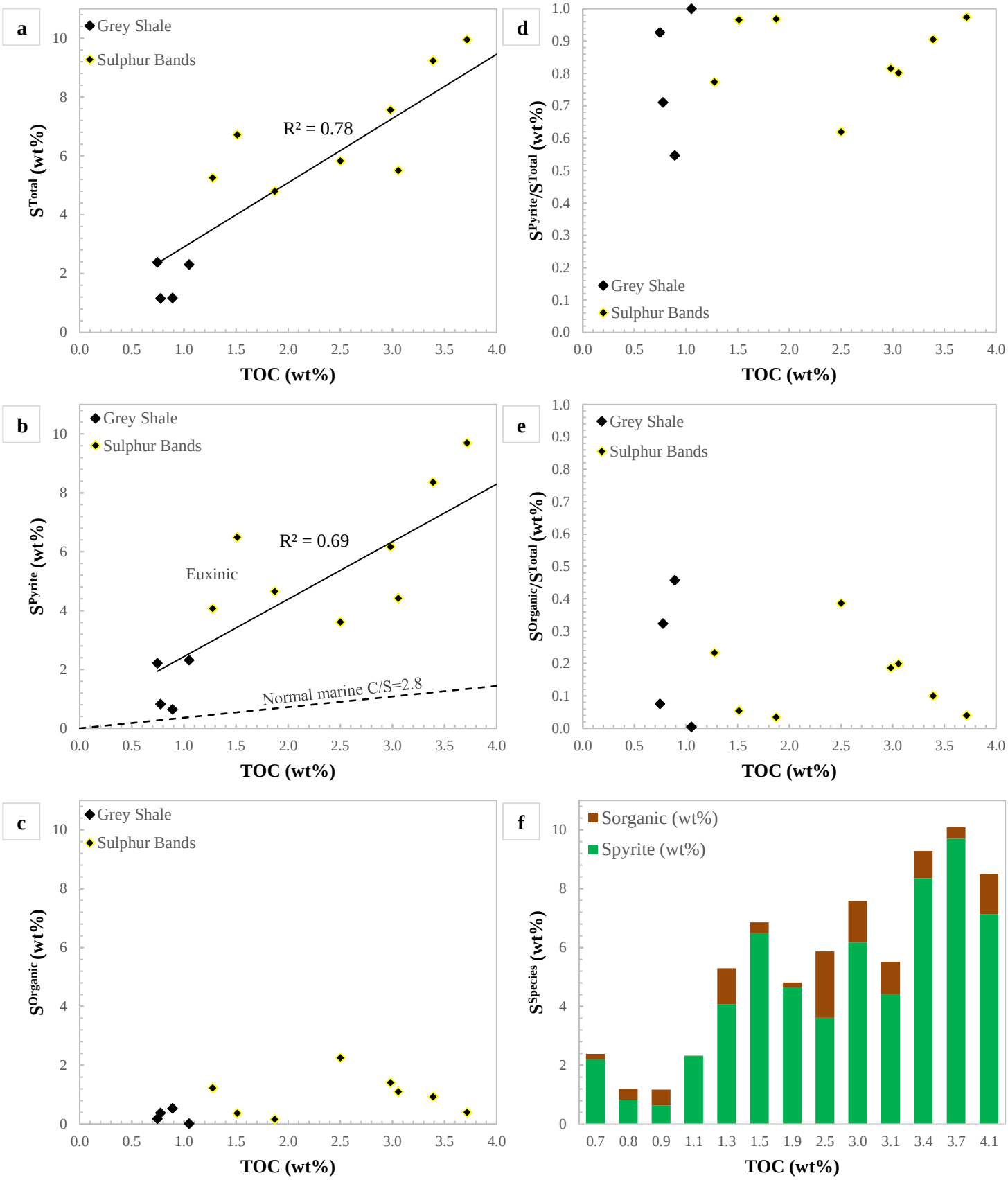

Figure 4. 3: Rock-Eval 7S sulphur parameters vs TOC for the North-Yorkshire section. Dashed line: Normal marine C/S relationship (Berner, 1982)

4.3.3- Somerset section: Blue Lias (Appendix J and N)

In the Somerset section, we observe a positive trend between TOC and S^{Total} for most of the samples with TOC contents < 9 wt% (Figure 4. 4a). This suggests that the intensity of bacterial sulphate reduction allowing formation of reduced sulphur species (HS^-, H_2S) was enhanced during deposition of organic-rich samples. Then, this intensity of bacterial sulphate reduction dropped in even organic-richer samples with TOC contents ≥ 9wt% (Figure 4. 4a) either due to a decreasing amount of SO_4^{2-} present in the depositional environment and/or by a decreasing input of metabolizable OM.

In Figure 4. 4b we observe that the carbonate-rich samples tend to have TOC/S^{Pyrite} ratios close to the TOC *vs* S^{Pyrite} relationship of normal marine sediments (Berner, 1982), while the clay-rich samples tend to have low S^{Pyrite} contents mostly around 0-2 wt%, except one sample where S^{Pyrite} = 3.4 wt% (Figure 4. 4b). This indicates that the pyritization process was generally limited in most of clay-rich samples. For clay-rich samples with TOC < 9 wt%, where the intensity of bacterial sulphate reduction was enhanced (Figure 4. 4a), incomplete pyritization can only be related to a limited concentration of reactive iron minerals. For the clay-rich samples with TOC ≥ 9 wt%, where the intensity of bacterial sulphate reduction was reduced (Figure 4. 4a), the pyritization process was limited by the amount of reduced sulphur species present in the depositional environment (Figure 4. 4a). Therefore, the S^{Pyrite} *vs* TOC relationships of the clay rich samples cannot be used as indicator of overlying water oxygenation, as this relationship is useful in environments where S^{Pyrite} formation is limited (Murray *et al.*, 1978; Devol and Ahmed, 1981; Berner, 1984; Pratt, 1984).

In general, we observe a positive trend between TOC and $S^{Organic}$ contents for most of the Somerset samples with TOC contents < 9wt%, except one sample in which strong pyritization (Figure 4. 4b) limited $S^{Organic}$ formation. Indeed, the organic-poor, mostly carbonate-rich samples have lower $S^{Organic}$ contents compared to the organic-rich/clay-rich samples (Figure 4. 4c). For samples with TOC contents ≥ 9wt%, both the amount of reduced sulphur (S^{Total}) and the formation of $S^{Organic}$ compounds were limited (Figure 4. 4c).

There is one sample with relative low TOC content (1.0 wt%), high S^{Total} content (2.60 wt%), high S^{Pyrite} content (2.3 wt%) and low $S^{Organic}$ content (0.3 wt%), the yellow sample in Figure 4. 4a, 4b, 4c, 4d, 4e. According to Leventhal (1995) sediments containing high sulphide sulphur (greater than 1 %) in association with low contents of organic C (generally less than 1 %) can be interpreted to result from later diagenetic or epigenetic addition of HS^- that reacted with available reactive iron to form pyrite. An alteration of this sample, as suggested by its high OI value (65 $mgCO_2/gTOC$), would also explain the low TOC content of this sample compared to its high S^{Total} content.

In Figure 4. 4d, 4e and 4f, we observe that the partitioning between S^{Pyrite} and $S^{Organic}$ in this sample set is widely distributed, ranging from samples that exclusively contain S^{Pyrite} to samples that only contain $S^{Organic}$. It is interesting to note that the carbonate-rich samples tend to have higher relative S^{Pyrite} contributions than the clay-rich samples, which is counter-intuitive as the reactive iron required to form pyrite is usually thought to be delivered from land, similar to clay.

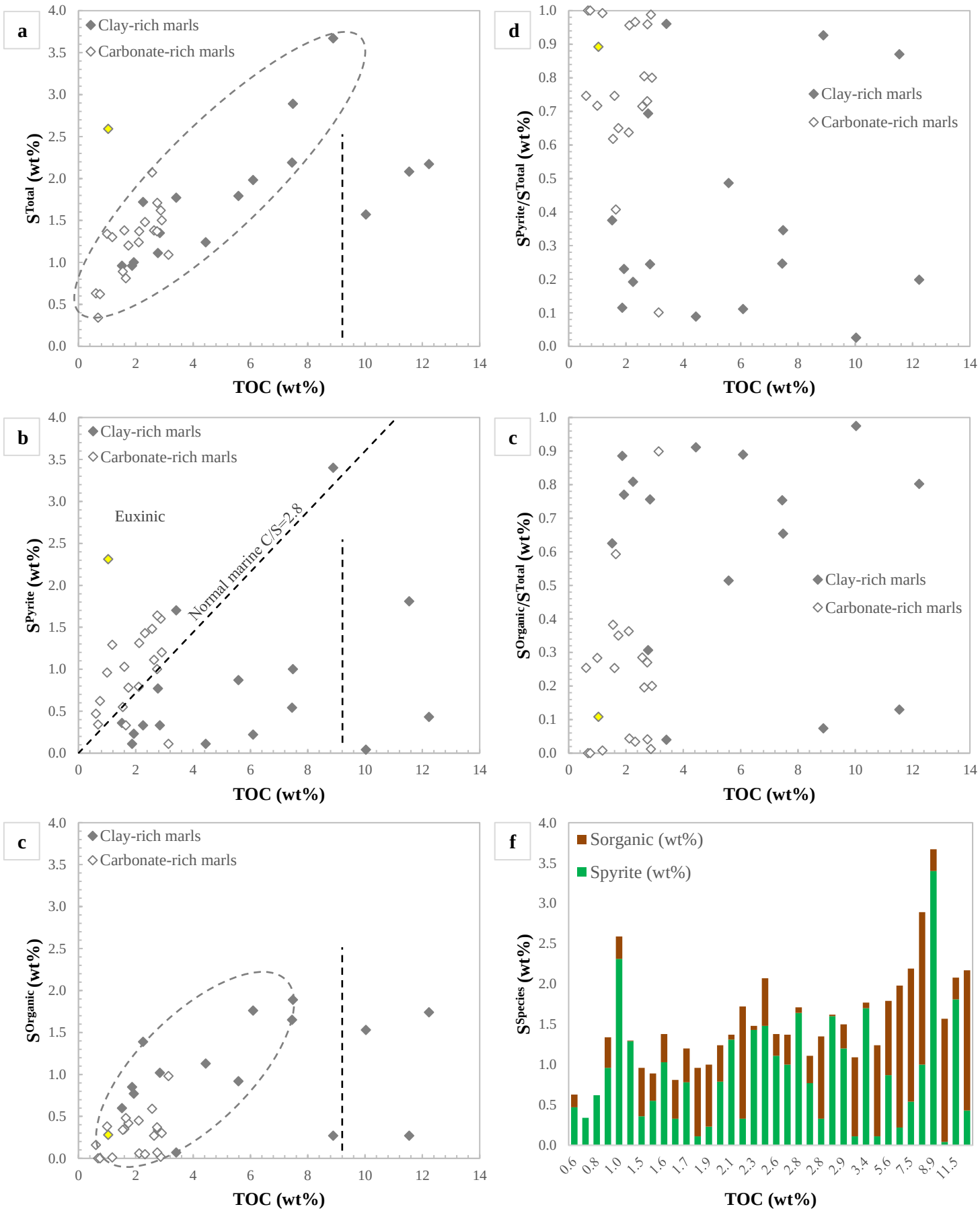

Figure 4. 4: Rock-Eval 7S sulphur parameters vs TOC for the Somerset section. Dashed line: Normal marine C/S relationship (Berner, 1982)

4.4- CONTRIBUTION OF NEW ROCK-EVAL 7S DATA IN THE DESCRIPTION OF OM PRESERVATION

4.4.1- Dorset section: Kimmeridge Clay Formation

Numerous studies have reconstructed the paleoenvironmental conditions responsible for the deposition of the KCF and postulated models to explain TOC variation in the Dorset section. Some models suggest that the organic-rich intervals are the result of increased primary productivity (e.g. Gallois, 1976; Bertrand and Lallier-Vergès, 1993; Lallier-Vergès *et al.*, 1993; Tribovillard *et al.*, 1994). It was assumed that enhanced primary productivity caused increased OM accumulation, leading to production of large quantities of H_2S which, in turn, could result in anoxic-euxinic conditions and enhanced OM preservation. Other models suggest enhanced preservation, due to anoxic bottom waters, is the primary cause of the depositions of the organic-rich intervals (e.g. Tyson *et al.*, 1979; Oschmann, 1988; Wignall and Myers, 1988; Matthews *et al.*, 2004; Weedon *et al.*, 2004). They argued that the interface between oxygenated and suboxic/anoxic waters cyclically rose and fell and, when falling below the sediment–water interface, caused diminished preservation of the settling OM and hence the deposition of less organic-rich facies. Our Rock-Eval 7S results support both models given that we obtained a positive correlation (R^2>0.9) between TOC and S^{Total}. Indeed, this result suggests an increase of the intensity of bacterial sulphate reduction either by higher amounts of metabolizable OM via enhanced primary productivity, or by the establishment of more anoxic conditions.

In addition of these two models, other environmental/climatic conditions have been suggested to impact the OM preservation in the Dorset section. Boussafir *et al.* (1995) argued that sulfurization of OM could play an important role in the preservation of OM. Our Rock-Eval 7S results, by showing a very good positive correlation (R^2>0.9 and intercept close to 0) between $S^{Organic}$ and TOC, are consistent with Boussafir *et al.* (1995) results. Another model by Armstrong *et al.* (2016) suggested that the fluctuations in OM burial in the KCF were controlled by orbitally paced changes in rainfall intensity beneath the ascending limb of the Hadley cell, i.e., under the direct influence of the intertropical convergence zone. We were not able to observe this impact of paleoclimate on OM preservation using Rock-Eval 7S data because the S^{Pyrite} content of the studied samples, the only parameter which has a direct link with precipitation, weathering and runoff dynamics in the hinterland, presents a low and a constant value

4.2.2- North Yorkshire section: Grey Shale Member

Rock-Eval 7S data suggest that OM preservation in the Grey Shale Member was related to redox conditions prevailing during deposition of this interval. Indeed, the organic-poor grey shale samples were deposited in relative well oxygenated water conditions compared to the organic-rich sulphur band samples which were characterised by anoxic-euxinic bottom water conditions. This is consistent with results from the detailed analyses of the Grey Shale Member, performed by (Salem, 2013), including TOC and total sulphur quantification, microscopy, iron speciation, trace element concentrations, molecular biomarkers, and bulk carbon and sulphur isotopes. Indeed, (Salem 2013) suggested highly variable redox conditions within the Grey Shale Member, with generally oxic conditions during the deposition of the organic-poor "grey shale", intercalated by some brief episodes of anoxic-euxinic bottom water conditions allowing the formation of the organic-rich "sulphur bands. Therefore, in this study, based on a simple and easy to compile Rock-Eval 7S dataset, we come to similar interpretations as the detailed, time-consuming study by (Salem, 2013).

The cm-scale geochemical records from the lower sulphur band, performed by (Salem, 2013), actually suggest significant short term variations in redox within the bed, with one full cycle from anoxia/euxinia to oxic conditions and back. In this study, with our data resolution being too low, we are not able to observe any internal redox condition within the individual sulphur bands.

(Salem, 2013) also showed that the grey shale samples directly below the sulphur bands showed less enrichment of TOC, reactive iron and trace elements, but still suggested conditions close to bottom water anoxia. Only further up the section, in the bioturbated grey shale, highly reactive iron and trace elements were significantly depleted, indicating a return to more oxic conditions. Our Rock-Eval 7S data confirm these results by showing that the grey shale samples, selected directly above and below the sulphur bands, have TOC/S^{Pyrite} ratios ranging from values close to the TOC vs S^{Pyrite} relationship for normal marine sediments (Berner, 1982) to values corresponding to anoxic-euxinic bottom water conditions. This suggests that either some of the grey shale samples directly below and above the sulphur bands were deposited during anoxic bottom water conditions, or the bottom waters were oxic during the deposition but pore waters became anoxic/euxinic shortly below the sediment-water interface, leading to a high pyritization degree underneath an oxic water column (Hardisty *et al.*, 2018; Raiswell *et al.*, 2018).

No impact of OM sulphurisation on OM preservation is observed in the Grey Shale Member. Indeed, the Rock-Eval 7S data show that OM sulphurisation was limited due to high concentration of reactive iron allowing S^{Pyrite} formation which consumed most of the available reduced sulphur species.

4.2.3- Somerset section: Blue Lias

For Somerset samples with TOC contents < 9 wt%, the Rock-Eval 7S dataset shows that generally clay-rich samples have higher TOC and S^{Total} contents compared to carbonate-rich samples, suggesting an increase in the intensity of bacterial sulphate reduction in organic-rich/clay-rich samples. This can be due to an establishment of more anoxic condition which would have led to an enhancement of sulphate reducing bacteria activity, or an increase in the input of metabolizable OM via primary production, or weaker dilution of both TOC and terrigenous clay by carbonate.

In addition to that, the carbonate-rich samples tend to have TOC/S^{Pyrite} ratios to close and following the TOC *vs* S^{Pyrite} relationship for normal marine sediments (Berner, 1982). However, in clay-rich samples, with S^{Pyrite} formation being limited, the S^{Pyrite} *vs* TOC relationships cannot be used as indicator of overlying water oxygenation (Murray *et al.*, 1978; Devol and Ahmed, 1981; Berner, 1984; Pratt, 1984).

Literature (Sellwood, 1970; Hesselbo *et al.*, 2004) suggests that OM preservation in the Somerset section is linked to bottom-water oxygenation. Indeed, the more carbonate-rich beds reflect well-oxygenated conditions, whereas the organic-rich facies represent anoxic conditions at the sea floor. Additional information from the Rock-Eval 7S data is the relative enhancement in the intensity of natural OM sulphurisation in clay-rich samples compared to carbonate-rich samples, which could contribute to the high OM preservation in clay-rich samples.

For Somerset samples with TOC contents ≥ 9wt%, we observe a drop in the intensity of bacterial sulphate reduction (Figure 4. 4a) leading to limited formation of S^{Pyrite} and $S^{Organic}$. This can be related either to a decreasing amount of dissolved sulphate (SO_4^{2-}) presents in the depositional environment and/or to a decreasing input of metabolizable OM, the two main elements required for bacterial sulphate reduction.

Generally, in the Somerset section, clay-rich samples tend to have lower relative S^{Pyrite} contributions than the carbonate-rich samples, while the intensity of bacterial sulphate reduction is higher in clay-rich compared to carbonate-rich samples. This is counter-intuitive given that the reactive iron required to form pyrite is usually thought to be associated to terrigenous, i.e., clay input, suggesting that pyrite formation in the Somerset section is to an extent independent of the terrigenous input. $S^{Organic}$ enrichment in the clay-rich samples can be explained by more rapid OM sulphurisation compared to S^{Pyrite} formation (Riedinger *et al.*, 2006; Raven *et al.*, 2016a; Raven *et al.*, 2016b). Indeed, it is possible that, in clay-rich samples, most of the reduced sulphur species were firstly used to form

$S^{Organic}$ compounds, limiting the potential for S^{Pyrite} formation. However, additional work is needed to confirm this assumption.

4.5- CONCLUSIONS

In this study, using only a rapid Rock-Eval 7S analysis, we obtained a targeted set of carbon and sulphur parameters to help describe factors of OM preservation in marine sediments. Indeed, the new Rock-Eval 7S parameters (S^{Pyrite} and $S^{Organic}$) defined in Chapter 3, combined with the classical Rock-Eval 7S parameters (TOC; HI; OI; Tmax; MinC; S^{Total}), were used as indicators of paleo-environmental conditions which impact OM preservation. In the Dorset and Somerset sections, the potential role of OM sulfurization on OM preservation has been assessed using $S^{Organic}$ *vs* TOC plots. In addition, S^{Pyrite} *vs* TOC plots have been useful to characterise the bottom water oxygenation, an important environmental factor of OM preservation, prevailing during deposition of the North Yorkshire section.

By using the advanced Rock-Eval 7S methodology, the first quick, efficient and reliable quantitative method that allows direct quantification of S^{Pyrite} and $S^{Organic}$ as well as the classical Rock-Eval 7S parameters (TOC; HI; OI; Tmax; MinC; S^{Total}) in a single and short analysis, we saved numerous analytical techniques and chemical treatments that might be required to obtain these different parameters. Therefore, as shown in this study, using Rock-Eval 7S is a significant time and money saving option which can be integrated in most paleo-environmental assessments.

Chapter 5: SUMMARY AND OUTLOOK

5.1-SUMMARY

The overall target of this PhD project has been to contribute to the understanding of source rock formation via the study of OM preservation in marine sediments. Indeed, this study aims to highlight and provide different new sulphur Rock-Eval 7S parameters that can be used for this purpose. This process first required developing and validating new analytical method for sulphur speciation and quantification on the Rock-Eval 7S system. The following points were studied:

- Calibration of Rock-Eval 7S for S^{Total} quantification: This involved determination of two sulphur calibration coefficients, KSO_2 pyrolysis and KSO_2 oxidation, for each phase of the Rock-Eval 7S analysis. Using these new calibration coefficients, we obtained that Rock-Eval 7S provides accurate quantification of the S^{Total} content of rock samples.

- Characterisation of Rock-Eval 7S sulphur signals of the different sulphur species found in marine sediments (S^{Pyrite}; $S^{Organic}$; $S^{Sulphates}$ and $S^{Elemental}$): We observed that the different sulphur species decompose at different specific ranges of temperatures, except S^{Pyrite} and $S^{Organic}$. These two sulphur species are degraded at different ranges of temperature during the pyrolysis phase allowing quantification of ${}_{Pyrolysis}S^{Pyrite}$ and ${}_{Pyrolysis}S^{Organic}$ but during the oxidation phase, they are degraded at the same temperature ranges. This limits the total S^{Pyrite} and $S^{Organic}$ direct quantification using the Rock-Eval 7S. Therefore, further analytical development was required to find a method for S^{Pyrite} and $S^{Organic}$ quantification using Rock-Eval 7S.

- Development of a method for S^{Pyrite} and $S^{Organic}$ quantification using Rock-Eval 7S: Knowing that with Rock-Eval 7S we can quantify ${}_{Pyrolysis}S^{Pyrite}$, the strategy here was to study pyrite thermal transformation during Rock-Eval 7S pyrolysis and its interaction with OM and minerals commonly found in organic rich marine sediments, in order to estimate the total S^{Pyrite} from the ${}_{Pyrolysis}S^{Pyrite}$, and then deduce the total $S^{Organic}$. The following formulas have been defined for S^{Pyrite} and $S^{Organic}$ quantification in organic rich marine sediments:

$$S^{Pyrite} = \frac{(1+\beta+\gamma)}{\alpha} \cdot {}_{Pyrolysis}S^{Pyrite}$$

$$S^{Organic} = S_{total} - S^{Pyrite}$$

In these formulas, the factor α is the percentage of ${}_{Pyrolysis}S^{Pyrite}$ of the total S^{Pyrite}. The factors β and γ are correction factors of the OM_{effect} and Min_{effect}, which aim to consider the amount of ${}_{Pyrolysis}S^{Pyrite}$ trapped in the OM and the mineral matrix during the pyrolysis phase.

- Validation of the new Rock-Eval 7S method for S^{Pyrite} and $S^{Organic}$ quantification: A set of organic rich marine sediment samples, and of sedimentary mixtures with known S^{Pyrite} and $S^{Organic}$ contents (sedimentary rocks containing only $S^{Organic}$ + pyrite) was selected and analysed to validate this new method. The results obtained show that the new Rock-Eval 7S method provides an accurate quantification of both S^{Pyrite} and $S^{Organic}$. We observed, nevertheless, a slight disparity of the Rock-Eval 7S method with independent analyses which can be linked to the calibration of the OM_{effect} and Min_{effect}, two important parameters of the Rock-Eval 7S method.

Once the development and the validation of this new Rock-Eval 7S method for S^{Pyrite} and $S^{Organic}$ quantification completed, its application to parametrise OM preservation has been highlighted in this study. This concerned the use of the new Rock-Eval 7S parameters, S^{Pyrite} and $S^{Organic}$, in addition to the classical Rock-Eval 7S carbon and sulphur parameters (TOC; HI; OI; Tmax; MinC; S^{Total}), to help the description of OM preservation in marine environments. Three sedimentary sections were studied, the Dorset section (KCF), the North-Yorkshire section (Grey Shale Member) and the Somerset section (Blue Lias Fm.). Only with a single Rock-Eval 7S analysis of samples from these sedimentary sections, we obtained relevant carbon and sulphur parameters that was used as indicators of paleoenvironmental conditions which impact OM preservation. Therefore, we save numerous analytical techniques and chemical treatments that might be required to obtain these different parameters.

This established new Rock-Eval 7S method for S^{Pyrite} and $S^{Organic}$ quantification has numerous other potential applications and opportunities. Indeed, it can provide useful data for a wide range of studies including petroleum exploration and production, paleoenvironmental/paleoclimate reconstruction, coal exploration and production and soil pollution.

5.2-OUTLOOK

5.2.1- Development of Rock-Eval 7S for S^{Pyrite} and $S^{Organic}$ quantification

In this study, a method for S^{Pyrite} and $S^{Organic}$ quantification using Rock-Eval 7S was developed and validated. To improve this method and/or widen its scope, additional work must be undertaken, including:

- Improvement of the calibration of Rock-Eval 7S method parameters (OM_{effect} and Min_{effect}): This will consist in studying, in more detail, the effect of OM and minerals on the amount of pyritic sulphur released during pyrolysis to improve calibration of OM_{effect} and Min_{effect}. The goal here is to consider the high geochemical and mineralogical variability of sedimentary rocks in order to improve accuracy of the Rock-Eval 7S method.

- Sulphate neoformation issues: More research must be done to understand, in more detail, the sulphate neoformation which occurs during Rock-Eval 7S analysis in order to find an accurate and valid method to distinguish real native sulphates from neoformed sulphates. This will allow the application of the Rock-Eval 7S method to sedimentary rocks containing a considerable amount of sulphate, which are essentially from evaporitic environments.

- Calibrating the Rock-Eval 7S method for other type of samples (recent sediments, soils, coals): In this study, the Rock-Eval 7S method for pyritic and organic sulphur quantification was calibrated to ancient sedimentary rocks. Therefore, further analytical development improvements are needed to extrapolate this method on other type of samples including recent sediments, soils, and coals. This will widen the scope of Rock-Eval 7S method to environmental sciences, soils sciences and coal exploration/production.

5.2.2- Using the Rock-Eval 7S carbon and sulphur properties as descriptors of OM preservation in DIONISOS sedimentary basin model

The longer-term perspective of this PhD project is to apply Rock-Eval 7S carbon and sulphur parameters as routine descriptors of OM preservation in basin models, linking them to the stratigraphic basin model Dionisos™, in particular its new module “Dionisos Organic Matter”.

5.2.2.1- Dionisos principle

Dionisos™ is a 3D stratigraphic model which has been developed at IFPEN over the past twenty two years (Granjeon, 1996; Granjeon and Joseph, 1999; Granjeon and Wolf, 2007; Granjeon, 2009; Granjeon, 2014). It allows simulation of the deposition and evolution of sedimentary systems over long time scales (tens to hundreds of millions of years) and distances (several tens to hundreds of kilometres). The application of the principle of mass balance and large-scale transport laws permit Dionisos™ to reconstruct the 3D evolution of facies distribution, sedimentation and erosion rates. This stratigraphic modelling is done over a given period of time, and at each time step, three factors are quantified (Figure 5. 1): (i) The accommodation space which corresponds to the space available for the sediments. It is obtained by adding the relative deformation of the basin (subsidence) and the eustatic variations; (ii)The sediment supply or production which corresponds to fluvial inputs (erosion of adjacent land) and/or in situ production of carbonates; (iii) The sediment transport which is defined from the large-scale sediment transport laws (Csato *et al.*, 2013; Granjeon, 2014).

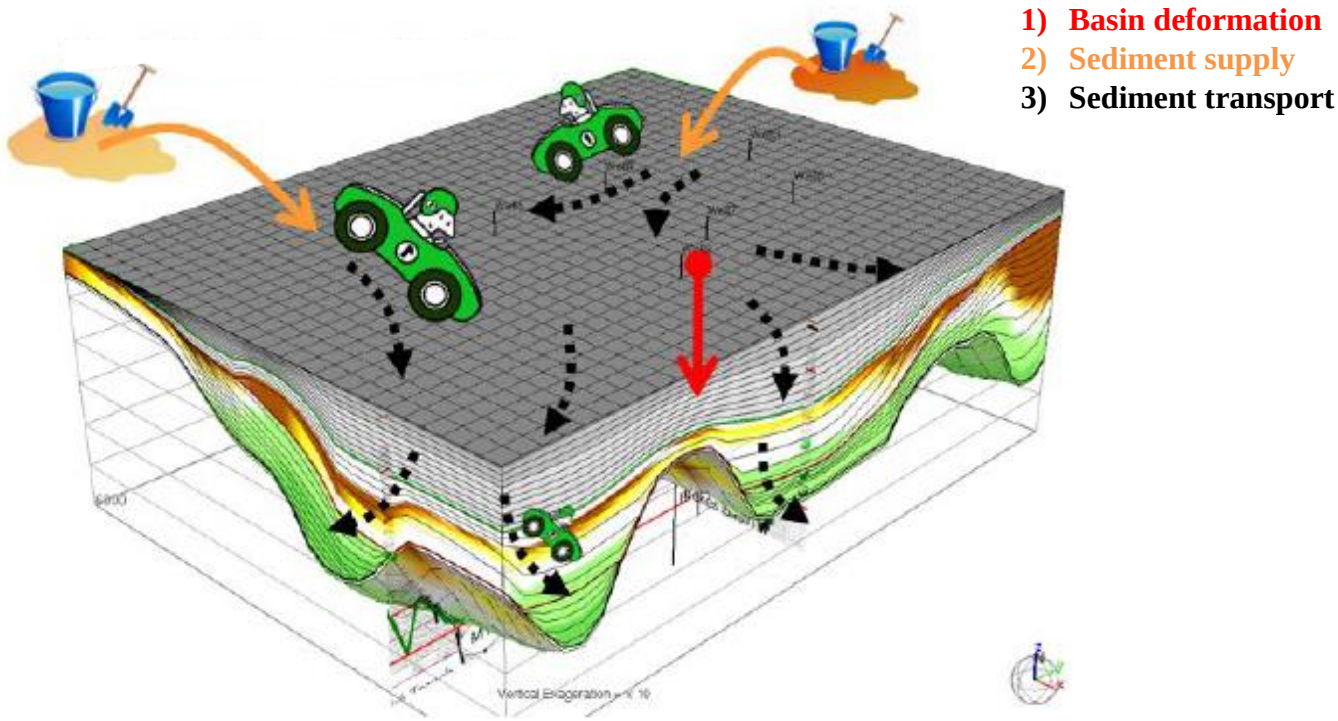

Figure 5. 1 : Quantified factor in Dionisos™ simulations

The new module of Dionisos™, "Dionisos Organic Matter", is currently being developed at IFP Energies Nouvelles (Granjeon and Chauveau, 2014). The new module is used to simulate the

distribution and quality of source rocks and gas/oil shales by modelling production, transport and preservation/degradation of organic matter at the basin scale. This simulation is done using parameters, some already provided by the normal stratigraphic modelling approach (e.g. bathymetry, basin morphology, sedimentation rate), and others specific to organic matter: primary productivity; rain rate of organic carbon; transport of organic matter; the oxygen level and the burial efficiency which corresponds to the degradation of organic matter on the first meters of burial.

5.2.2.2- Using the Rock-Eval 7S carbon and sulphur properties as descriptors of OM preservation in DIONISOS sedimentary basin model

Organic matter preservation is currently simulated in Dionisos Organic Matter from two parameters: the oxygen level and the burial efficiency. The use of oxygen level is based on the fact that organic matter degradation is most effective in an oxic environment, while anoxic conditions favour the preservation of organic matter. The oxygen level is determined from an equation based on Mann and Zweigel (2008). It is expressed as a value ranging from 0 (totally anoxic environment) to 1 (environment completely oxygenated). It is determined over a vertical profile defined from a surface oxygen level, a primary productivity and a deep mixing coefficient. The burial efficiency is mainly controlled by sedimentation rate (Betts and Holland, 1991) and environmental redox conditions (Tyson, 1995). In Dionisos Organic Matter, the burial efficiency is calculated from the sedimentation rate provided by the normal stratigraphic model and the oxygen level.

We have seen in this study that relevant Rock-Eval 7S carbon and sulphur geochemical parameters can be used to accurately describe OM preservation. The outlook will be to integrate these new Rock-Eval 7S descriptors of OM preservation to Dionisos Organic Matter. This aims to provide improved input variables to Dionisos, to expand the existing Dionisos parameters for OM preservation.

APPENDIX

Appendix A: Rock-Eval 7S sulphur calibration (SO_2 signals of Elemental sulphur and B2323 coal samples)

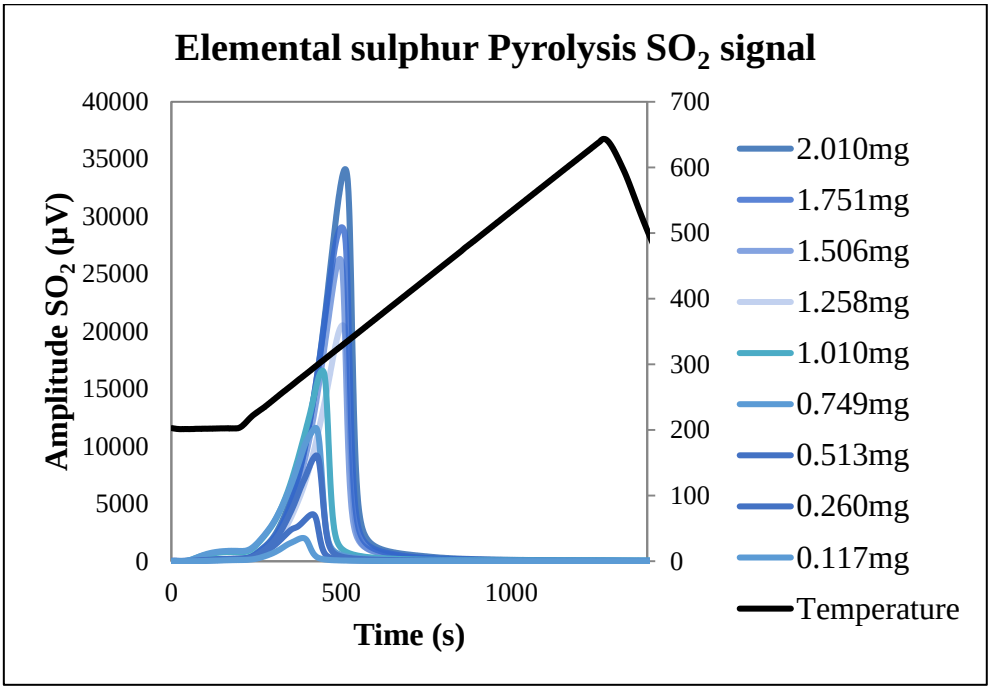

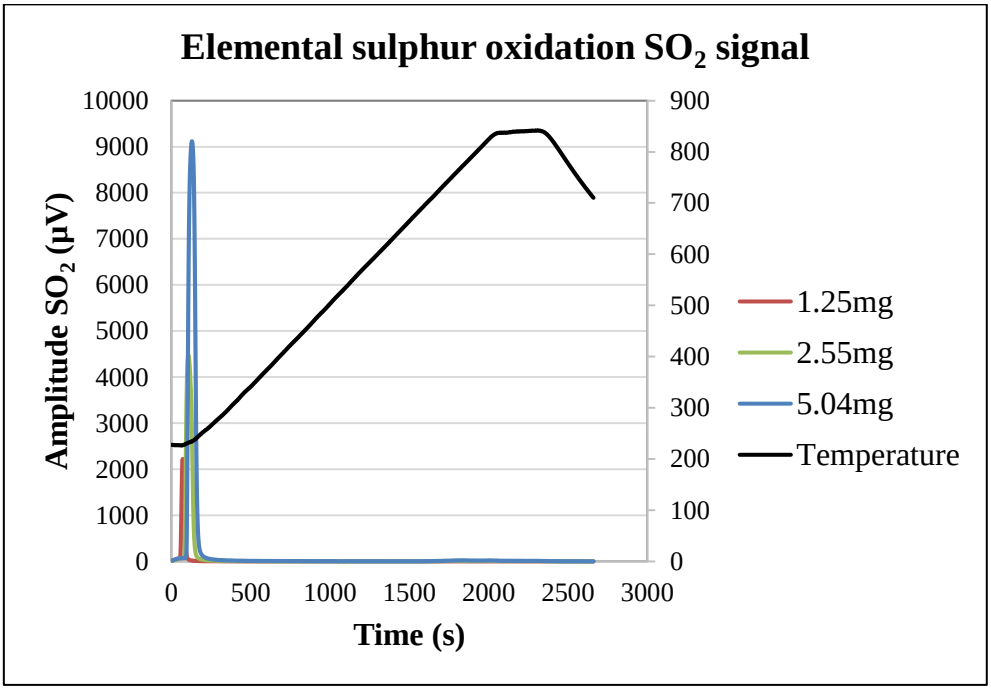

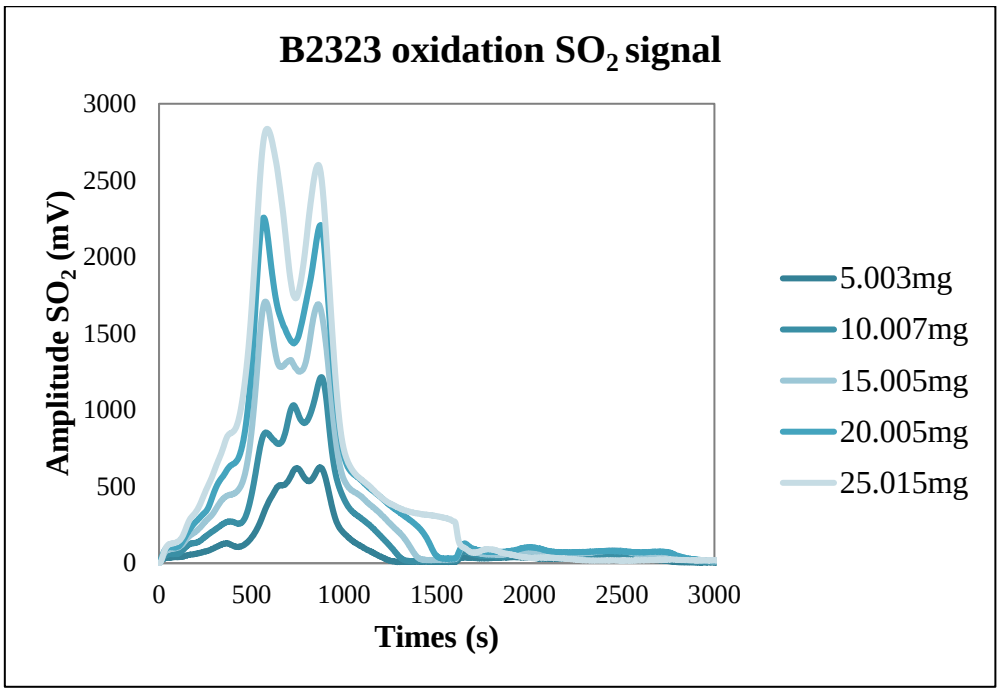
B2323 oxidation SO2 signal
Amplitude SO2 (mV)
3000
2500
2000
1500
1000
500
0
0
500
1000
1500
2000
2500
3000
Times (s)
5.003mg
10.007mg
15.005mg
20.005mg
25.015mg

Appendix B: Rock-Eval 7S sulphur calibration: Determination of the KSO_2 coefficients

Pyrolysis reference sample: Elemental sulphur

TS (%)	Sample mass (mg)	Sulphur mass (mg)	100*Sulphur mass (µg)	Peaks area µV.s
100	0.260	0.260	26000	506622
100	0.513	0.513	51300	1045283
100	0.749	0.749	74900	1602437
100	1.010	1.010	101000	2147351
100	0.119	0.119	11900	217763
100	0.117	0.117	11700	240875
100	0.264	0.264	26400	518773
100	0.510	0.510	51000	1029022
100	0.760	0.760	76000	1572353
100	1.003	1.003	100300	2083895
100	1.258	1.258	125800	2643205
100	1.249	1.249	124900	2601284
100	1.506	1.506	150600	3188868
100	1.505	1.505	150500	3161569
100	1.751	1.751	175100	3765059
100	1.749	1.749	174900	3830116
100	2.014	2.014	201400	4311044
100	2.010	2.010	201000	4328505

Oxidation reference sample: Coal B2323

TS (%)	Sample mass (mg)	Sulphur mass (mg)	10000*sulphur mass (µg)	Peak area µV.s
3.42	5.003	0.171	1711026	332567
3.42	10.007	0.342	3422394	650416
3.42	15.005	0.513	5131710	1016850
3.42	20.005	0.684	6841710	1338309
3.42	25.005	0.855	8551710	1634105

Appendix C: Rock-Eval 7S sulphur calibration: Assessment of the calibration coefficients

Samples	RE 7S TS (wt.%)	Standard deviation (wt.%)	Infrared TS (wt.%)	Error bars (wt.%)
Orbagnoux BR9ca	1.13	0.10	1.11	0.10
Orbagnoux BR9h	2.44	0.10	2.28	0.10
Orbagnoux BR9f	3.49	0.10	3.49	0.10
Orbagnoux DR9ca	11.77	0.10	12.32	0.30
Orbagnoux DR9h	13.66	0.10	14.20	0.30
Orbagnoux DR9f	14.68	0.10	14.54	0.30
Samples	RE 7S TS (wt.%)	Standard deviation (wt.%)	LECO TS (wt.%)	Error bars (wt.%)
North Yorkshire 03	2.38	0.07	2.52	0.20
North Yorkshire 09	6.69	0.07	6.62	0.20
North Yorkshire 10	9.85	0.24	9.87	0.20
North Yorkshire 11	9.20	0.08	9.75	0.20
North Yorkshire 12	8.00	0.39	7.87	0.20
North Yorkshire 13	7.56	0.11	7.22	0.20
North Yorkshire 14	5.22	0.08	4.74	0.20
North Yorkshire 15	1.17	0.04	0.90	0.20
North Yorkshire 17	2.47	0.31	2.10	0.20
North Yorkshire 18	5.51	0.08	4.84	0.20
North Yorkshire 40	1.07	0.17	1.13	0.20
North Yorkshire 44	4.72	0.15	4.51	0.20
North Yorkshire 50	5.62	0.45	5.14	0.20

Appendix D: SO_2 pyrolysis sulphur signals (Altered pyrite *vs* Normal pyrite)

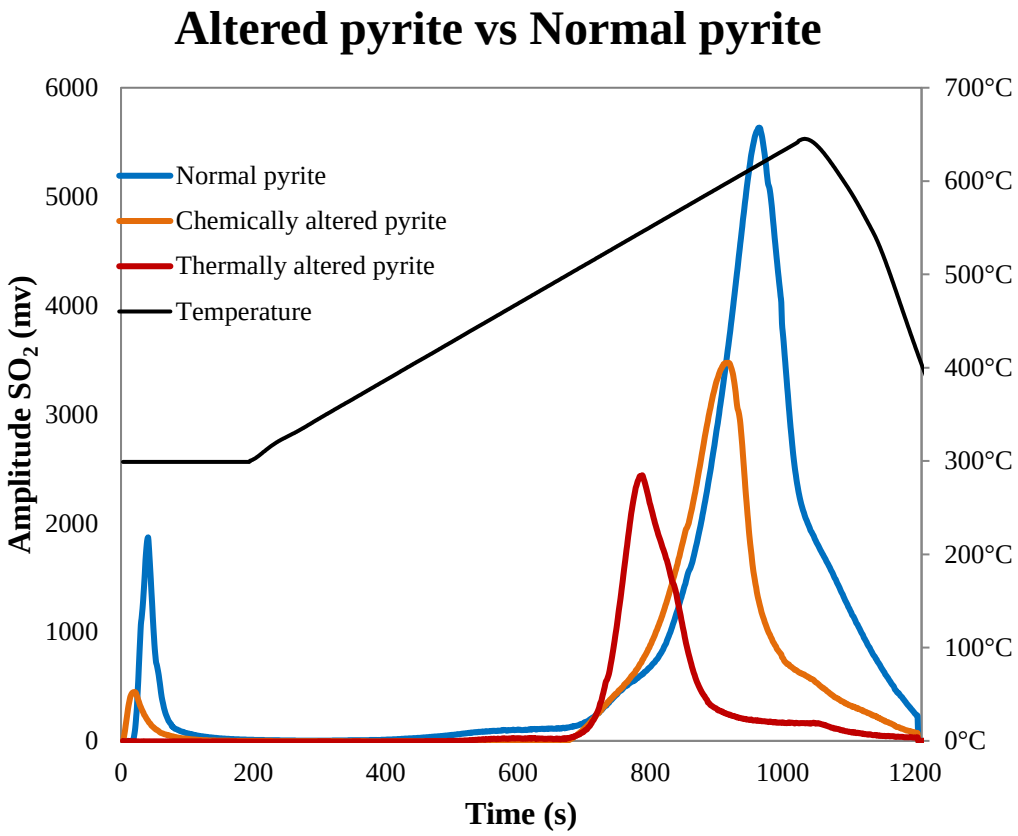

Appendix E: Rock-Eval 7S signals Type II and Type III Kerogens, Pyrite and mixtures “Pyrite + Kerogens”

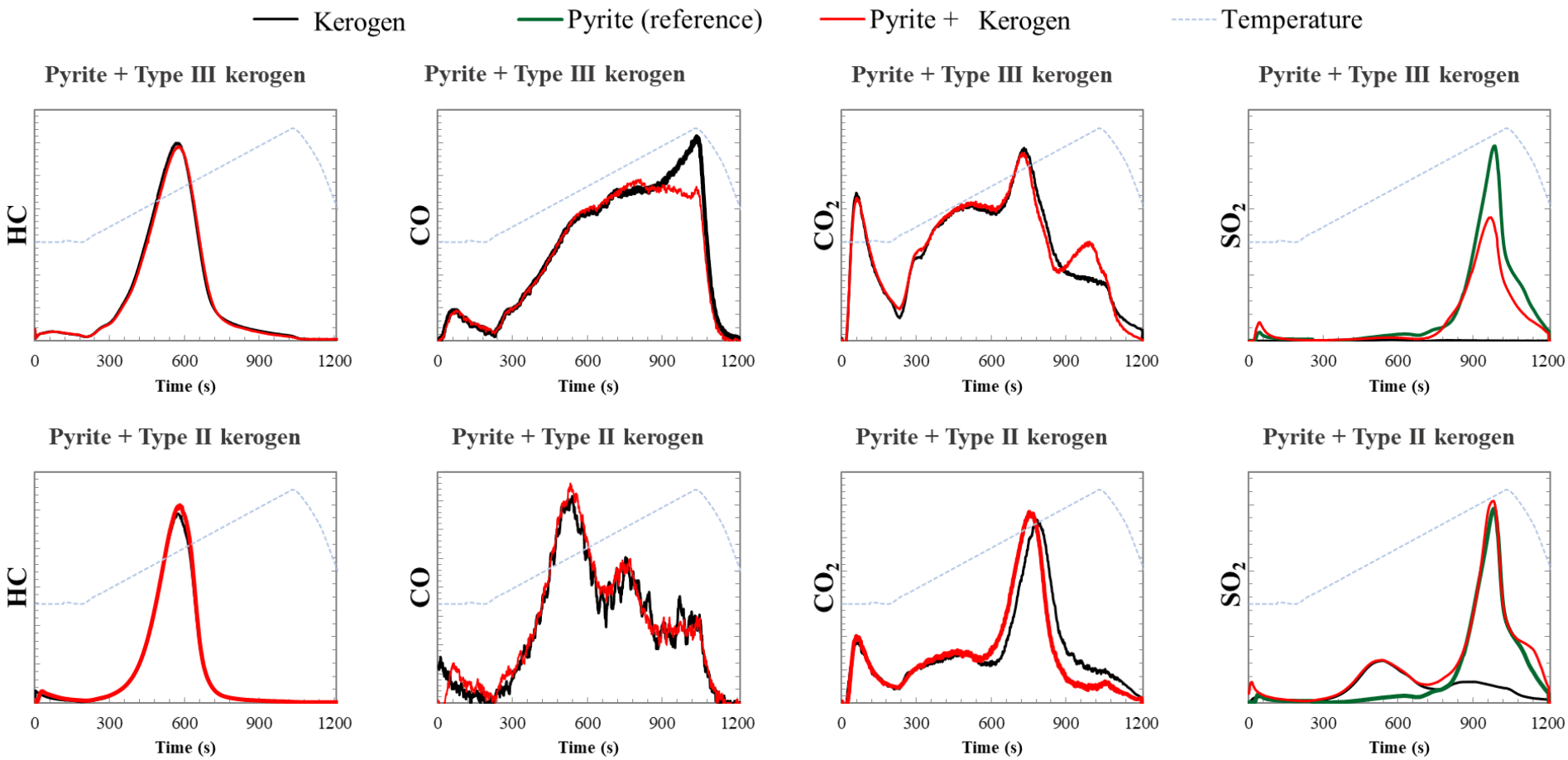

Appendix F: Rock-Eval 7S results of mixture "Pure igneous pyrite + Kerogen": Raw data

	Mixture weight (mg)	Kerogen weight (mg)	$_{Pyrolysis}S^{Kerogen}$ (wt%)	Pyrite weight (mg)	$_{Pyrolysis}S^{Pyrite}$ (wt%)	Pyrite proportion in mixture (mg/mg)	Kerogen proportion in mixture (mg/mg)
Type I-Green River Shale-01	6.1	4.0	0.8	2.0	23.4	0.3	0.7
Type I-Green River Shale-02	6.0	3.8	1.5	2.0	23.4	0.3	0.7
Type II-Shiste carton-Paris-01	6.1	4.0	6.1	2.0	23.4	0.3	0.7
Type II-Shiste carton-Paris-02	6.0	4.0	5.1	2.0	23.4	0.3	0.7
Type II-Shiste carton-Grandville-01	6.1	4.0	8.9	2.0	23.4	0.3	0.7
Type II-Shiste carton-Grandville-02	6.0	4.0	9.0	2.0	23.4	0.3	0.7
Type II-ODP 959-130-137-01	6.0	4.0	11.8	2.0	23.4	0.3	0.7
Type II-ODP 959-130-137-02	6.0	4.0	11.7	2.0	23.4	0.3	0.7
Type II-ODP 959-46-57-01	6.0	4.0	11.9	2.0	23.4	0.3	0.7
Type II-ODP 959-46-57-02	6.0	4.0	12.0	2.0	23.4	0.3	0.7
Type II-ODP 959-81-88-01	6.0	4.0	12.4	2.0	23.4	0.3	0.7
Type II-ODP 959-81-88-02	6.0	4.0	12.6	2.0	23.4	0.3	0.7
Type II Oxidized (2 days)-Shiste carton-01	6.0	4.0	7.8	2.0	23.4	0.3	0.7
Type II Oxidized (2 days)-Shiste carton-02	6.0	4.0	7.7	2.0	23.4	0.3	0.7
Type II Oxidized (5 days)-Shiste carton-01	6.0	4.0	7.3	2.0	23.4	0.3	0.7
Type II Oxidized (5 days)-Shiste carton-02	6.0	4.0	7.6	2.0	23.4	0.3	0.7
Type II Oxidized (11 days)-Shiste carton-01	6.0	4.0	6.8	2.0	23.4	0.3	0.7
Type II Oxidized (11 days)-Shiste carton-02	6.0	4.0	7.2	2.0	23.4	0.3	0.7
Type IIS-PHOSPHORIA-01	6.0	4.0	7.4	2.0	23.4	0.3	0.7
Type IIS-PHOSPHORIA-02	6.1	4.0	7.8	2.0	23.4	0.3	0.7
Type III-Calvert Bluff-01	6.1	4.0	0.7	2.0	23.4	0.3	0.7
Type III-Calvert Bluff-02	6.0	4.0	0.4	2.0	23.4	0.3	0.7
Type III-Oxidized (2 days)-Calvert Bluff-01	6.0	4.0	0.2	2.0	23.4	0.3	0.7
Type III-Oxidized (2 days)-Calvert Bluff-02	6.1	4.0	0.3	2.0	23.4	0.3	0.7
Type III-Oxidized (5 days)-Calvert Bluff-01	6.0	4.0	0.1	2.0	23.4	0.3	0.7
Type III-Oxidized (5 days)-Calvert Bluff-02	6.0	4.0	0.3	2.0	23.4	0.3	0.7

	Mixture weight (mg)	Type II Kerogen weight (mg)	$_{Pyrolysis}S^{Type\ II\ kerogen}$ (wt%)	$^{SD}{}_{Pyrolysis}S^{Type\ II\ kerogen}$ (wt%)	Type III Kerogen weight (mg)	$_{Pyrolysis}S^{Type\ III\ kerogen}$ (wt%)	$^{SD}{}_{Pyrolysis}S^{Type\ III\ kerogen}$ (wt%)	Pyrite weight (mg)	$_{Pyrolysis}S^{Pyrite}$ (wt%)	Pyrite proportion in mixture (mg/mg)	Type II Kerogen proportion in mixture (mg/mg)	Type III Kerogen proportion in mixture (mg/mg)
Mixture (Type II +Type III)-A-01	6.3	2.2	5.60	0.86	2.2	0.23	0.22	1.9	23.4	0.30	0.35	0.35
Mixture (Type II +Type III)-A-02	5.95	2.0	5.60	0.86	2.0	0.23	0.22	2.0	23.4	0.34	0.33	0.33
Mixture (Type II +Type III)-A-03	6.02	2.0	5.60	0.86	2.0	0.23	0.22	2.1	23.4	0.34	0.33	0.33
Mixture (Type II +Type III)-B-01	5.92	1.0	5.60	0.86	3.0	0.23	0.22	2.0	23.4	0.33	0.16	0.51
Mixture (Type II +Type III)-B-02	6.07	1.0	5.60	0.86	3.0	0.23	0.22	2.1	23.4	0.34	0.16	0.49
Mixture (Type II +Type III)-B-03	6.21	1.1	5.60	0.86	3.0	0.23	0.22	2.1	23.4	0.33	0.18	0.48

Appendix G: Rock-Eval 7S results of mixture "Pure igneous pyrite + Kerogen": Processed data

	Expected pyrolysis $S^{Mixtures}$ (wt%)	Expected pyrolysis $S^{Mixtures\ mean}$ (wt%)	Expected pyrolysis $S^{Mixtures\ SD}$ (wt%)	Obtained pyrolysis $S^{Mixtures}$ (wt%)	Obtained pyrolysis $S^{Mixtures\ mean}$ (wt%)	Obtained pyrolysis $S^{Mixtures\ SD}$ (wt%)	**OM_{effect}**	**Max OM_{effect}**	**Min OM_{effect}**	**SD OM_{effect}**
Type I-Green River Shale-01	8.3	8.6	0.4	8.0	8.4	0.7	**1.6**	**6.4**	**-3.8**	**2.3**
Type I-Green River Shale-02	8.8			8.9						
Type II-Shiste carton-Paris-01	11.8	11.5	0.5	11.2	11.1	0.1	**3.1**	**7.1**	**-1.3**	**5.1**
Type II-Shiste carton-Paris-02	11.2			11.1						
Type II-ODP 959-130-137-01	15.7	15.7	0.1	12.9	13.3	0.7	**15.3**	**15.6**	**14.9**	**0.6**
Type II-ODP 959-130-137-02	15.6			13.7						
Type II-ODP 959-46-57-01	15.7	15.8	0.1	13.7	13.8	0.1	**12.6**	**13.0**	**12.2**	**0.8**
Type II-ODP 959-46-57-02	15.8			13.8						
Type II-ODP 959-81-88-01	16.1	16.2	0.1	14.8	14.8	0.0	**8.1**	**8.8**	**7.4**	**1.2**
Type II-ODP 959-81-88-02	16.2			14.9						
Type II-Shiste carton-Grandville-01	13.7	13.7	0.1	12.5	12.4	0.2	**10.0**	**10.4**	**9.6**	**0.7**
Type II-Shiste carton-Grandville-02	13.8			12.3						
Type II Oxidized (2 days)-Shiste carton-01	13.0	13.0	0.0	10.2	10.4	0.2	**20.0**	**20.1**	**19.9**	**0.2**
Type II Oxidized (2 days)-Shiste carton-02	12.9			10.5						
Type II Oxidized (5 days)-Shiste carton-01	12.7	12.8	0.2	8.3	8.3	0.0	**35.4**	**36.2**	**34.6**	**1.4**
Type II Oxidized (5 days)-Shiste carton-02	12.9			8.3						
Type II Oxidized (11 days)-Shiste carton-01	12.3	12.5	0.3	7.9	8.0	0.2	**35.7**	**37.1**	**34.2**	**2.6**
Type II Oxidized (11 days)-Shiste carton-02	12.6			8.2						
Type IIS-PHOSPHORIA-01	12.7	12.8	0.2	12.4	12.6	0.2	**2.2**	**3.9**	**0.4**	**3.1**
Type IIS-PHOSPHORIA-02	13.0			12.7						
Type III-Calvert Bluff-01	8.3	8.2	0.2	6.2	6.3	0.2	**26.2**	**24.5**	**21.1**	**3.0**
Type III-Calvert Bluff-02	8.1			6.4						
Type III-Oxidized (2 days)-Calvert Bluff-01	7.9	7.9	0.0	6.4	6.4	0.0	**22.4**	**19.8**	**19.2**	**0.5**
Type III-Oxidized (2 days)-Calvert Bluff-02	7.9			6.4						
Type III-Oxidized (5 days)-Calvert Bluff-01	7.9	7.9	0.1	6.1	6.1	0.1	**26.2**	**23.4**	**22.2**	**1.1**
Type III-Oxidized (5 days)-Calvert Bluff-02	8.0			6.2						

	Expected pyrolysis $S^{Mixtures}_{mean}$ (wt%)	Expected pyrolysis $S^{Mixtures}_{max}$ (wt%)	Expected pyrolysis $S^{Mixtures}_{min}$ (wt%)	Average expected pyrolysis $S^{Mixtures}_{mean}$ (wt%)	Average expected pyrolysis $S^{Mixtures}_{max}$ (wt%)	Average Expected pyrolysis $S^{Mixtures}_{min}$ (wt%)	Obtained pyrolysis $S^{Mixtures}$ (wt%)	Average obtained pyrolysis $S^{Mixtures}$ (wt%)	SD obtained pyrolysis $S^{Mixtures}$ (wt%)	**OM_{effect}**	**Max OM_{effect}**	**Min OM_{effect}**	**SD OM_{effect}**
Mixture (Types II+ III)-A01	9.2	9.5	8.8	9.7	10.0	9.3	8.48	9.0	0.9	**6.8**	**10.2**	**3.2**	**7.4**
Mixture (Types II+ III)-A02	9.9	10.3	9.6				9.52						
Mixture (Types II + III)-A03	9.9	10.3	9.5				9.01						
Mixture (Types II + III)-B01	8.8	9.1	8.6	9.0	9.2	8.7	7.78	7.6	0.3	**14.8**	**17.2**	**12.3**	**6.2**
Mixture (Types II + III)-B02	9.1	9.3	8.8				7.63						
Mixture (Types II +III)-B03	9.0	9.2	8.7				7.47						

Appendix H: Rock-Eval 7S results of mixture "Pure igneous pyrite + Mineral"

Clay minerals (Kaolinite + Illite + Smectite) carbonate minerals (Calcite + Dolomite + Siderite)

	Mixture weight (mg)	Mineral weight (mg)	$_{Pyrolysis}S^{Mineral}$ (wt%)	Pyrite weight (mg)	Expected pyrolysis $S^{Mixtures}$ = $_{Pyrolysis}S^{Pyrite}$ (wt%)	Obtained pyrolysis $S^{Mixtures}$ (wt%)	**Min_{effect}**	**Mean Min_{effect}**	**SD Min_{effect}**
Kaolinite-01	60.0	58.0	0.0	2.0	23.4	23.3	**0.4**	**0.0**	**3.0**
Kaolinite-02	60.0	58.0	0.0	2.0	23.4	24.1	**-2.7**		
Illite-01	60.0	58.0	0.0	2.0	23.4	23.4	**0.1**	**0.0**	**1.0**
Illite-02	60.0	58.0	0.0	2.0	23.4	23.6	**-0.9**		
Smectite-01	60.0	58.0	0.0	2.0	23.4	14.5	**38.1**	**39.9**	**3.0**
Smectite-02	60.0	58.0	0.0	2.0	23.4	13.7	**41.6**		
Calcite-01	60.0	58.0	0.0	2.1	23.4	9.3	**60.5**	**60.2**	**1.0**
Calcite-02	60.0	57.9	0.0	2.1	23.4	9.4	**59.9**		
Dolomite-01	60.0	58.0	0.0	2.1	23.4	5.0	**78.6**	**79.1**	**1.0**
Dolomite-02	60.0	58.0	0.0	2.1	23.4	4.8	**79.5**		
Sidérite-01	60.0	58.0	0.0	2.0	23.4	1.4	**94.1**	**95.0**	**2.0**
Sidérite-02	60.0	58.0	0.0	2.0	23.4	1.0	**95.9**		
100%clay minerals+0%carbonate minerals-01	60.0	58.0	0.0	2.0	23.4	21.5	**8.4**	**6.4**	**2.0**
100%clay minerals+0%carbonate minerals-02	60.0	58.0	0.0	2.1	23.4	22.2	**5.5**		
100%clay minerals+0%carbonate minerals-03	60.0	58.0	0.0	2.0	23.4	22.2	**5.5**		
93%clay minerals+7%carbonate minerals-01	60.0	58.0	0.0	2.0	23.4	13.6	**42.2**	**39.8**	**2.0**
93%clay minerals+7%carbonate minerals-02	60.0	58.0	0.0	2.0	23.4	14.4	**38.4**		
93%clay minerals+7%carbonate minerals-03	60.0	58.0	0.0	2.0	23.4	14.3	**39.0**		
69%clay minerals+31%carbonate minerals-01	60.0	58.0	0.0	2.0	23.4	7.9	**66.2**	**65.8**	**1.0**
69%clay minerals+31%carbonate minerals-02	60.0	58.0	0.0	2.0	23.4	8.1	**65.4**		
50%clay minerals+50%carbonate minerals-01	60.0	58.0	0.0	2.0	23.4	6.1	**73.9**	**77.4**	**4.0**
50%clay minerals+50%carbonate minerals-02	60.0	58.0	0.0	2.0	23.4	5.0	**78.5**		
50%clay minerals+50%carbonate minerals-02	60.0	58.0	0.0	2.0	23.4	4.7	**79.9**		
26%clay minerals+ 4% carbonate minerals-01	60.0	58.0	0.0	2.0	23.4	1.9	**91.7**	**91.8**	**0.0**
26%clay minerals+74%carbonate minerals-02	60.0	58.0	0.0	2.0	23.4	1.9	**91.9**		
0%clay minerals+100%carbonate minerals-01	60.0	58.0	0.0	2.0	23.4	2.1	**91.1**	**94.3**	**3.0**
0%clay minerals+100%carbonate minerals-02	60.0	58.0	0.0	2.0	23.4	1.1	**95.5**		
0%clay minerals+100%carbonate minerals-03	60.0	58.0	0.0	2.0	23.4	0.8	**96.4**		

	Mixture weight (mg)	Mineral weight (mg)	$_{Pyrolysis}S^{Mineral}$ (wt%)	Pyrite weight (mg)	Expected pyrolysis $S^{Mixtures} = {}_{Pyrolysis}S^{Pyrite}$ (wt%)	Obtained pyrolysis $S^{Mixtures}$ (wt%)	**Min_{effect}**	**Mean Min_{effect}**	**SD Min_{effect}**
100% Kaolinite + 0% Calcite-01	60.0	58.0	0.0	2.0	23.4	23.3	**0.4**	**0.0**	**3.0**
100% Kaolinite + 0% Calcite-02	60.0	58.0	0.0	2.0	23.4	24.1	**-2.7**		
88% Kaolinite + 12% Calcite-01	60.0	58.0	0.0	2.0	23.4	17.0	**27.3**	**26.9**	**1.0**
88% Kaolinite + 12% Calcite-02	60.0	58.0	0.0	2.0	23.4	17.2	**26.5**		
71% Kaolinite + 29% Calcite-01	60.0	58.0	0.0	2.0	23.4	14.8	**36.7**	**34.9**	**3.0**
71% Kaolinite + 29% Calcite-02	60.0	58.0	0.0	2.0	23.4	15.7	**33.2**		
49% Kaolinite + 51% Calcite-01	60.0	58.0	0.0	2.0	23.4	14.5	**38.1**	**38.2**	**1.0**
49% Kaolinite + 51% Calcite-02	60.0	58.0	0.0	2.0	23.4	14.5	**38.3**		
26% Kaolinite + 74% Calcite-01	60.0	58.0	0.0	2.0	23.4	13.9	**40.8**	**42.2**	**3.0**
26% Kaolinite + 74% Calcite-02	60.0	58.0	0.0	2.0	23.4	13.2	**43.5**		
0% Kaolinite + 100% Calcite-01	60.0	58.0	0.0	2.1	23.4	9.3	**60.5**	**60.2**	**1.0**
0% Kaolinite + 100% Calcite-02	60.0	57.9	0.0	2.1	23.4	9.4	**59.9**		
100% Smectite + 0% Siderite-01	60.0	58.0	0.0	2.0	23.4	14.5	**38.1**	**39.9**	**3.0**
100% Smectite + 0% Siderite-02	60.0	58.0	0.0	2.0	23.4	13.7	**41.6**		
91% Smectite + 9% Siderite-01	60.0	57.9	0.0	2.1	23.4	6.6	**71.9**	**72.4**	**1.0**
91% Smectite + 9% Siderite-02	60.0	57.9	0.0	2.1	23.4	6.4	**72.8**		
71% Smectite + 29% Siderite-01	60.0	58.0	0.0	2.0	23.4	2.9	**87.7**	**87.7**	**0.0**
71% Smectite + 29% Siderite-02	60.0	58.0	0.0	2.0	23.4	2.9	**87.7**		
50% Smectite + 50% Siderite-01	60.0	58.1	0.0	1.9	23.4	2.4	**89.6**	**89.6**	**0.0**
50% Smectite + 50% Siderite-02	60.0	58.1	0.0	1.9	23.4	2.4	**89.6**		
26% Smectite + 74% Siderite-01	60.0	58.0	0.0	2.0	23.4	0.3	**98.8**	**98.8**	**0.0**
26% Smectite + 74% Siderite-02	60.0	58.0	0.0	2.0	23.4	0.3	**98.8**		
0% Smectite + 100% Siderite-01	60.0	58.0	0.0	2.0	23.4	1.4	**94.1**	**95.0**	**2.0**
0% Smectite + 100% Siderite-02	60.0	58.0	0.0	2.0	23.4	1.0	**95.9**		

Appendix I: Rock-Eval 7S CO_2 signal of mixtures "Pyrite + carbonates"

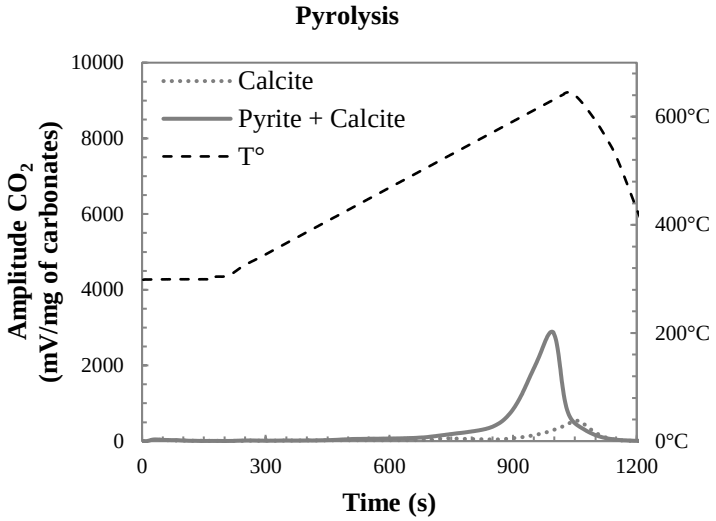

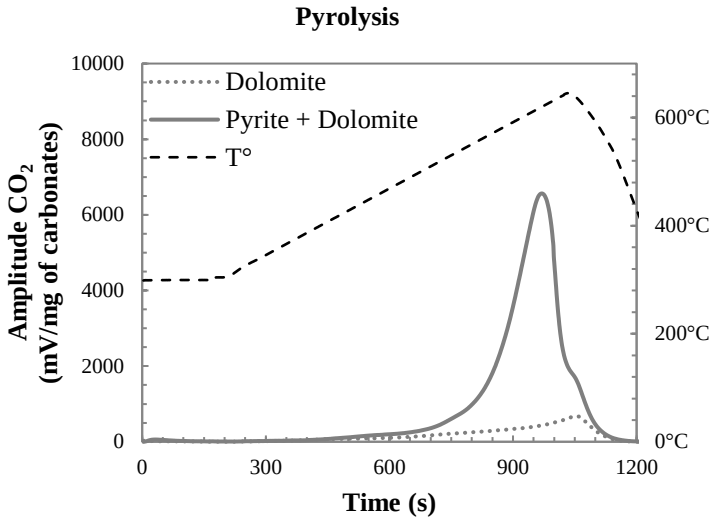

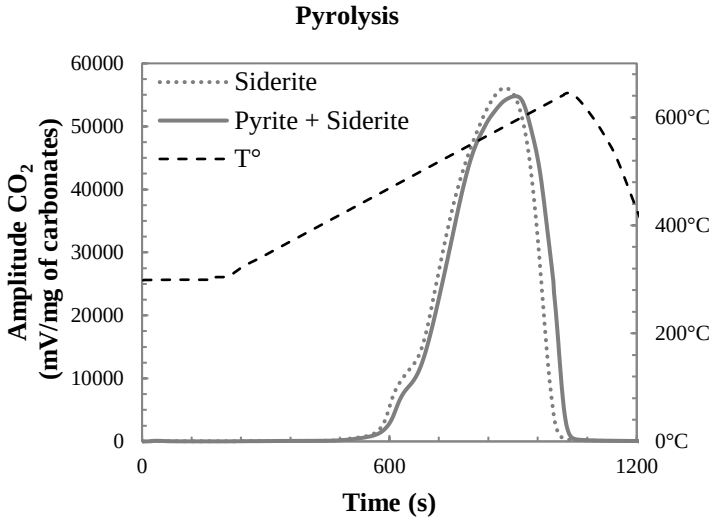

Appendix J: S^{Pyrite} and $S^{Organic}$ quantification using Rock-Eval 7S

Grey Shale Member samples

Analysis	$_{Pyrolysis}S^{Pyrite}$ (wt%)	MINC (wt%)	HI (mgHC/grock)	OI ($mgCO_2$/grock)	S^{Total} (wt%)	$S^{Total\ mean}$ (wt%)	SD	S^{Pyrite} (wt.%)	$S^{Pyrite\ mean}$ (wt.%)	SD	$S^{Organic}$ (wt%)	$S^{Organic\ mean}$ (wt%)	SD
NY171323-01	0.51	0.11	135	17	2.3	2.4	0.10	2.31	2.2	0.18	0.13	0.2	0.27
NY171323-02	0.56	0.11	127	17	2.4			2.11			0.23		
NY171329-01	1.7	0.15	251	16	6.7	6.7	0.05	6.59	6.5	0.18	0.42	0.4	0.23
NY171329-02	1.72	0.19	259	16	6.8			6.39			0.31		
NY171330-01	2.37	0.3	419	13	10.1	10.0	0.17	9.74	9.7	0.08	0.24	0.4	0.25
NY171330-02	2.41	0.3	422	14	9.9			9.65			0.55		
NY171331-01	2.03	0.32	385	16	9.3	9.2	0.04	8.47	8.4	0.19	0.75	0.9	0.24
NY171331-02	2.15	0.3	409	10	9.2			8.25			1.1		
NY171332-01	1.55	0.33	447	9	8.3	8.2	0.13	5.95	7.1	2.09	2.17	1.4	2.22
NY171332-02	1.52	0.38	453	14	8.1			8.31			0.55		
NY171333-01	1.39	0.27	329	16	7.5	7.6	0.17	6.65	6.2	0.85	1.01	1.4	1.02
NY171333-02	1.65	0.27	344	14	7.7			5.69			1.81		
NY171334-01	0.99	0.13	129	26	5.3	5.3	0.05	4.15	4.1	0.14	1.13	1.2	0.19
NY171334-02	0.98	0.18	137	30	5.2			3.99			1.32		
NY171335-01	0.2	0.15	145	22	1.1	1.2	0.05	0.82	0.8	0.01	0.45	0.4	0.06
NY171335-02	0.18	0.16	145	25	1.2			0.83			0.3		
NY171337-01	0.56	0.15	152	28	2.3	2.3	0.10	2.38	2.3	0.12	0.01	0.0	0.21
NY171337-02	0.59	0.17	156	28	2.4			2.25			0.01		
NY171338-01	1.03	0.5	418	16	5.6	5.5	0.08	4.39	4.4	0.04	1.08	1.1	0.12
NY171338-02	1.02	0.51	423	10	5.5			4.44			1.12		
NY171360-01	0.15	0.53	140	15	1.2	1.2	0.00	0.68	0.6	0.07	0.5	0.5	0.07
NY171360-02	0.16	0.5	141	15	1.2			0.6			0.57		
NY171364-01	1.12	0.29	258	14	4.8	4.8	0.02	4.71	4.7	0.11	0.1	0.2	0.12
NY171364-02	1.14	0.28	263	14	4.8			4.59			0.23		
NY171370-01	0.79	0.24	209	21	6.0	5.8	0.21	3.88	3.6	0.47	1.9	2.3	0.68
NY171370-02	0.88	0.23	206	21	5.7			3.35			2.61		

KCF samples

Analysis	$_{Pyrolysis}S^{Pyrite}$ (wt%)	MINC (wt%)	HI (mgHC/grock)	OI ($mgCO_2$/grock)	S^{Total} (wt%)	$S^{Total\ mean}$ (wt%)	SD	S^{Pyrite} (wt.%)	$S^{Pyrite\ mean}$ (wt.%)	SD	$S^{Organic}$ (wt%)	$S^{Organic\ mean}$ (wt%)	SD
Dorset172327-01	0.01	11.2	689	47	0.3	0.3	0.0	0.2	0.2	0.0	0.1	0.1	0.0
Dorset172327-02	0.01	11.2	574	40	0.3			0.2			0.1		
Dorset172329-01	0.29	3.6	679	14	6.1	6.2	0.2	1.1	1.4	0.4	4.9	4.8	0.6
Dorset172329-02	0.41	3.2	726	19	6.3			1.6			4.6		
Dorset172330-01	0.21	0.4	490	17	1.9	2.0	0.1	0.8	0.9	0.0	1.1	1.1	0.1
Dorset172330-02	0.22	0.5	486	21	2.0			0.9			1.1		
Dorset172332-01	0.39	2.0	682	11	7.2	7.3	0.1	1.5	1.9	0.7	5.7	5.4	0.8
Dorset172332-02	0.6	1.0	779	13	7.3			2.3			5.0		
Dorset172333-01	0.31	2.5	605	13	3.1	3.2	0.1	1.2	1.3	0.1	1.9	1.9	0.2
Dorset172333-01	0.33	2.74	608	24	3.2			1.3			1.9		
Dorset172334-01	0.02	7.76	401	32	0.6	0.5	0.1	0.2	0.3	0.1	0.3	0.2	0.2
Dorset172334-02	0.03	8.20	421	47	0.5			0.3			0.1		
Dorset172335-01	0.04	9.80	759	18	1.7	1.7	0.1	0.9	1.0	0.2	0.7	0.7	0.3
Dorset172335-02	0.05	10.42	758	23	1.8			1.2			0.6		
Dorset172336-01	0.15	2.77	703	13	3.4	3.5	0.1	0.6	0.7	0.2	2.8	2.7	0.4
Dorset172336-02	0.22	2.42	705	16	3.5			0.9			2.7		

Validation mixtures: (Phosphoria: PHOS43 Limagne: S18-02RB Orbagnoux: ORBA)

Analysis	$_{Pyrolysis}S^{Pyrite}$ (wt%)	MINC (wt%)	HI (mgHC/g rock)	OI ($mgCO_2$/ grock)	S^{Total} (wt%)	$S^{Total\ mean}$ (wt%)	SD	S^{Pyrite} (wt.%)	$S^{Pyrite\ mean}$ (wt.%)	SD	$S^{Organic}$ (wt%)	$S^{Organic\ mean}$ (wt%)	SD
PHOS43-P1-01	0.3	0.4	369	61	3.5	3.5	0.0	1.4	1.6	0.2	2.1	2.0	0.2
PHOS43-P102	0.4	0.4	372	62	3.5			1.7			1.9		
PHOS43-P2-01	0.7	0.4	374	61	4.9	4.9	0.0	3.0	2.8	0.3	1.9	2.1	0.3
PHOS43-P2-02	0.6	0.4	375	61	4.9			2.7			2.3		
S18-2RB-P1-01	0.2	0.1	556	38	1.2	1.2	0.0	0.9	0.9	0.2	0.3	0.3	0.2
S18-2RB-P2-01	0.4	0.1	549	38	1.9	1.9	0.0	1.7	1.7	0.2	0.3	0.3	0.2
S18-2RB-P3-01	0.4	0.1	548	40	2.5	2.5	0.0	1.9	1.9	0.2	0.6	0.6	0.2
S18-2RB-P4-01	0.5	0.1	543	40	3.1	3.1	0.0	2.3	2.3	0.2	0.8	0.8	0.2
ORBA9CA-P1-01	0.1	10.8	869	25	3.1	3.1	0.0	1.4	1.7	0.6	1.7	1.4	0.6
ORBA9CA-P1-02	0.1	10.8	883	23	3.1			2.0			1.0		
ORBA9CA-P2-01	0.1	10.5	905	23	4.6	4.6	0.0	3.1	3.5	0.6	1.5	1.1	0.6
ORBA9CA-P2-02	0.2	10.5	893	25	4.6			3.8			0.8		
ORBA9CB-P1-01	0.2	0.9	835	11	1.6	1.6	0.0	0.9	0.9	0.0	0.7	0.7	0.0
ORBA9CB-P1-02	0.2	0.8	838	9	1.5			0.9			0.7		
ORBA9CB-P2-01	0.5	0.8	827	11	2.4	2.4	0.1	1.9	1.8	0.1	0.6	0.6	0.0
ORBA9CB-P2-02	0.4	0.8	824	11	2.4			1.7			0.6		
ORBA9CB-P3-01	0.6	0.8	792	14	3.2	3.1	0.2	2.5	2.4	0.1	0.8	0.7	0.1
ORBA9CB-P3-02	0.6	0.8	792	14	3.1			2.4			0.7		
ORBA9CB-P4-01	0.8	0.8	799	10	3.9	3.9	0.1	3.2	3.3	0.1	0.7	0.6	0.1
ORBA9CB-P4-02	0.9	0.8	787	13	3.9			3.4			0.6		

Validation mixtures: (Phosphoria: PHOS43 Limagne: S18-02RB Orbagnoux: ORBA)

Analysis	$_{Pyrolysis}S^{Pyrite}$ (wt%)	MINC (wt%)	HI (mgHC/grock)	OI ($mgCO_2$/grock)	S^{Total} (wt%)	$S^{Total\ mean}$ (wt%)	SD	S^{Pyrite} (wt.%)	$S^{Pyrite\ mean}$ (wt.%)	SD	$S^{Organic}$ (wt%)	$S^{Organic\ mean}$ (wt%)	SD
ORBA9KA-P1-01	0.0	11.0	948	23	1.7	1.6	0.1	0.7	0.7	0.0	1.0	1.0	0.1
ORBA9KA-P1-02	0.0	11.0	951	22	1.6			0.7			0.9		
ORBA9KA-P2-01	0.0	10.8	968	24	2.4	2.4	0.0	1.1	1.3	0.4	1.3	1.1	0.4
ORBA9KA-P2-02	0.1	10.8	962	27	2.4			1.6			0.9		
ORBA9KA-P3-01	0.1	10.8	978	27	3.3	3.3	0.0	2.0	2.2	0.4	1.3	1.0	0.4
ORBA9KA-P3-02	0.1	10.8	976	28	3.3			2.5			0.8		
ORBA9KA-P4-01	0.2	10.6	995	25	4.1	4.1	0.0	3.6	3.6	0.0	0.5	0.5	0.0
ORBA9KA-P4-02	0.2	10.6	979	29	4.1			3.6			0.5		
ORBA9M-P1-01	0.0	11.5	948	35	1.3	1.3	0.0	0.7	0.7	0.0	0.6	0.6	0.0
ORBA9M-P1-02	0.0	11.4	920	37	1.3			0.7			0.6		
ORBA9M-P2-01	0.1	11.3	933	52	2.2	2.2	0.0	2.0	1.8	0.3	0.2	0.4	0.3
ORBA9M-P2-02	0.1	11.3	959	37	2.2			1.6			0.6		
ORBA9M-P3-01	0.2	11.1	975	40	2.9	2.9	0.0	2.7	2.7	0.0	0.2	0.2	0.0
ORBA9M-P3-02	0.2	11.1	980	35	2.9			2.7			0.2		
ORBA9M-P4-01	0.2	11.0	995	42	3.7	3.7	0.0	3.5	3.5	0.0	0.3	0.3	0.0
ORBA9M-P4-02	0.3	11.0	1007	42	3.7			3.5			0.3		

Somerset samples

Analysis	$_{Pyrolysis}S^{Pyrite}$ (wt%)	MINC (wt%)	HI (mgHC/grock)	OI ($mgCO_2$/grock)	S^{Total} (wt%)	S^{Pyrite} (wt.%)	$S^{Organic}$ (wt%)
EQ01	0.0	9.4	67	249	0.2	0.2	0.0
EQ02	0.1	5.9	203	71	1.3	1.3	0.0
EQ03	0.2	4.0	157	65	2.6	2.3	0.3
EQ04	0.1	4.4	327	35	1.1	0.8	0.3
EQ05	0.0	4.8	217	92	1.0	0.4	0.6
EQ06	0.0	10.0	36	263	0.2	0.2	0.0
EQ07	0.0	7.2	55	237	0.6	0.6	0.0
EQ08	0.1	4.4	529	25	1.8	0.9	0.9
EQ09	0.1	5.1	392	58	2.1	1.5	0.6
EQ10	0.0	10.0	91	223	0.2	0.2	0.0
EQ11	0.1	5.9	394	27	1.4	1.3	0.1
EQ13	0.2	4.7	505	23	1.8	1.7	0.1
EQ14	0.1	5.9	156	88	1.3	1.0	0.4
EQ15	0.4	4.3	541	16	3.7	3.4	0.3
EQ16	0.3	3.3	608	20	2.9	1.0	1.9
EQ17	0.0	4.4	494	25	2.0	0.2	1.8
EQ18	0.1	5.9	474	29	1.5	1.2	0.3
EQ19	0.1	5.5	419	40	1.4	1.0	0.4
EQ20	0.1	5.0	388	37	1.4	1.1	0.3
EQ21	0.1	5.5	119	129	1.5	0.8	0.7
EQ22	0.0	9.7	46	426	0.1	0.0	0.1
EQ23	0.0	6.9	89	189	1.0	0.5	0.5
EQ24	0.0	10.6	42	457	0.0	0.0	0.0
EQ25	0.0	7.6	143	79	0.6	0.3	0.0
EQ26	0.0	3.8	599	18	2.2	0.5	0.2
EQ27	0.0	6.2	381	29	1.1	0.4	1.7
EQ28	0.1	6.6	388	33	1.5	0.1	1.0
EQ29	0.1	7.3	349	37	0.9	1.4	0.1
EQ30	0.0	7.2	343	32	0.8	0.6	0.3
EQ31	0.2	5.0	442	24	1.6	0.3	0.5
EQ32	0.0	4.8	389	36	1.4	1.6	0.0
EQ33	0.1	5.6	368	43	1.2	0.3	1.0
EQ34	0.0	6.5	236	153	0.8	0.8	0.4
EQ35	0.0	8.5	161	123	0.2	0.3	0.5
EQ36	0.0	8.1	205	64	0.3	0.2	0.0
EQ37	0.1	6.6	80	106	1.3	0.6	0.7
EQ38	0.1	4.1	545	21	2.2	0.5	1.7
EQ39	0.2	4.8	899	8	2.1	1.8	0.3
EQ40	0.2	5.6	420	30	1.7	1.6	0.1
EQ41	0.1	5.9	357	50	1.2	0.8	0.5
EQ44	0.0	3.5	588	20	1.6	*0.0*	*1.5*
EQ45	0.0	4.4	445	42	1.2	*0.1*	*1.1*
EQ46	0.0	3.7	197	116	2.1	*0.3*	*1.8*
EQ47	0.0	3.6	252	43	1.7	*0.3*	*1.4*
EQ48	0.0	4.6	280	52	1.0	*0.2*	*0.8*
EQ49	0.1	8.2	233	66	0.6	*0.6*	*0.0*
EQ50	0.0	5.9	144	111	1.2	*0.3*	*1.0*
EQ51	0.0	4.8	295	58	1.0	*0.1*	*0.9*
EQ52	0.1	5.1	292	61	1.4	*1.0*	*0.4*
EQ53	0.0	9.3	237	124	0.2	*0.0*	*0.2*

Appendix K: S^{Pyrite} and $S^{Organic}$ quantification using elemental analysis method

Grey Shale Member samples

Analysis	S^{Total} (wt%)	$S^{Total\ mean}$ (wt%)	SD	S^{Pyrite} (wt.%)	$S^{Pyrite\ mean}$ (wt.%)	SD	$S^{Organic}$ (wt%)	$S^{Organic\ mean}$ (wt%)	SD
NY171323-01	2.02	2.0	*0.02*	2.20	2.2	*0.39*	-0.18	0.0	*0.41*
NY171323-02	2.02			2.20			-0.18		
NY171329-01	5.71	5.7	*0.05*	5.66	5.7	*1.00*	0.05	0.0	*1.05*
NY171329-02	5.71			5.66			0.05		
NY171330-01	8.67	8.7	*0.09*	8.55	8.5	*1.51*	0.12	0.1	*1.61*
NY171330-02	8.67			8.55			0.12		
NY171331-01	7.60	7.6	*0.09*	7.50	7.5	*1.33*	0.09	0.1	*1.42*
NY171331-02	7.60			7.50			0.09		
NY171332-01	6.75	6.7	*0.08*	6.55	6.5	*1.16*	0.20	0.2	*1.24*
NY171332-02	6.75			6.55			0.20		
NY171333-01	5.95	6.0	*0.07*	5.77	5.8	*1.02*	0.18	0.2	*1.09*
NY171333-02	5.95			5.77			0.18		
NY171334-01	3.76	3.8	*0.04*	3.44	3.4	*0.61*	0.32	0.3	*0.64*
NY171334-02	3.76			3.44			0.32		
NY171335-01	1.07	1.1	*0.01*	0.93	0.9	*0.16*	0.14	0.1	*0.18*
NY171335-02	1.07			0.93			0.14		
NY171337-01	2.41	2.4	*0.03*	2.41	2.4	*0.43*	0.00	0.0	*0.46*
NY171337-02	2.41			2.41			0.00		
NY171338-01	5.03	5.0	*0.05*	4.87	4.9	*0.86*	0.16	0.2	*0.92*
NY171338-02	5.03			4.87			0.16		
NY171360-01	1.18	1.2	*0.01*	1.17	1.2	*0.21*	0.01	0.0	*0.22*
NY171360-02	1.18			1.17			0.01		
NY171364-01	4.25	4.3	*0.04*	3.91	3.9	*0.69*	0.35	0.3	*0.73*
NY171364-02	4.25			3.91			0.35		
NY171370-01	4.61	4.6	*0.05*	4.09	4.1	*0.72*	0.52	0.5	*0.78*
NY171370-02	4.61			4.09			0.52		

KCF samples

Analysis	S^{Total} (wt%)	$S^{Total\ mean}$ (wt%)	SD	S^{Pyrite} (wt.%)	$S^{Pyrite\ mean}$ (wt.%)	SD	$S^{Organic}$ (wt%)	$S^{Organic\ mean}$ (wt%)	SD
Dorset172327-01	0.28	0.3	*0.01*	0.19	0.2	*0.03*	0.09	0.1	*0.04*
Dorset172327-02	0.28			0.19			0.09		
Dorset172329-01	6.01	6.0	*0.12*	1.34	1.3	*0.24*	4.67	4.7	*0.35*
Dorset172329-02	6.01			1.34			4.67		
Dorset172330-01	1.94	1.9	*0.03*	1.17	1.2	*0.21*	0.78	0.8	*0.24*
Dorset172330-02	1.94			1.17			0.78		
Dorset172332-01	6.93	6.9	*0.13*	1.44	1.4	*0.26*	5.49	5.5	*0.38*
Dorset172332-02	6.93			1.44			5.49		
Dorset172333-01	2.98	3.0	*0.06*	2.10	2.1	*0.37*	0.87	0.9	*0.43*
Dorset172333-01	2.98			2.10			0.87		
Dorset172334-01	0.43	0.4	*0.01*	0.48	0.5	*0.09*	-0.06	0.0	*0.09*
Dorset172334-02	0.43			0.48			-0.06		
Dorset172335-01	1.53	1.5	*0.04*	0.58	0.6	*0.10*	0.95	0.9	*0.15*
Dorset172335-02	1.53			0.58			0.95		
Dorset172336-01	3.37	3.4	*0.06*	2.29	2.3	*0.41*	1.08	1.1	*0.47*
Dorset172336-02	3.37			2.29			1.08		

Appendix L: S^{Pyrite} and $S^{Organic}$ quantification in validation mixtures

Validation mixtures (Phosphoria: PHOS43 Limagne: S18-02RB Orbagnoux: ORBA)

Analysis	$S^{Organic}$ (wt%)	$S^{Organic\ mean}$ (wt%)	SD	S^{Pyrite} (wt.%)	$S^{Pyrite\ mean}$ (wt.%)	SD	S^{Total} (wt%)	$S^{Total\ mean}$ (wt%)	SD
Phos43-P1mg-01	1.8	1.8	0.0	1.7	1.7	0.1	3.4	3.4	0.1
Phos43-P1mg-02	1.8		0.0	1.7		0.1	3.4		
Phos43-P2mg-01	1.7	1.7	0.0	3.2	3.2	0.1	4.9	4.9	0.2
Phos43-P2mg-02	1.7		0.0	3.2		0.1	5.0		
S18-2RB-P1mg-01	0.4	0.4	0.0	0.9	0.9	0.0	1.2	1.2	0.1
S18-2RB-P2mg-01	0.4	0.4	0.0	1.7	1.7	0.1	2.0	2.0	0.1
S18-2RB-P3mg-01	0.4	0.4	0.0	2.5	2.5	0.1	2.8	2.8	0.1
S18-2RB-P4mg-01	0.3	0.3	0.0	3.2	3.2	0.1	3.6	3.6	0.2
9ca-P1mg-01	1.2	1.2	0.0	1.8	1.8	0.1	2.9	2.9	0.1
9ca-P1mg-02	1.2		0.0	1.8		0.1	3.0		
9ca-P2mg-01	1.1	1.1	0.0	3.4	3.4	0.1	4.6	4.6	0.2
9ca-P2mg-02	1.1		0.0	3.4		0.1	4.6		
9cb-P1mg-01	0.6	0.6	0.0	0.9	0.9	0.0	1.6	1.6	0.1
9cb-P1mg-02	0.6		0.0	0.9		0.0	1.6		
9cb-P2mg-01	0.6	0.6	0.0	1.8	1.8	0.1	2.4	2.4	0.1
9cb-P2mg-02	0.6		0.0	1.8		0.1	2.4		
9cb-P3mg-01	0.6	0.6	0.0	2.6	2.6	0.1	3.2	3.2	0.1
9cb-P3mg-02	0.6		0.0	2.6		0.1	3.2		
9cb-P4mg-01	0.6	0.6	0.0	3.4	3.4	0.1	4.0	4.0	0.2
9cb-P4mg-02	0.6		0.0	3.4		0.1	4.0		

Validation mixtures (Phosphoria: PHOS43 Limagne: S18-02RB Orbagnoux: ORBA)

Analysis	$S^{Organic}$ (wt%)	$S^{Organic\ mean}$ (wt%)	SD	S^{Pyrite} (wt.%)	$S^{Pyrite\ mean}$ (wt.%)	SD	S^{Total} (wt%)	$S^{Total\ mean}$ (wt%)	SD
9ka-P1mg-01	0.7	0.7	0.0	0.9	0.9	0.0	1.6	1.6	0.1
9ka-P1mg-02	0.7		0.0	0.9		0.0	1.6		
9ka-P2mg-01	0.7	0.7	0.0	1.8	1.8	0.1	2.4	2.4	0.1
9ka-P2mg-02	0.7		0.0	1.8		0.1	2.4		
9ka-P3mg-01	0.7	0.7	0.0	2.6	2.6	0.1	3.3	3.3	0.1
9ka-P3mg-02	0.7		0.0	2.6		0.1	3.3		
9ka-P4mg-01	0.6	0.6	0.0	3.4	3.4	0.1	4.1	4.1	0.2
9ka-P4mg-02	0.6		0.0	3.4		0.1	4.1		
9m-P1mg-01	0.3	0.3	0.0	0.9	0.9	0.0	1.2	1.2	0.1
9m-P1mg-02	0.3		0.0	0.9		0.0	1.2		
9m-P2mg-01	0.3	0.3	0.0	1.8	1.8	0.1	2.1	2.1	0.1
9m-P2mg-02	0.3		0.0	1.8		0.1	2.1		
9m-P3mg-01	0.3	0.3	0.0	2.6	2.6	0.1	2.9	2.9	0.1
9m-P3mg-02	0.3		0.0	2.6		0.1	2.9		
9m-P4mg-01	0.3	0.3	0.0	3.4	3.4	0.1	3.7	3.7	0.2
9m-P4mg-02	0.3		0.0	3.4		0.1	3.7		

Appendix M: XRD Characterisation

Grey Shale Member samples

Samples	%Clay minerals	%Quartz	%Pyrite
NY171323-01	29	68	3
NY171329-01	21	71	8
NY171330-01	21	70	9
NY171331-01	25	62	13
NY171332-01	31	55	14
NY171333-01	35	58	8
NY171334-01	33	63	4
NY171335-01	39	56	5
NY171337-01	43	49	8
NY171338-01	45	48	6
NY171360-01	50	47	3
NY171364-01	42	51	7
NY171370-01	54	44	2

Somerset samples

Samples	%Carbonate minerals	%Quartz	%Clay minerals	%Pyrite	%Other
EQ1	5	36	58	1	
EQ2	70	13	15	2	
EQ3	52	12	31	2	3
EQ4	60	12	26	2	
EQ5	66	9	24	1	
EQ6	94	3	4	0	
EQ7	80	6	13	0	2
EQ8	57	14	22	3	5
EQ9	67	10	20	4	
EQ10	93	3	4	0	
EQ11	72	14	12	2	
EQ12	45	23	28	4	
EQ13	59	15	23	3	
EQ14	72	10	16	2	
EQ15	57	15	22	6	
EQ16	46	20	29	5	
EQ17	60	14	24	3	
EQ18	72	14	10	3	
EQ19	69	13	16	2	
EQ20	65	16	15	4	
EQ21	71	10	18	2	
EQ22	88	5	6	1	
EQ23	71	11	16	2	
EQ24	86	6	6	2	
EQ25	80	9	9	2	
EQ26	54	19	22	4	
EQ27	74	11	12	3	
EQ28	78	10	10	2	
EQ29	71	14	12	4	
EQ30	79	9	10	2	
EQ31	65	15	17	3	
EQ32	70	12	15	3	
EQ33	82	13	4	1	
EQ34	66	19	13	3	
EQ35	85	10	5	0	
EQ36	90	6	3	1	
EQ37	78	11	8	3	
EQ38	66	15	15	4	
EQ39	62	16	19	3	
EQ40	64	16	16	3	
EQ41	55	21	21	3	
EQ44	54	15	29	2	
EQ45	55	13	30	1	
EQ46	73	17	10	0	
EQ47	50	14	33	2	
EQ48	63	17	18	2	
EQ49	85	7	6	3	
EQ50	78	9	11	1	
EQ51	59	13	26	2	
EQ52	72	14	14	0	
EQ53	90	5	5	0	

Appendix N: Basic Rock-Eval 7S parameters

Dorset, North-Yorkshire, Somerset sections

Sections	Samples	Tmax (°C)	TOC (wt%)	MinC (wt%)	HI (mgHC/grock)	OI ($mgCO_2$/grock)	TS (wt%)
North-Yorkshire	GR-3	432	0.7	0.1	131	17	2.4
	SB-9	422	1.5	0.2	255	16	6.7
	SB-10	422	3.7	0.3	421	14	10.0
	SB-11	423	3.4	0.3	397	13	9.2
	SB-12	422	4.1	0.4	450	12	8.2
	SB-13	423	3.0	0.3	337	15	7.6
	SB-14	426	1.3	0.2	133	28	5.3
	GR-15	435	0.8	0.2	145	24	1.2
	GR-17	433	1.1	0.2	154	28	2.3
	SB-18	428	3.1	0.5	421	13	5.5
	GR-40	434	0.9	0.5	141	15	1.2
	GR-44	433	1.9	0.3	261	14	4.8
	GR-50	425	2.5	0.2	208	21	5.8
Dorset	SSK52130	414	2.4	11.2	488	19	0.3
	SSK52132	413	26.8	3.4	731	12	6.2
	SSK52133	422	6.6	0.4	704	15	2.0
	SSK52134	417	36.9	1.5	607	19	7.3
	SSK52135	421	9.5	2.6	703	17	3.2
	SSK52137	429	1.5	8.0	411	40	0.5
	SSK52138	414	6.7	10.1	759	21	1.7
	SSK52139	425	18.6	2.6	632	44	3.5
Somerset	EQ01	67	0.28	9.44	67	249	0.2
	EQ02	203	1.18	5.93	203	71	1.3
	EQ03	157	1.04	3.98	157	65	2.6
	EQ04	327	2.77	4.4	327	35	1.1
	EQ05	217	1.52	4.8	217	92	1.0
	EQ06	36	0.17	10	36	263	0.2
	EQ07	55	0.46	7.18	55	237	0.6
	EQ08	529	5.58	4.38	529	25	1.8
	EQ09	392	2.57	5.07	392	58	2.1
	EQ10	91	0.29	9.96	91	223	0.2
	EQ11	394	2.12	5.87	394	27	1.4
	EQ13	505	3.41	4.72	505	23	1.8
	EQ14	156	1	5.88	156	88	1.3
	EQ15	541	8.89	4.25	541	16	3.7
	EQ16	608	7.48	3.26	608	20	2.9
	EQ17	494	6.09	4.35	494	25	2.0
	EQ18	474	2.91	5.92	474	29	1.5
	EQ19	419	2.74	5.45	419	40	1.4
	EQ20	388	2.64	5.01	388	37	1.4
	EQ21	119	0.85	5.45	119	129	1.5
	EQ22	46	0.21	9.65	46	426	0.1
	EQ23	89	0.65	6.85	89	189	1.0
	EQ24	42	0.13	10.61	42	457	0.0
	EQ36	143	0.61	7.63	205	64	0.6
	EQ25	599	12.23	3.75	143	79	2.2
	EQ26	381	3.14	6.19	599	18	1.1
	EQ27	388	2.32	6.55	381	29	1.5
	EQ28	349	1.55	7.32	388	33	0.9
	EQ29	343	1.65	7.17	349	37	0.8
	EQ30	442	2.87	5.02	343	32	1.6
	EQ31	389	2.84	4.81	442	24	1.4
	EQ32	368	1.74	5.59	389	36	1.2
	EQ33	236	0.96	6.46	368	43	0.8

Sections	Samples	Tmax (ºC)	TOC (wt%)	MinC (wt%)	HI (mgHC/grock)	OI ($mgCO_2$/grock)	TS (wt%)
Somerset	EQ34	161	0.6	8.47	236	153	0.2
	EQ35	205	0.68	8.11	161	123	0.3
	EQ37	80	0.62	6.58	80	106	1.3
	EQ38	545	7.45	4.06	545	21	2.2
	EQ39	899	11.54	4.83	899	8	2.1
	EQ40	420	2.75	5.62	420	30	1.7
	EQ41	357	2.1	5.92	357	50	1.2
	EQ44	588	10.03	3.53	588	20	1.6
	EQ45	445	4.44	4.38	445	42	1.2
	EQ46	197	1.59	3.73	197	116	2.1
	EQ47	252	2.25	3.62	252	43	1.7
	EQ48	280	1.93	4.63	280	52	1.0
	EQ49	233	0.75	8.17	233	66	0.6
	EQ50	144	0.96	5.87	144	111	1.2
	EQ51	295	1.87	4.84	295	58	1.0
	EQ52	292	1.6	5.09	292	61	1.4
	EQ53	237	0.72	9.26	237	124	0.2

Appendix O: Rock-Eval 7S standard deviation estimation for less than 10 analysis

$$S_{RE\ 7S} = \frac{W_{RE\ 7S}}{d_n}$$

$$S_{RE\ 7S} = Rock - Eval\ 7S\ standard\ deviation$$

$$W_{RE\ 7S} = Range\ between\ the\ largest\ and\ the\ smallest\ values$$

$$dn = Tabulated\ values\ as\ a\ function\ of\ n\ in\ the\ hypothesis\ of\ a\ normal\ distribution$$

$$n = Number\ of\ analysis.$$

$$\boldsymbol{n \Longrightarrow dn}$$
$$\mathbf{2 \Longrightarrow 1.13}$$
$$\mathbf{3 \Longrightarrow 1.69}$$
$$\mathbf{4 \Longrightarrow 2.06}$$
$$\mathbf{5 \Longrightarrow 2.33}$$
$$\mathbf{6 \Longrightarrow 2.53}$$
$$\mathbf{7 \Longrightarrow 2.70}$$
$$\mathbf{8 \Longrightarrow 2.70}$$
$$\mathbf{9 \Longrightarrow 2.97}$$
$$\mathbf{10 \Longrightarrow 3.08}$$

REFERENCES

Aboussou, A., Lamoureux-Var, V., Pillot, D., Kowalewski, I., Garcia, B., Wagner, T., Buckman, J.O., März, C., 2017. Procédé pour la quantification du soufre pyritique et du soufre organique d'un echantillon de roche. Patent: FR 17/58.413.

Aboussou, A., Lamoureux-Var, V., Pillot, D., Kowalewski, I., Garcia, B., Wagner, T., März, C., 2018. Procédé pour la quantification du soufre pyritique et du soufre organique d'un échantillon de roche (Perfectionnement). Patent: FR 18/56.042.

Acholla, F.V., Orr, W.L., 1993. Pyrite removal from kerogen without altering organic matter: The chromous chloride method. Energy Fuels 7, 406–410.

Amrani, A., 2014. Organosulfur Compounds: Molecular and Isotopic Evolution from Biota to Oil and Gas. Annu. Rev. Earth Planet. Sci. 42, 733–768.

Anadón, P., Rosell, L., Talbot, M.R., 1992. Carbonate replacement of lacustrine gypsum deposits in two Neogene continental basins, eastern Spain. Sedimentary Geology 78, 201–216.

Anderson, T.F., Kruger, J., Raiswell, R., 1987. C-S-Fe relationships and the isotopic composition of pyrite in the New Albany Shale of the Illinois Basin, U.S.A. Geochimica et Cosmochimica Acta 51, 2795–2805.

Armstrong, H.A., Wagner, T., Herringshaw, L.G., Farnsworth, A.J., Lunt, D.J., Harland, M., Imber, J., Loptson, C., Atar, E.F.L., 2016. Hadley circulation and precipitation changes controlling black shale deposition in the Late Jurassic Boreal Seaway. Paleoceanography 31, 1041–1053.

Arnarson, T.S., Keil R. G., 2001. Organic–mineral interactions in marine sediments studied using density fractionation and X-ray photoelectron spectroscopy. Organic Geochemistry 32, 1401–1415.

Arndt, S., Hetzel, A., Brumsack, H.-J., 2009. Evolution of organic matter degradation in Cretaceous black shales inferred from authigenic barite: A reaction-transport model. Geochimica et Cosmochimica Acta 73, 2000–2022.

Attar, A., Dupuis, F., 1979. The Rate and the Fundamental Mechanisms of the Reaction of Hydrogen Sulfide with the Basic Minerals in Coal. Industrial and Engineering Chemistry Process Design and Development 18, 607–618.

Aycard, M., Derenne, S., Largeau, C., Mongenot, T., Tribovillard, N., Baudin, F., 2003. Formation pathways of proto-kerogens in Holocene sediments of the upwelling influenced Cariaco Trench, Venezuela. Organic Geochemistry 34, 701–718.

Barrabe, L., 1932. Oil in Limagne Area, France. AAPG Bulletin 16.

Baudin, F., Tribovillard, N.-P., Trichet, J., 2007. Géologie de la matière organique. Vuibert; Société géologique de France, Paris.

Bauer, D., Vogt, T., Klinger, M., Masset, P.J., Otto, M., 2014. Direct determination of sulfur species in coals from the argonne premium sample program by solid sampling electrothermal vaporization inductively coupled plasma optical emission spectrometry. Analytical Chemistry 86, 10380–10388.

Behar, F., Beaumont, V., De B. Penteado, H. L., 2001. Rock-Eval 6 Technology: Performances and Developments. Oil & Gas Science and Technology - Rev. IFP 56, 111–134.

Behar, F., Lorant, F., Lewan, M., 2008. Role of NSO compounds during primary cracking of a Type II kerogen and a Type III lignite. Organic Geochemistry 39, 1–22.

Berner, R.A., 1970. Sedimentary pyrite formation. American Journal of Science, 1970, 1–23.

Berner, R.A., 1982. Burial of organic carbon and pyrite sulfur in the modern ocean: Its geochemical and environmental significance. American Journal of Science 282, 451–473.

Berner, R.A., 1984. Sedimentary pyrite formation: An update. Geochimica et Cosmochimica Acta 48, 605–615.

Berner, R.A., Raiswell, R., 1983. Burial of organic carbon and pyrite sulfur in sediments over phanerozoic time: a new theory. Geochimica et Cosmochimica Acta 47, 855–862.

Berner, R.A., Raiswell, R., 1984. C/S method for distinguishing freshwater from marine sedimentary rocks. Geology 12, 365–368.

Bertrand, P., Lallier-Vergès, E., 1993. Past sedimentary organic matter accumulation and degradation controlled by productivity. Nature 364, 786–788.

Betts, J.N., Holland, H.D., 1991. The oxygen content of ocean bottom waters, the burial efficiency of organic carbon, and the regulation of atmospheric oxygen. Atmospheric Oxygen Variation Through Geologic Time 97, 5–18.

Bishop, J., 1988. The barite-opal-organic carbon association in oceanic particulate matter. Nature 332, 341–343.

Bock, M.J., Mayer L. M., 2000. Mesodensity organo–clay associations in a near-shore sediment. Marine Geology 163, 65–75.

Bolin, T.B., 2010. Direct Determination of Pyrite Content in Argonne Premium Coals by the Use of Sulfur X-ray Near Edge Absorption Spectroscopy (S-XANES). Energy Fuels 24, 5479–5482.

Bolin, T.B., 2014. S-XANES analysis of thermal iron sulfide transformations in a suite of Argonne Premium Coals: A study of particle size effects during pyrolysis. International Journal of Coal Geology 131, 200–213.

Boussafir, M., Gelin, F., Lallier-Vergès, E., Derenne, S., Bertrand, P., Largeau, C., 1995. Electron microscopy and pyrolysis of kerogens from the Kimmeridge Clay Formation, UK: Source organisms, preservation processes, and origin of microcycles. Geochimica et Cosmochimica Acta 59, 3731–3747.

Boussafir, M., Lallier-Vergès, E., 1997. Accumulation of organic matter in the Kimmeridge Clay Formation (KCF): An update fossilisation model for marine petroleum source-rocks. Marine and Petroleum Geology 14, 75–83.

Boyabat, N., Özer, A.K., Bayrakçeken, S., Gülaboğlu, M., 2004. Thermal decomposition of pyrite in the nitrogen atmosphere. Fuel Processing Technology 85, 179–188.

Brothers, L.A., Engel, M.H., Elmore, R.D., 1996. The late diagenetic conversion of pyrite to magnetite by organically complexed ferric iron. Chemical Geology 130, 1–14.

Burdige, D.J., 2007. Preservation of organic matter in marine sediments: Controls, mechanisms, and an imbalance in sediment organic carbon budgets? Chemical Reviews 107, 467–485.

Burdige, D.J., Gardner, K.G., 1998. Molecular weight distribution of dissolved organic carbon in marine sediment pore waters. Marine Chemistry 62, 45–64.

Burgos, P., Madejón, P., Madejón, E., Girón, I., Cabrera, F., Murillo, J.M., 2013. Natural remediation of an unremediated soil twelve years after a mine accident: Trace element mobility and plant composition. Journal of Environmental Management 114, 36–45.

Calvert, S.E., Pedersen, T.F., 1992. Organic carbon accumulation and preservation in marine sediments: How important is anoxia? In: Whelan, J. K. & Farrington, J. W. (Ed.), Productivity, Accumulation and Preservation of Organic Matter in Recent and Ancient Sediments. Columbia Univ. Press, New York.

Canfield, D.E., 1989. Reactive iron in marine sediments. Geochimica et Cosmochimica Acta 53, 619–632.

Canfield, D.E., 1994. Factors influencing organic carbon preservation in marine sediments. Chemical Geology 114, 315–329.

Canfield, D.E., Raiswell, R., 1999. The evolution of the sulfur cycle. American Journal of Science 299, 697–723.

Canfield, D.E., Raiswell, R., Westrich, J.T., Reaves, C.M., Berner, R.A., 1986. The use of chromium reduction in the analysis of reduced inorganic sulfur in sediments and shales. Chemical Geology 54, 149–155.

Chen, H., Li, B., Zhang B., 2000. Decomposition of pyrite and the interaction of pyrite with coal organic matrix in pyrolysis and hydropyrolysis. Fuel 79, 1627–1631.

Chowns, T.M., 1966. Depositional environment of the Cleveland ironstone series. Nature 211, 1286–1287.

Claypool, G.E., Kaplan, I.R., 1974. The Origin and Distribution of Methane in Marine Sediments. In: Kaplan, I.R. (Ed.), Natural gases in marine sediments. Plenum Press, New York, pp. 99–139.

Cleyle, P.J., Caley, W.F., Stewart, L., whiteway, S.G., 1984. Decomposition of pyrite and trapping of sulphur in a coal matrix during pyrolysis of coal. Fuel 63, 1579–1582.

Coats, A.W., Bright, N.F.H., 1966. The kinetics of the thermal decomposition of pyrite. Can. J. Chem. 44, 1191–1195.

Csato, I., Granjeon, D., Catuneanu, O., Baum, G.R., 2013. A three-dimensional stratigraphic model for the Messinian crisis in the Pannonian Basin, eastern Hungary. Basin Res 25, 121–148.

Curiale, J.A., Curtis, J.B., 2016. Organic geochemical applications to the exploration for source-rock reservoirs - A review. Journal of Unconventional Oil and Gas Resources 13, 1–31.

Davis, J.B., Kirkland, D.W., 1970. Native sulfur deposition in the Castile Formation, Culberson County, Texas. Economic Geology 65, 107–121.

Deconinck, J.-F., Hesselbo, S.P., Debuisser, N., Averbuch, O., Baudin, F., Bessa, J., 2003. Environmental controls on clay mineralogy of an Early Jurassic mudrock (Blue Lias Formation, southern England). International Journal of Earth Sciences 92, 255–266.

Dehairs, F., Chesselet, R., Jedwab, J., 1980. Discrete suspended particles of barite and the barium cycle in the open ocean. Earth and Planetary Science Letters 49, 528–550.

Demaison, G.J., Moore, G.T., 1980. Anoxic environments and oil source bed genesis. Organic Geochemistry 2, 9–31.

Devol, A.H., Ahmed, S.I., 1981. Are high rates of sulphate reduction associated with anaerobic oxidation of methane? Nature 291, 407–408.

Durand, B., 1980. Kerogen insoluble organic matter from Swan v sedimentary rocks. Editions Technip, Paris.

Dymond, J., Suess, E., Lyle, M., 1992. Barium in Deep-Sea Sediment: A Geochemical Proxy for Paleoproductivity. Paleoceanography 7, 163–181.

Efthimiadis, E.A., Sotirchos, S.V., 1992. Sulfidation of Limestone-Derived Calcines. Industrial and Engineering Chemistry Research 31, 2311–2321.

Emerson, S., 1984. Organic carbon preservation in marine sediments: The carbon cycle and atmospheric CO2 natural variations Archean to present. Chapman conference papers 1984.

Energy Information Administration 2012, 2012. Energy Information Administration. Annual Energy Outlook 2012 with Projection to 2035 DOE/EIA-0383(2012).

Espitalie, J., Deroo, G., Marquis, F., 1985. La pyrolyse Rock-Eval et ses applications. Première partie. Rev. Inst. Fr. Pét. 40, 563–579.

Espitalie, J., Deroo, G., Marquis, F., 1986. La pyrolyse Rock-Eval et ses applications. Troisième partie. Rev. Inst. Fr. Pét. 41, 73–89.

Ferdelman, T.G., 1988. The Distribution of Sulfur, Iron, Manganese, Copper and Uranium in a Salt Marsh Sediment Core as Determined by a Sequential Extraction Method. University of Delaware, USA.

Ferdelman, T.G., Church, T.M., Luther, G.W., 1991. Sulfur enrichment of humic substances in a Delaware salt marsh sediment core. Geochimica et Cosmochimica Acta 55, 979–988.

Filley, T.R., Freeman, K.H., Wilkin, R.T., Hatcher, P.G., 2002. Biogeochemical controls on reaction of sedimentary organic matter and aqueous sulfides in holocene sediments of Mud Lake, Florida. Geochimica et Cosmochimica Acta 66, 937–954.

Francois, R., 1987. A study of sulphur enrichment in the humic fraction of marine sediments during early diagenesis. Geochimica et Cosmochimica Acta 51, 17–27.

Freeman, K.H., Wakeham, S.G., Hayes, J.M., 1994. Predictive isotopic biogeochemistry: Hydrocarbons from anoxic marine basins. Compound-Specific Isotope Analysis in Biogeochemistry and Petroleum Research 21, 629–644.

Frimmel, F.H., Christman, R.F., Bracewell, J.M., 1988. Humic substances and their role in the environment: Report of the Dahlem Workshop on Humic Substances and Their Role in the Environment, Berlin 1987, March 29-April 3. Wiley, Chichester [West Sussex], New York.

Fruit, D., Elmore, R.D., Halgedahl, S., 1995. Remagnetization of the folded Belden Formation, northwest Colorado. Journal of Geophysical Research 100, 15,009–15,023.

Gallois, R.W., 1976. Coccolith blooms in the Kimmeridge Clay and origin of North Sea Oil. Nature 259, 473–475.

Garner, L.H., 2014. Understanding the combined variability of sulphur and carbon in sulphur-rich kerogen from a marine shale using Rock-Eval 7S., School of Civil Engineering and Geosciences, Newcastle University, UK.

Garrels, R.M., Lerman, A., 1984. Coupling of the sedimentary sulfur and carbon cycles - an improved model. American Journal of Science 284, 989–1007.

Gelin, F., Volkman, J.K., Largeau, C., Derenne, S., Sinninghe Damsté, J.S., Leeuw, J.W. de, 1999. Distribution of aliphatic, nonhydrolyzable biopolymers in marine microalgae. Organic Geochemistry 30, 147–159.

Giblin, A.E., Howarth, R.W., 1984. Porewater evidence for a dynamic sedimentary iron cycle in salt marshes. Limnology and Oceanography 29, 47–63.

Goldhaber, M.B., Kaplan, I.R., 1974. The sulfur cycle: In: Goldberg, E.D. (Ed.) The sea: ideas and observations on progress in the study of the seas, Wiley/Interscience, New York .

Granjeon, D., 1996. Modélisation stratigraphique déterministe: Conception et applications d'un modèle diffusif 3D multilithologique, PhD thesis, Université de Rennes I, France.

Granjeon, D., 2009. 3-D Stratigraphic Modeling of Sedimentary Basins. AAPG Search and Discovery Article #90090©2009. AAPG Annual Convention and Exhibition, Denver, Colorado 2009.

Granjeon, D., 2014. 3D forward modelling of the impact of sediment transport and base level cycles on continental margins and incised valleys: 16. In: Martinius, A.W., Ravnås, R., Howell, J.A., Steel, R.J., Wonham, J.P. (Eds.), From Depositional Systems to Sedimentary Successions on the Norwegian Continental Margin. Wiley-Blackwell, pp. 453–472.

Granjeon, D., Chauveau, B., 2014. Sedimentary basin development method using stratigraphic simulation coupled with an organic matter production and degradation model. Patent: US20140163883 A1. 12-6-2014.

Granjeon, D., Joseph, P., 1999. Concepts and Applications of A 3-D Multiple Lithology, Diffusive Model in Stratigraphic Modeling. In: Harbaugh, J.W., Watney, W.L., Rankey, E.C., Slingerland, R., Goldstein, R.H., Franseen, E.K. (Eds.), Numerical Experiments in Stratigraphy: Recent Advances in Stratigraphic and Sedimentologic Computer Simulations. SEPM Society for Sedimentary Geology.

Granjeon, D., Wolf, S., 2007. 3D stratigraphic modeling in complex tectonics area. AAPG Search and Discovery Article #90063©2007. AAPG Annual Convention and Exhibition, Denver, Colorado 2007.

Griffith, E.M., Paytan, A., 2012. Barite in the ocean - occurrence, geochemistry and palaeoceanographic applications. Sedimentology 59, 1817–1835.

Gryglewicz, G., Jasieńko, S., 1992. The behaviour of sulphur forms during pyrolysis of low-rank coal. Fuel 71, 1225–1229.

Guo, Q., Zhu, G., Strauss, H., Peters, M., Chen, T., Yang, J., Wei, R., Tian, L., Han, X., 2015. Tracing the sources of sulfur in Beijing soils with stable sulfur isotopes. Journal of Geochemical Exploration 161, 112–118.

Hallam, A., 1981. A revised sea-level curve for the early Jurassic. Journal of the Geological Society 138, 735–743.

Hallam, A., Sellwood, B.W., 1976. Middle Mesozoic Sedimentation in Relation to Tectonics in the British Area. The Journal of Geology 84, 301–321.

Hallam, L., 1975. Jurassic Environments. Cambridge University Press, Cambridge.

Hardisty, D.S., Riedinger, N., Gill, B.C., Johnston, D.T., Reinhard, C.T., Planavasky, N.J., Asael, D., Rouxel, O., Owens, J.O., Lyons, T.W., 2018. Detection of sulfidic pore fluids beneath an oxic water column: a comparison of sequential Fe and Mo paleoredox proxies at FOAM. American Journal of Science.

Hartman, M., Svoboda, K., Trnka, O., Čermák, J., 2002. Reaction between hydrogen sulfide and limestone calcines. Industrial and Engineering Chemistry Research 41, 2392–2398.

Hartnett, H.E., Keil, R.G., Hedges, J.I., Devol, A.H., 1998. Influence of oxygen exposure time on organic carbon preservation in continental margin sediments. Nature 391, 572–574.

Hedges, J.I., Keil, R.G., 1995. Sedimentary organic matter preservation: an assessment and speculative synthesis. Marine Chemistry 49, 81–115.

Henkel, S., Mogollón, J.M., Nöthen, K., Franke, C., Bogus, K., Robin, E., Bahr, A., Blumenberg, M., Pape, T., Seifert, R., März, C., Lange, G.J. de, Kasten, S., 2012. Diagenetic barium cycling in Black Sea sediments - A case study for anoxic marine environments. Geochimica et Cosmochimica Acta 88, 88–105.

Henneke, E., Luther III, G.W., Lange, G.J. de, Hoefs, J., 1997. Sulphur speciation in anoxic hypersaline sediments from the eastern Mediterranean Sea. Geochimica et Cosmochimica Acta 61, 307–321.

Herbin, J.P., Fernandez-Martinez, J.L., Geyssant, J.R., Albani, A., Deconinck, J.F., Proust, J.N., Colbeaux, J.P., Vidier, J.P., 1995. Sequence stratigraphy of source rocks applied to the study of the Kim meridgian/Tithonian in the north-west European shelf (Dorset/UK, Yorkshire/UK and Boulonnais/France). Marine and Petroleum Geology 12, 177–194.

Hesselbo, S.P., Jenkyns, H.C., 1995. A comparison of the Hettangian to Bajocian successions of Dorset and Yorkshire. In: Taylor P.D. (Ed.), Field Geology of the British Jurassic, Taylor P.D. ed. Geological Society of London, London.

Hesselbo, S.P., Robinson, S.A., Surlyk, F., 2004. Sea-level change and facies development across potential Triassic-Jurassic boundary horizons, SW Britain. Journal of the Geological Society 161, 365–379.

Hu, G., Dam-Johansen, K., Wedel, S., Hansen, J.P., 2006. Decomposition and oxidation of pyrite. Progress in Energy and Combustion Science 32, 295–314.

Huc, A., Lallier-Verges, E., Bertrand, P., Carpentier, B., Hollander, D., 1992. Organic matter response to change of depositional environment in Kimmeridgian shales, Dorset, U.K. In: Whelan, J.K., Farrington, J.W., Hunt, J.M. (Eds.), Organic matter. Productivity, accumulation, and preservation in recent and ancient sediments. Columbia University Press, New York.

Huc, A.Y., 1977. Contribution of Organic Geochemistry to a Paleoecological Outline of Toarcian Oil Sales in the Eastern Paris Basin. Analysis of Insoluble Organic Matter (Kerogens). [Contribution de la Géochmie organique a une esquisse paleoecologique des schistes bitumineux du Toarcien de l'Est du bassin de paris. Etude de la matiere organique insoluble (kerogenes).]. Rev Inst Fr Pet 32, 703–718.

Huc, A.-Y., 2013. Geochemistry of fossils fuels: From conventional to unconventional hydrocarbon systems. TECHNIP, Paris.

Huerta-Diaz, M.A., Morse, J.W., 1990. A quantitative method for determination of trace metal concentrations in sedimentary pyrite. Marine Chemistry 29, 119–144.

Hunger, S., Benning, L.G., 2007. Greigite: a true intermediate on the polysulfide pathway to pyrite. Geochemical transactions 8, 1.

Hutcheon, I., 1998. The potential role of pyrite oxidation in corrosion and reservoir souring. Journal of Canadian Petroleum Technology 37, 27–31.

Ibarra, J., Palacios, J., Moliner, R., Bonet, A.J., 1994. Evidence of reciprocal organic matter-pyrite interactions affecting sulfur removal during coal pyrolysis. Fuel 73, 1046–1050.

Jacobs, L., Emerson, S., Skei, J., 1985. Partitioning and transport of metals across the O2 H2S interface in a permanently anoxic basin: Framvaren Fjord, Norway. Geochimica et Cosmochimica Acta 49, 1433–1444.

Jahnke, R.A., 1990. Early diagenesis and recycling of biogenic debris at the seafloor, Santa Monica Basin, California. J Mar Res 48, 413–436.

Jenkyns, H.C., 1985. The early Toarcian and Cenomanian-Turonian anoxic events in Europe: comparisons and contrasts. Geologische Rundschau 74, 505–518.

Jenkyns, H.C., Jones, C.E., Gröcke, D.R., Hesselbo, S.P., Parkinson, D.N., 2002. Chemostratigraphy of the Jurassic System: Applications, limitations and implications for palaeoceanography. Journal of the Geological Society 159, 351–378.

Jensen, H., Connan, J., Bjorøy, M., Hall, K., Wold, S., 1998. Geoelf sulphur analyser: Quantification of thermally extractable and pyrolysable organic and mineral sulphur in source rocks. Organic Geochemistry 28, 87–110.

Karthe, S., Szargan, R., Suoninen, E., 1993. Oxidation of pyrite surfaces: a photoelectron spectroscopic study. Applied Surface Science 72, 157–170.

Keil, R.G., Tsamakis, E., Fuh, C.B., Giddings, J.C., Hedges, J.I., 1994. Mineralogical and textural controls on the organic composition of coastal marine sediments: Hydrodynamic separation using SPLITT-fractionation. Geochimica et Cosmochimica Acta 58, 879–893.

Kelemen, S.R., Sansone, M., Walters, C.C., Kwiatek, P.J., Bolin, T., 2012. Thermal transformations of organic and inorganic sulfur in Type II kerogen quantified by S-XANES. Geochimica et Cosmochimica Acta 83, 61–78.

Kelly, D.P., Wood, A.P., 2000. Reclassification of some species of Thiobacillus to the newly designated genera Acidithiobacillus gen. nov., Halothiobacillus gen. nov. and Thermithiobacillus gen. nov. International Journal of Systematic and Evolutionary Microbiology 50, 511–516.

Kennedy, M.J., Löhr, S.C., Fraser, S.A., Baruch, E.T., 2014. Direct evidence for organic carbon preservation as clay-organic nanocomposites in a Devonian black shale; from deposition to diagenesis. Earth and Planetary Science Letters 388, 59–70.

Kennedy, M.J., Wagner, T., 2011. Clay mineral continental amplifier for marine carbon sequestration in a greenhouse ocean. Proceedings of the National Academy of Sciences of the United States of America 108, 9776–9781.

Knicker, H., 2004. Stabilization of N-compounds in soil and organic-matter-rich sediments - What is the difference? Marine Chemistry 92, 167–195.

Kolonic, S., Sinninghe Damsté, J.S., Böttcher, M.E., Kuypers, M.M.M., Kuhnt, W., Beckmann, B., Scheeder, G., Wagner, T., 2006. Geochemical characterization of Cenomanian/Turonian black shales from the Tarfaya basin (SW morocco). Journal of Petroleum Geology 25, 325–350.

Lafargue, E., Marquis, F., Pillot, D., 1998. Rock-Eval 6 applications in hydrocarbon exploration, production, and soil contamination studies. Revue de l'Institut Francais du Petrole 53, 421–437.

Lallier-Vergès, E., Bertrand, P., Huc, A.Y., Bückel, D., Tremblay, P., 1993. Control of the preservation of organic matter by productivity and sulphate reduction in Kimmeridgian shales from Dorset (UK). Marine and Petroleum Geology 10, 600–605.

Lalonde, K., Mucci, A., Ouellet, A., Gélinas, Y., 2012. Preservation of organic matter in sediments promoted by iron. Nature 483, 198–200.

Lambert, J.M., Simkovich, G., Walker, P.L., 1980. Production of pyrrhotites by pyrite reduction. Fuel 59, 687–690.

Lamoureux-Var, V., Lorant, F., 2005. Experimental evaluation of H2S yields in reservoir rocks submitted to steam injection. 13th European Symposium on Improved Oil Recovery 2005.

Landais, P., Michels, R., Benkhedda, Z., Kister, J., Dereppe, J.-M., 1991. Behavior of Oxidized Type II Kerogen during Artificial Maturation. Energy and Fuels 5, 860–866.

Larter, S.R., Solli, H., Douglas, A.G., Lange, F. de, Leeuw, J.W. de, 1979. Occurrence and significance of prist-1-ene in kerogen pyrolysates [5]. Nature 279, 405–408.

Leeuw, J.W. de, Largeau, C., 1993. A Review of Macromolecular Organic Compounds That Comprise Living Organisms and Their Role in Kerogen, Coal, and Petroleum Formation. In: Stehli, F.G., Jones, D.S., Engel, M.H., Macko, S.A. (Eds.), Organic Geochemistry, vol. 11. Springer US, Boston, MA. Topics in Geobiology, pp. 23–72.

Leventhal, J.S., 1983. An interpretation of carbon and sulfur relationships in Black Sea sediments as indicators of environments of deposition. Geochimica et Cosmochimica Acta 47, 133–137.

Leventhal, J.S., 1987. Carbon and sulfur relationships in Devonian shales from the Appalachian Basin as an indicator of environment of deposition. American Journal of Science 287, 33–49.

Leventhal, J.S., 1995. Carbon-sulfur plots to show diagenetic and epigenetic sulfidation in sediments. Geochimica et Cosmochimica Acta 59, 1207–1211.

Lewan, M.D., Bjorøy, M., Dolcater, D.L., 1986. Effects of thermal maturation on steroid hydrocarbons as determined by hydrous pyrolysis of Phosphoria Retort Shale. Geochimica et Cosmochimica Acta 50, 1977–1987.

Lewan, M.D., Ruble, T.E., 2002. Comparison of petroleum generation kinetics by isothermal hydrous and nonisothermal open-system pyrolysis. Organic Geochemistry 33, 1457–1475.

Love, L.G., Amstutz, G.C., 1966. Review of microscopic pyrite from the Devonian Chattanooga shale and Rammelsberg Banderz. Fortschr. Mineral, 1966, 273–309.

Lückge, A., Horsfield, B., Littke, R., Scheeder, G., 2002. Organic matter preservation and sulfur uptake in sediments from the continental margin off Pakistan. Organic Geochemistry 33, 477–488.

Lyons, T.W., 1997. Sulfur isotopic trends and pathways of iron sulfide formation in upper holocene sediments of the anoxic black sea. Geochimica et Cosmochimica Acta 61, 3367–3382.

Lyons, T.W., Berner, R.A., 1992. Carbon-sulfur-iron systematics of the uppermost deep-water sediments of the Black Sea. Chemical Geology 99, 1–27.

Machado, M.E., Fontanive, F.C., Oliveira, J.V. de, Caramão, E.B., Zini, C.A., 2011. Identification of organic sulfur compounds in coal bitumen obtained by different extraction techniques using comprehensive two-dimensional gas chromatography coupled to time-of-flight mass spectrometric detection. Analytical and bioanalytical chemistry, 2011, 2433–2444.

Mackenzie, A.S., Hoffmann, C.F., Maxwell, J.R., 1981. Molecular parameters of maturation in the Toarcian shales, Paris Basin, France-III. Changes in aromatic steroid hydrocarbons. Geochimica et Cosmochimica Acta 45, 1345–1355.

Mann, U., Zweigel, J., 2008. Modelling Source-Rock Distribution and Quality Variations: The Organic Facies Modelling Approach. In: Boer, P. de, Postma, G., van der Zwan, K., Burgess, P., Kukla, P. (Eds.), Analogue and Numerical Modelling of Sedimentary Systems: From Understanding to Prediction. Wiley-Blackwell, Oxford, UK, pp. 239–274.

Matthews, A., Morgans-Bell, H.S., Emmanuel, S., Jenkyns, H.C., Erel, Y., Halicz, L., 2004. Controls on iron-isotope fractionation in organic-rich sediments (Kimmeridge Clay, Upper Jurassic, Southern England). Geochimica et Cosmochimica Acta 68, 3107–3123.

Mayer, L.M., 1994. Relationships between mineral surfaces and organic carbon concentrations in soils and sediments. Chemical Geology 114, 347–363.

Mayer, L.M., 1999. Extent of coverage of mineral surfaces by organic matter in marine sediments. Geochimica et Cosmochimica Acta 63, 207–215.

Mongenot, T., Derenne, S., Largeau, C., Tribovillard, N.-P., Lallier-Vergès, E., Dessort, D., Connan, J., 1999. Spectroscopic, kinetic and pyrolytic studies of kerogen from the dark parallel laminae facies of the sulphur-rich Orbagnoux deposit (Upper Kimmeridgian, Jura). Organic Geochemistry 30, 39–56.

Morgans-Bell, H.S., Coe, A.L., Hesselbo, S.P., Jenkyns, H.C., Weedon, G.P., Marshall, J., Tyson, R.V., Williams, C.J., 2001. Integrated stratigraphy of the Kimmeridge Clay Formation (Upper Jurassic) based on exposures and boreholes in South Dorset, UK. Geological Magazine 138, 511–539.

Morse, J.W., Cornwell, J.C., 1987. Analysis and distribution of iron sulfide minerals in recent anoxic marine sediments. Marine Chemistry 22, 55–69.

Mossmann, J.-R., Aplin, A.C., Curtis, C.D., Coleman, M.L., 1991. Geochemistry of inorganic and organic sulphur in organic-rich sediments from the Peru Margin. Geochimica et Cosmochimica Acta 55, 3581–3595.

Müller, P.J., Suess, E., 1979. Productivity, sedimentation rate, and sedimentary organic matter in the oceans—I. Organic carbon preservation. Deep Sea Research Part A. Oceanographic Research Papers 26, 1347–1362.

Murray, J.W., Grundmanis, V., Smethie, W.M., 1978. Interstitial water chemistry in the sediments of Saanich Inlet. Geochimica et Cosmochimica Acta 42, 1011–1026.

Odom, I.E., 1983. Smectite clay minerals: properties and uses. Philosophical Transactions of the Royal Society of London (Series) A: Mathematical and Physical Sc 311, 391–409.

Orr, W.L., 1986. Kerogen/asphaltene/sulfur relationships in sulfur-rich Monterey oils. Organic Geochemistry 10, 499–516.

Oschmann, W., 1988. Kimmeridge clay sedimentation — A new cyclic model. Palaeogeography, Palaeoclimatology, Palaeoecology 65, 217–251.

Passier, H.F., Luther III, G.W., Lange, G.J. de, 1997. Early diagenesis and sulphur speciation in sediments of the Oman Margin, northwestern Arabian Sea. Deep-Sea Research Part II: Topical Studies in Oceanography 44, 1361–1380.

Peckmann, J., Paul, J., Thiel, V., 1999. Bacterially mediated formation of diagenetic aragonite and native sulfur in Zechstein carbonates (Upper Permian, Central Germany). Sedimentary Geology 126, 205–222.

Petsch, S., Berner, R., Eglinton, T., 2000. A field study of the chemical weathering of ancient sedimentary organic matter. Organic Geochemistry 31, 475–487.

Pettijohn, F.J., 1957. Sedimentary rocks. Harper and Brothers, New York.

Philippot, P., van Zuilen, M., Lepot, K., Thomazo, C., Farquhar, J., van Kranendonk, M.J., 2007. Early Archaean Microorganisms Preferred Elemental Sulfur, Not Sulfate. Science 317, 1534–1537.

Pillot, D., Deville, E., Prinzhofer, A., 2013. Identification and Quantification of Carbonate Species Using Rock-Eval Pyrolysis. Oil Gas Sci. Technol. – Rev. IFP Energies nouvelles 69, 341–349.

Piper, D.Z., Calvert, S.E., 2009. A marine biogeochemical perspective on black shale deposition. Earth-Science Reviews 95, 63–96.

Poulton, S.W., Krom, M.D., Raiswell, R., 2004. A revised scheme for the reactivity of iron (oxyhydr)oxide minerals towards dissolved sulfide. Geochimica et Cosmochimica Acta 68, 3703–3715.

Powell, J.H., 2010. Jurassic sedimentation in the Cleveland Basin: A review. Proceedings of the Yorkshire Geological Society 58, 21–72.

Pratt, M.L., 1984. Influence of Paleoenvironmental Factors on Preservation of Organic Matter in Middle Cretaceous Greenhorn Formation, Pueblo, Colorado 68, 1146–1159.

Premuzic, E.T., Benkovitz, C.M., Gaffney, J.S., Walsh, J.J., 1982. The nature and distribution of organic matter in the surface sediments of world oceans and seas. Organic Geochemistry 4, 63–77.

Price, L.C., Wenger, L.M., 1992. The influence of pressure on petroleum generation and maturation as suggested by aqueous pyrolysis. Organic Geochemistry 19, 141–159.

Raiswell, R., Berner, R.A., 1985. Pyrite formation in euxinic and semi-euxinic sediments. American Journal of Science, 1985, 710–724.

Raiswell, R., Berner, R.A., 1986. Pyrite and organic matter in Phanerozoic normal marine shales. Geochimica et Cosmochimica Acta 50, 1967–1976.

Raiswell, R., Buckley, F., Berner, R.A., Anderson, T.F., 1988. Degree of pyritization of iron as a paleoenvironmental indicator of bottom-water oxygenation. Journal of Sedimentary Petrology 58, 812–819.

Raiswell, R., Hardisty, D.S., Lyons, T.W., Canfield, D.E., Owens, J.D., Planavsky, N.J., Poulton, S.W., Reinhard, C.T., 2018. The iron paleoredox proxies: A guide to the pitfalls, problems and proper practice. American Journal of Science 318, 491–526.

Ransom, B., Bennett, R.H., Baerwald, R., Shea, K., 1997. 5TEM6 study of in situ organic matter on continental margins: occurrence and the "monolayer" hypothesis. Marine Geology 138, 1–9.

Rashid, M.A., 1985. Geochemistry of marine humic compounds. Springer-Verlag, New York.

Raven, M.R., Sessions, A.L., Adkins, J.F., Thunell, R.C., 2016a. Rapid organic matter sulfurization in sinking particles from the Cariaco Basin water column. Geochimica et Cosmochimica Acta 190, 175–190.

Raven, M.R., Sessions, A.L., Fischer, W.W., Adkins, J.F., 2016b. Sedimentary pyrite δ34S differs from porewater sulfide in Santa Barbara Basin: Proposed role of organic sulfur. Geochimica et Cosmochimica Acta 186, 120–134.

Riboulleau, A., Baudin, F., Deconinck, J.-F., Derenne, S., Largeau, C., Tribovillard, N., 2003. Depositional conditions and organic matter preservation pathways in an epicontinental environment: The Upper Jurassic Kashpir Oil Shales (Volga Basin, Russia). Palaeogeography, Palaeoclimatology, Palaeoecology 197, 171–197.

Riedinger, N., Brunner, B., Krastel, S., Arnold, G.L., Wehrmann, L.M., Formolo, M.J., Beck, A., Bates, S.M., Henkel, S., Kasten, S., Lyons, T.W., 2017. Sulfur Cycling in an Iron Oxide-Dominated, Dynamic Marine Depositional System: The Argentine Continental Margin. Frontiers in Earth Science 5, 33.

Riedinger, N., Kasten, S., Gröger, J., Franke, C., Pfeifer, K., 2006. Active and buried authigenic barite fronts in sediments from the Eastern Cape Basin. Earth and Planetary Science Letters 241, 876–887.

Rimmer, S.M., Thompson, J.A., Goodnight, S.A., Robl, T.L., 2004. Multiple controls on the preservation of organic matter in Devonian-Mississippian marine black shales: Geochemical and petrographic evidence. Palaeogeography, Palaeoclimatology, Palaeoecology 215, 125–154.

Ruble, T.E., Lewan, M.D., Philip, R.P., 2001. New insights on the Green River petroleum system in the Uinta basin from hydrous pyrolysis experiments. AAPG Bulletin 85, 1333–1371.

Russell, J.M., Werne, J.P., 2009. Climate change and productivity variations recorded by sedimentary sulfur in Lake Edward, Uganda/D. R. Congo. Chemical Geology 264, 337–346.

Salem, N., 2013. Geochemical characterisation of the Pliensbachian-Toarcian boundary during the onset of the Toarcian Oceanic Anoxic Event. North Yorkshire, UK, PhD thesis, Newcastle University, UK.

Sarret, G., Mongenot, T., Connan, J., Derenne, S., Kasrai, M., Michael Bancroft, G., Largeau, C., 2002. Sulfur speciation in kerogens of the Orbagnoux deposit (Upper Kimmeridgian, Jura) by XANES spectroscopy and pyrolysis. Organic Geochemistry 33, 877–895.

Sellwood, B.W., 1970. The relation of trace fossils to small scale sedimentary cycles in the British Lias. Trace Fossils 3, 489–504.

Sinninghe Damste, J.S., Leeuw, J.W. de, 1990. Analysis, structure and geochemical significance of organically-bound sulphur in the geosphere: State of the art and future research. Organic Geochemistry 16, 1077–1101.

Sinninghe Damsté, J.S., Eglinton, T.I., Leeuw, J.W. de, Schenck, P.A., 1989. Organic sulphur in macromolecular sedimentary organic matter: I. Structure and origin of sulphur-containing moieties in kerogen, asphaltenes and coal as revealed by flash pyrolysis. Geochimica et Cosmochimica Acta 53, 873–889.

Sinninghe Damsté, J.S., Irene, W., Rijpstra, C., Leeuw, J.W. de, Schenck, P.A., 1988. Origin of organic sulphur compounds and sulphur-containing high molecular weight substances in sediments and immature crude oils. Organic Geochemistry 13, 593–606.

Sinninghe Damsté, J.S., Kok, M.D., Köster, J., Schouten, S., 1998. Sulfurized carbohydrates: an important sedimentary sink for organic carbon? Earth and Planetary Science Letters 164, 7–13.

Sinninghe Damsté, J.S., las Heras, F. de, van Bergen, P.F., Leeuw, J.W. de, 1993. Characterization of Tertiary Catalan lacustrine oil shales: Discovery of extremely organic sulphur-rich Type I kerogens. Geochimica et Cosmochimica Acta 57, 389–415.

Sinninghe Damsté, J.S., Xavier, F., Heras, C., Leeuw, J., 1992. Molecular analysis of sulphur-rich brown coals by flash pyrolysis-gas chromatography-mass spectrometry. The Type III-S kerogen. Journal of Chromatography A 607, 361–376.

Speight, J.G., 2005. Handbook of Coal Analysis. Wiley.

Stamatakis, M.G., Hein, J.R., 1993. Origin of barite in Tertiary marine sedimentary rocks from Lefkas Island, Greece. Economic Geology 88, 91–103.

Suits, N., Arthur, M.A., Dean, W., 1993. C–S–Fe systematics in Peru margin muds. Geol. Soci. Amer. Abstr 25, A199 1993.

Sweeney, R.E., 1972. Pyritization During Diagenesis of Marine Sediments, PhD thesis, University of California, USA.

Sweeney, R.E., Kaplan, I.R., 1973. Pyrite framboid formation: Laboratory synthesis and marine sediments. Economic Geology 68, 618–634.

Tegelaar, E.W., Leeuw, J.W. de, Derenne, S., Largeau, C., 1989. A reappraisal of kerogen formation. Geochimica et Cosmochimica Acta 53, 3103–3106.

Tissot, B.P., Welte, D.H., 1978. Petroleum formation and occurrence: A new approach to oil and gas exploration. Springer-Verlag, Berlin, New York.

Torres, M.E., Brumsack, H.J., Bohrmann, G., Emeis, K.C., 1996. Barite fronts in continental margin sediments: A new look at barium remobilization in the zone of sulfate reduction and formation of heavy barites in diagenetic fronts. Chemical Geology 127, 125–139.

Tribovillard, N., Hatem, E., Averbuch, O., Barbecot, F., Bout-Roumazeilles, V., Trentesaux, A., 2015. Iron availability as a dominant control on the primary composition and diagenetic overprint of organic-matter-rich rocks. Chemical Geology 401, 67–82.

Tribovillard, N., Trentesaux, A., Ramdani, A., Baudin, F., Riboulleau, A., 2004. Controls on organic accumulation in late Jurassic shales of northwestern Europe as inferred from trace-metal geochemistry. Bulletin de la Societe Geologique de France 175, 491–506.

Tribovillard, N., Trichet, J., Défarge, C., Trentesaux, A., 1999. Jurassic lagoonal environments and quasi-abiotic platy limestone accumulation: Microbial interventions. Sedimentology 46, 1183–1197.

Tribovillard, N.-P., Desprairies, A., Lallier-Vergès, E., Bertrand, P., Moureau, N., Ramdani, A., Ramanampisoa, L., 1994. Geochemical study of organic-matter rich cycles from the Kimmeridge Clay Formation of Yorkshire (UK): productivity versus anoxia. Palaeogeography, Palaeoclimatology, Palaeoecology 108, 165–181.

Tuttle, M.L., Goldhaber, M.B., 1993. Sedimentary sulfur geochemistry of the Paleogene Green River Formation, western USA: Implications for interpreting depositional and diagenetic processes in saline alkaline lakes. Geochimica et Cosmochimica Acta 57, 3023–3039.

Tyson, R.V., 1995. Sedimentary Organic Matter. Springer Netherlands, Dordrecht.

Tyson, R.V., Pearson, T.H., 1991. Modern and ancient continental shelf anoxia: an overview. Geological Society, London, Special Publications 58, 1–24.

Tyson, R.V., Wilson, R.L., Downie, C., 1979. A stratified water column environmental model for the type Kimmeridge Clay. Nature 277, 377–380.

Uteyev, R., 2011. Etude thermodynamique et expérimentale du cycle géochimique du soufre dans les bassins sédimentaires, PhD thesis, Université Henri Poincaré, France.

Vairavamurthy, A., Mopper, K., Taylor, B.F., 1992. Occurrence of particle-bound polysulfides and significance of their reaction with organic matters in marine sediments. Geophys. Res. Lett. 19, 2043–2046.

Vairavamurthy, M.A., Maletic, D., Wang, S., Manowitz, B., Eglinton, T., Lyons, T., 1997. Characterization of sulfur-containing functional groups in sedimentary humic substances by X-ray absorption near-edge structure spectroscopy. Energy and Fuels 11, 546–553.

Vairavamurthy, M.A., Wang, S., Khandelwal, B., Manowitz, B., Ferdelman, T., Fossing, H., 1995. Sulfur Transformations in Early Diagenetic Sediments from the Bay of Conception, Off Chile. In: Vairavamurthy, M.A., Schoonen, M.A.A.,

Eglinton, T.I., Luther, G.W., Manowitz, B. (Eds.), Geochemical Transformations of Sedimentary Sulfur, vol. 612. American Chemical Society, Washington, DC. ACS Symposium Series, pp. 38–58.

Vandenbroucke, M., Largeau, C., 2007. Kerogen origin, evolution and structure. Organic Geochemistry 38, 719–833.

Veto, I., Hetényi, M., Hámor-Vidó, M., Hufnagel, H., Haas, J., 2000. Anaerobic degradation of organic matter controlled by productivity variation in a restricted Late Triassic basin. Organic Geochemistry 31, 439–452.

Volzone, C., 2007. Retention of pollutant gases: Comparison between clay minerals and their modified products. Applied Clay Science 36, 191–196.

Von-Breymann, M.T., Emeis, K., Suess, E., 1992. Water depth and diagenetic constraints on the use of barium as a palaeoproductivity indicator. Geological Society, Special Publication, London.

Wagner, T., 2002. Late Cretaceous to early Quaternary organic sedimentation in the eastern Equatorial Atlantic. Palaeogeography, Palaeoclimatology, Palaeoecology 179, 113–147.

Warrington, G., Ivimey-Cook, H.C., 1995. The Late Triassic and Early Jurassic of coastal sections in west Somerset and south and mid-Glamorgan. In: Taylor P.D. (Ed.), Field Geology of the British Jurassic, Taylor P.D. ed. Geological Society of London, London.

Weedon, G.P., Coe, A.L., Gallois, R.W., 2004. Cyclostratigraphy, orbital tuning and inferred productivity for the type Kimmeridge Clay (Late Jurassic), Southern England. Journal of the Geological Society 161, 655–666.

Werne, J.P., Hollander, D.J., Lyons, T.W., Sinninghe Damsté, J.S., 2004. Organic sulfur biogeochemistry: Recent advances and future research directions. Sulfur Biogeochemistry: Past and Present, 135–150.

Werne, J.P., Lyons, T.W., Hollander, D.J., Schouten, S., Hopmans, E.C., Sinninghe Damsté, J.S., 2008. Investigating pathways of diagenetic organic matter sulfurization using compound-specific sulfur isotope analysis. Geochimica et Cosmochimica Acta 72, 3489–3502.

Westrich, J.T., 1983. The consequences and controls of bacterial sulfate reduction in marine sediments, PhD thesis, Yale University, USA.

Wignall, P.B., Myers, K.J., 1988. Interpreting benthic oxygen levels in mudrocks: A new approach. Geology 16, 452.

Wilkin, R.T., Barnes, H.L., 1997. Pyrite formation in an anoxic estuarine basin. American Journal of Science 297, 620–650.

Williamson, A., Johnson, M.S., 1981. Reclamation of Metalliferous Mine Wastes. In: Lepp, N.W. (Ed.), Effect of Heavy Metal Pollution on Plants: Metals in the Environment. Springer Netherlands, Dordrecht, pp. 185–212.

Yperman, J., Franco, D., Mullens, J., van Poucke, L.C., Gryglewicz, G., Jasienko, S., 1995. Determination of sulfur groups in pyrolysed low-rank coal by atmospheric-pressure t.p.r. Fuel 74, 1261–1266.

Yrjas, K.P., Zevenhoven, C., Hupa, M.M., 1996. Hydrogen Sulfide Capture by Limestone and Dolomite at Elevated Pressure. 1. Sorbent Performance. Industrial and Engineering Chemistry Research 35, 176–183.

Zaback, D.A., Pratt, L.M., 1992. Isotopic composition and speciation of sulfur in the Miocene Monterey Formation: Reevaluation of sulfur reactions during early diagenesis in marine environments. Geochimica et Cosmochimica Acta 56, 763–774.

Zeng, T., Arnold, W.A., Toner, B.M., 2013. Microscale characterization of sulfur speciation in lake sediments. Environmental science & technology 47, 1287–1296.